DISSECTING THE FUNCTION OF FARP1 AND RHO GTPASES IN SEMAPHORIN-PLEXIN SIGNALING: STRUCTURAL PERSPECTIVE

APPROVED BY SUPERVISORY COMMITTEE

Xuewu Zhang, Ph.D.

Joseph Albanesi, Ph.D.

Lily Huang, Ph.D.

Jose Rizo-Rey, Ph.D.

Paul Sternweis, Ph.D.

Dedicated to my beautiful wife and my family for their endless love and support in this long journey.

DISSECTING THE REGULATION OF FARP1 AND RHO GTPASES IN SEMAPHORIN-PLEXIN SIGNALING: STRUCTRUAL PERSPECTIVE

by

YI-CHUN KUO

DISSERTATION / THESIS

Presented to the Faculty of the Graduate School of Biomedical Sciences

The University of Texas Southwestern Medical Center at Dallas

In Partial Fulfillment of the Requirements

For the Degree of

DOCTOR OF PHILOSOPHY

The University of Texas Southwestern Medical Center at Dallas

Dallas, Texas

December, 2017

DISSECTING THE REGULATION OF FARP1 AND RHO GTPASES IN SEMAPHORIN-PLEXIN SIGNALING: STRUCTRUAL PERSPECTIVE

Publication No. _____

Yi-Chun Kuo, Ph.D.

The University of Texas Southwestern Medical Center at Dallas, 2017

Supervising Professor: Xuewu Zhang, Ph.D.

The Semaphorin-Plexin signaling is important for regulating axon guidance. Binding of Semaphorin to the Plexin receptor induces the dimerization of Plexin and stimulates its cytoplasmic GAP activity towards Rap, resulting in cytoskeleton re-organization. The growth cone of an axon then turns around, which ultimately leads to the repulsive guidance of the axon. Structural studies by our laboratory and others have revealed how the RapGAP activity of

Plexin cytoplasmic region is stimulated by dimerization, how the Semaphorin ligand interacts with Plexin ectodomain, and how extracellular domains prevent Plexin from premature activation. Several downstream effectors interacting with Plexin cytoplasmic domain were found; however, the molecular mechanisms by which these effectors regulate Plexin signaling remain largely unknown. Our laboratory was interested in one of the effectors named FARP. Previous studies in our laboratory determined the crystal structures of the functional units of FARP1 and FARP2 but failed to detect any GEF activity *in vitro*. A recent screening with yeast two-hybrid identified a RhoGTPase, Rif, as a novel interacting protein for FARP1. To investigate how Rif/FARP1 interaction is involved in Plexin signaling, I determined the crystal structure of Rif-bound FARP1. This complex structure explains the functional roles that FARP1 and Rif might exert in dendritic spine formation and neurite outgrowth. Also, the N-terminal FERM domain of FARPs is known to interact with the cytoplasmic domain of Plexin. To interrogate how FERM interacts with Plexin and how this interaction might regulate Plexin signaling, I characterized the interaction of FERM with Plexin both biophysically and biochemically. The last question that I attempted to address in this dissertation is how a RhoGTPase, RhoD, inhibits activation of Plexin. RhoD was known for its remarkable inhibitory effect on Plexin signaling presumably through binding to the defined RhoGTPase binding domain of Plexin. The structure of Rac1 or Rnd1 in complex with Plexin did not explain how this binding regulates Plexin activity. I solved the crystal structure of the RhoD/Plexin complex. Modeling of this structure with that of Plexin active dimer in the context of the plasma membrane reveals a mechanism by which RhoD inhibits Plexin

activation. Structure studies in this dissertation added another layer of comprehension on how the Semaphorin-Plexin signaling is regulated.

TABLE OF CONTENTS

PRIOR PUBLICATIONS

1. Wu, X., L. S. Zhang, J. Toombs, **Y. C. Kuo**, J. T. Piazza, R. Tuladhar, Q. Barrett, C. W. Fan, X. Zhang, L. D. Walensky, M. Kool, S. Y. Cheng, R. Brekken, J. T. Opferman, D. R. Green, T. Moldoveanu and L. Lum (2017). "Extra-mitochondrial prosurvival BCL-2 proteins regulate gene transcription by inhibiting the SUFU tumour suppressor." Nat Cell Biol **19**(10): 1226-1236.

2. Tao, C., W. L. Holland, Q. A. Wang, M. Shao, L. Jia, K. Sun, X. Lin, **Y. C. Kuo**, J. A. Johnson, R. Gordillo, J. K. Elmquist and P. E. Scherer (2017). "Short-Term Versus Long-Term Effects of Adipocyte Toll-Like Receptor 4 Activation on Insulin Resistance in Male Mice." Endocrinology **158**(5): 1260-1270.

3. Sun, X., J. C. Chuang, M. Kanchwala, L. Wu, C. Celen, L. Li, H. Liang, S. Zhang, T. Maples, L. H. Nguyen, S. C. Wang, R. A. Signer, M. Sorouri, I. Nassour, X. Liu, J. Xu, M. Wu, Y. Zhao, **Y. C. Kuo**, Z. Wang, C. Xing and H. Zhu (2016). "Suppression of the SWI/SNF Component Arid1a Promotes Mammalian Regeneration." Cell Stem Cell **18**(4): 456-466.

4. Kuo, Y. C. and X. Zhang (2016). "Regulation of Plexin: A Ring of Structural Twists and Turns." Neuron **91**(3): 497-499.

5. He, X., **Y. C. Kuo**, T. J. Rosche and X. Zhang (2013). "Structural basis for autoinhibition of the guanine nucleotide exchange factor FARP2." Structure **21**(3): 355-364.

6. Kuo, Y. C., K. Y. Huang, C. H. Yang, Y. S. Yang, W. Y. Lee and C. W. Chiang (2008). "Regulation of phosphorylation of Thr-308 of Akt, cell proliferation, and survival by the B55alpha regulatory subunit targeting of the protein phosphatase 2A holoenzyme to Akt." J Biol Chem **283**(4): 1882-1892.

LIST OF FIGURES

LIST OF TABLES

LIST OF ABBREVIATIONS

GTP – Guanosine 5′-triphosphate

GDP – Guanosine 5′-diphosphate

SUMO – Small ubiquitin-like modifier

Upl – Ubl-specific protease

PCR – Polymerase chain reaction

GCN4 – General control non-repressed 4

DTT – Dithiothreitol

TCEP – Tris(2-carboxyethyl)phosphine hydrochloride

SCD – Synthetic complete glucose

RT – Room temperature

MANT-GTP – 2'-(or-3')-*O*-(*N*-Methylanthraniloyl) Guanosine 5'-Triphosphate

GST – Glutathione-S-transferase.

BSA – Bovine serum albumin

GAP – GTPase-activating protein

GEF – Guanine nucleotide exchange factor

FERM – 4.1, ezrin, radixin and moesin

FARP – FERM, RhoGEF (ARHGEF) and pleckstrin domain protein

RBD – RhoGTPase binding domain

CHAPTER ONE :

OVERVIEW OF SEMAPHORIN/PLEXIN SIGNALING

SEMAPHORIN/PLEXIN SIGNALING

Relevance

Semaphorin and Plexin

Semaphorins are a family of secreted or transmembrane proteins that can regulate cell-cell interactions as well as cell morphology, differentiation, and function. Plexins are a large family of cell surface receptors for the axon guidance molecules Semaphorins (Kruger et al., 2005; Tran et al., 2007). Semaphorin-Plexin signaling is essential for the regulation of neuronal network formation, immune system development, and angiogenesis (Gu and Giraudo, 2013; Kumanogoh and Kikutani, 2013; Neufeld et al., 2012; Pasterkamp, 2012). Aberrance in Semaphorin-Plexin pathways has been implicated in various diseases including neurological disorders and cancer (Capparuccia and Tamagnone, 2009; Rujescu et al., 2007; Worzfeld and Offermanns, 2014).

Semaphorins are secreted or membrane-associated multi-domain proteins (Pasterkamp and Kolodkin, 2003) that have been grouped into eight classes according to their structural elements and sequence similarity (1999). Individual Semaphorins are designated by a letter code. Currently, more than 20 types of Semaphorin are found. All Semaphorins

contain a conserved Sema domain containing ~400 residues. The structure of Sema domain adopts a seven-blade β-propeller fold (Antipenko et al., 2003; Love et al., 2003). The size of Semaphorins varies depending on what other domains they harbor in addition to the Sema domain and PSI (Plexins, Semaphorins, and Integrins) domain. Classes 1, 4, 5, 6 and 7 Semaphorin are membrane-associated, whereas classes 2 and 3 and the viral Semaphorins are secreted (Kruger et al., 2005). (Figure 1-1)

Plexins are type I transmembrane receptors for Semaphorins. Plexins are grouped into four classes (A–D) by sequence homology. Individual Plexins are further designated by a number code. The extracellular region of Plexins have multi-domains including an N-terminal Sema domain for Semaphorin binding, three PSI domains, and three IPT (Ig-like, Plexins and Transcription factors) domains. The Plexin intracellular domain is highly conserved among different Plexins and shares GAP (GTPase-activating protein) domain homology. This GAP-homology domain is divided into two portions in primary sequence by an insertion of a RhoGTPase binding domain (RBD) (Kruger et al., 2005; Tong and Buck, 2005) (Figure 1-1). Binding of dimeric Semaphorin to the Sema domain of Plexin induces the dimerization of the cytoplasmic domains of Plexin and stimulates its RapGAP activity (Wang et al., 2012).

Plexin cytoplasmic domain

Signaling mechanism

In the absence of Semaphorin, the cytoplasmic domain of Plexin is inactive. GTP-

bound Rap functions as a critical activator of integrin for promoting cell adhesion to extracellular matrix (Gloerich and Bos, 2011). Binding of Semaphorin to Plexin stimulates its cytoplasmic GAP activity to facilitate the intrinsic GTP hydrolysis of Rap (Wang et al., 2012). Inactive GDP-bound Rap causes inactivation of integrin and weakens cell-extracellular matrix adhesion, leading to Plexin-mediated axonal repulsion and cell collapse (Wang et al., 2012) (Figure 1-2).

Overall architecture

The primary sequence of the intracellular region of Plexin has an N-terminal juxtamembrane (JM) helix, two halves of GAP-homology domains separated by an insertion segment RBD. Crystal structure of the intracellular region of Plexin revealed that two separated GAP-homology domains form an entire GAP domain; RBD resides at one side of the GAP domain (He et al., 2009) (Figure 1-3). The JM helix that connects the transmembrane region to the GAP domain wraps around the GAP domain and has a regulatory role in the process of Plexin activation. The GAP domain is the enzymatic domain essential for Plexin signaling. Mutation of the catalytic "arginine finger" residue abolishes GAP activity of Plexin. The RBD binds to a subset of RhoGTPases, such as Rac1, Rnd1, and RhoD, in their GTP–bound active state (Driessens et al., 2001; Rohm et al., 2000; Vikis et al., 2000; Zanata et al., 2002).

Plexin activation mechanism

Semaphorin binding to the extracellular Sema domain of Plexin receptor induces the dimerization of intracellular region of Plexin. Dimerization of Plexin intracellular region stimulates its GAP activity (Wang et al., 2012). Structural details of the activation process of Plexin intracellular region was revealed in (Wang et al., 2013). Plexin dimerization induces a large-scale conformational change and opens up the GAP domain to allow Rap binding. A JM helix of Plexin dimerizes with that from another Plexin molecule (Wang et al., 2013). Plexin dimer structure shows that the C-terminal portion of JM helices (JM-C) form multiple interactions that are important for Plexin active dimer formation. In the Plexin monomer structure (3IG3), the JM helix is divided into two halves by the kink in the middle (He et al., 2009). The JM-C constitutes several interactions with the GAP domain. Comparing the structures of the inactive monomer with the active dimer structure shows that JM dislodges from GAP domain, straighten to form a continuous helix, and rotate by ~90˚ to dimerize (Pascoe et al., 2015; Wang et al., 2013). (Figure 1-4)

RhoGTPases

The Rho family of small GTPases (RhoGTPases) constitutes part of the Ras superfamily and consists of 20 members, which can be classified into eight groups (Vega and Ridley, 2008). RhoGTPases are well known because of their roles in regulating cytoskeletal rearrangements, cell polarity, cell motility, axon guidance, and vesicle trafficking (Heasman and Ridley, 2008). RhoGTPases are molecular switches since they cycle between an active GTP-bound state and an inactive GDP-bound state. The switch I and II of RhoGTPases adopt

different conformations between these two states (Vetter and Wittinghofer, 2001). In the GTP-bound active conformation, RhoGTPases interact with a variety of effector proteins including actin regulators, kinases, and adaptor proteins through the switch regions, thereby regulating cell behavior. This GTP/GDP cycling is mainly regulated by two types of protein (Bos et al., 2007; Ridley, 2011). Guanine nucleotide exchange factors (GEFs) catalyze the exchange of GDP for GTP, thus activating the GTPase whereas GTPase-activating proteins (GAPs) facilitate the intrinsic GTP hydrolysis rate of the GTPase, thereby inactivating it.

The development of intricate neuronal networks requires a series of steps that begins with migration from its birthplace, initiation of the navigation process dictated by guidance cues, neurite outgrowth, and ultimately forms connections with destined targets, allowing neurons to communicate. RhoGTPases are critical regulators in various aspects of neuronal development, including neurite outgrowth and differentiation, axon pathfinding, and dendritic spine formation and maintenance, as they control the dynamics of the actin cytoskeleton in response to stimuli through various cell surface receptors (Bishop and Hall, 2000; Bokoch, 2003; Luo, 2002; Miki and Takenawa, 2003; Millard et al., 2004; Riento and Ridley, 2003; Toyofuku et al., 2005; Van Aelst and D'Souza-Schorey, 1997; Wennerberg et al., 2003; Zanata et al., 2002).

RhoGTPase regulation of Plexin signaling

The primary sequence of Plexin intracellular region has an insertion segment in between two halves of GAP-homology segments. The insertion segment was shown to bind

RhoGTPases such as Rac1, RND1 and RhoD, and was thus referred to as the RhoGTPase Binding Domain (RBD) (Driessens et al., 2001; Hu et al., 2001; Oinuma et al., 2003; Rohm et al., 2000; Tong et al., 2007; Turner et al., 2004; Vikis et al., 2002; Vikis et al., 2000; Zanata et al., 2002). Crystal structure of Plexin intracellular region showed that RBD forms a ubiquitin-like fold and resides next to GAP domain (He et al., 2009). One side of the RBD forms several interactions with the GAP domain while many hydrophobic residues on the other surface are utilized to pack against the switch II region of RhoGTPases in the GTP-bound active state. A series of studies found that RBD interacts directly with some RhoGTPases in a GTP-dependent manner through yeast two-hybrid and biochemical co-purification (Driessens et al., 2001; Hu et al., 2001; Oinuma et al., 2003; Rohm et al., 2000; Turner et al., 2004; Vikis et al., 2000; Zanata et al., 2002). A later systematic study has shown that the RBD of PlexinB1 binds Rac1, Rac2, Rac3, Rnd1, Rnd2, Rnd3, and RhoD, but not RhoA, Cdc42, RhoG or Rif (Fansa et al., 2013). Among these RhoGTPases, Rnd1 is sufficient to trigger Plexin signaling and initiate COS7 cell collapse even in the absence of Semaphorin. In contrast, RhoD blocks Semaphorin-induced collapse.

RhoGTPase was initially thought downstream the Plexin signaling since binding of RhoGTPases to RBD sequesters them from effectors; however, binding affinity between RhoGTPase to RBD is weaker than those to effectors (Fansa et al., 2013; Hota and Buck, 2009; Tong et al., 2007; Wang et al., 2011). In other words, RBD is unlikely able to compete with effectors for RhoGTPases. A later study found that COS7 collapse induced by a constitutively activated version of Plexin A1 does not require Rac, indicating that Rac acts

upstream of Plexin to regulate the activity of the receptor (Turner et al., 2004). Consistently, another study discovered that active Rac stimulates the localization of Plexin B1 to the cell surface, suggesting an inside-out regulation (Vikis et al., 2002). *In vitro* biochemical study found that addition of Rac or Rnd1 did not increase Plexin GAP activity (Wang et al., 2012). Structural studies of Rac1-bound Plexin suggested that the RBD-bound Rac is far away from the GAP active site and it's unlikely to help Rap binding. Meanwhile, this binding did not induce a significant conformational change of the GAP domain (Bell et al., 2011; Wang et al., 2012) (Figure 1-5). Several lines of evidence suggest that plasma membrane may play an important role in Plexin regulation by RhoGTPases.

FARP1 and FARP2

FARP1 and its close homolog FARP2 are large multi-domain proteins sharing the same domain architectures. FARPs contain a 4.1, ezrin, radixin and moesin (FERM) domain, a Dbl-homology (DH) domain and two pleckstrin homology (PH) domains. Because of harboring the DH domain, which is the GEF domain for RhoGTPases (RhoGEF), FARPs were thought a category of Dbl-family GEF. FARP1 is also known as a chondrocyte-derived ezrin-like protein (CDEP) and pleckstrin homology domain-containing family C member 2 (PLEKHC2) (Koyano et al., 1997); FARP2 is also known as the FERM domain-including RhoGEF (FIR) and the FGD1-related Cdc42-GEF (FRG) (Koyano et al., 1997; Miyamoto et al., 2003). Functional studies of FARP1 and FARP2 have been focused primarily on their roles in regulation of neuronal development and morphology because of their abundant

expression in neurons at the developmental stage and in the adult brain (Kawakita et al., 2003; Koyano et al., 1997; Kubo et al., 2002; Murata et al., 2006).

FARP1 and FARP2 in the regulation of neuronal development

Zhuang et al. showed that FARP1 is necessary and sufficient to promote the dendritic growth of lateral motor column (LMC) (Zhuang et al., 2009). Moreover, their study revealed that FARP1 serves as a specific effector of Semaphorin 6A and Plexin A4 signaling to regulate LMC dendritic growth, and its RhoGEF domain is necessary for this function. More recently, Cheadle et al. identified Farp1 as a novel synapse-organizing molecule through a proteomic analysis (Cheadle and Biederer, 2012). Their study showed that Farp1 promotes the structural dynamics of dendritic filopodia and their stability early in development. In mature neurons, Farp1 regulates the number of spines and is required to promote synapse formation. Notably, FARP1 increases F-actin polymerization in spine heads.

Toyofuku et al. showed that FARP2 associates directly with Plexin A1. Semaphorin 3A binding induces the dissociation of FARP2 from Plexin A1, resulting in activation of FARP2's RacGEF activity. Together with other biochemical results, FARP2 is indicated required for Semaphorin 3A-mediated repulsion of outgrowing axons and suppression of neuronal adhesion (Toyofuku et al., 2005). Recently, FARP2 has also been found to be involved in the Plexin-mediated regulation of bone homeostasis (Hayashi et al., 2012; Takegahara et al., 2010).

Domain architectures and structures of FARP1 and FARP2

FARPs contain the central DH-PH domains, which is the canonical feature of the Dbl-family GEFs for RhoGTPases (Rossman et al., 2005). The N-terminal FERM domain is linked to the DH domain by a ~200-residue flexible linker. The second PH domain (referred to as PH2) is connected to the first PH domain (PH1) by a ~70-residue linker. Previous studies have suggested that FARP1 and FARP2 act on different RhoGTPases. FARP1 has been identified as a RhoAGEF (Koyano et al., 2001), whereas the substrate for FARP2 remains controversial. Some studies suggested that FARP2 is a GEF for Rac1 (Kubo et al., 2002; Toyofuku et al., 2005) whereas others have shown that FARP2 is active towards Cdc42 (Fukuhara et al., 2004; Fukuyama et al., 2005; Miyamoto et al., 2003; Murata et al., 2006).

The DH domain in all the Dbl-family RhoGEFs is the functional unit responsible for catalyzing GTP/GDP exchange, through interacting with the guanine nucleotide-binding switch I and II regions in the RhoGTPase and thereby ejecting the bound guanine nucleotide (Rossman et al., 2005). The PH domain in the conserved DH-PH module of many RhoGEFs regulates GEF activity through interactions with the DH domain and/or the RhoGTPase substrate (Chhatriwala et al., 2007; Derewenda et al., 2004; Kristelly et al., 2004; Lutz et al., 2007; Rossman et al., 2003; Rossman et al., 2002). Extra domains outside of the DH-PH module diverge significantly among the Dbl-family RhoGEFs (Rossman et al., 2005), providing additional diversified mechanisms for regulating the catalytic activity of the DH domain (Ahmad and Lim, 2010; Bielnicki et al., 2011; Chen et al., 2011; Chrencik et al.,

2008; Mitin et al., 2007; Murayama et al., 2007; Rapley et al., 2008; Solski et al., 2004; Yohe et al., 2008; Yohe et al., 2007; Yu et al., 2010; Zheng et al., 2009).

To understand the regulation mechanisms, our laboratory has determined crystal structures of the DH domain and the DH-PH1-PH2 domains of FARP2, and the DH-PH1-PH2 domains of FARP1 (He et al., 2013). The structures reveal a multi-layered auto-inhibition mechanism that involves the C-terminal portion of the last helix in the DH domain, the two PH domains, and two inter-domain linkers (Figure 1-6). This auto-inhibited conformation is distinct from that of other RhoGEFs characterized in previous structural studies.

Puzzle remained for the regulation mechanism of FARP1 and FARP2

Although the structures of DH-PH1-PH2 of FARPs were solved, the regulation mechanism is still puzzling. We could not detect any GEF activity of FARP2 towards any type of RhoGTPases using various auto-inhibition-disrupting mutants of DH-PH1-PH2 *in vitro*. Sequence alignment of the DH domain of FARP1 and FARP2 showed that the catalytic residue for GEF activity is mutated in FARP1. Lack of activity renders the puzzle remained: how FARPs regulate neuronal development. Whether FARPs indeed function as the RhoGEFs or they serve as signaling scaffolds for signal transduction? These intriguing questions need further investigation.

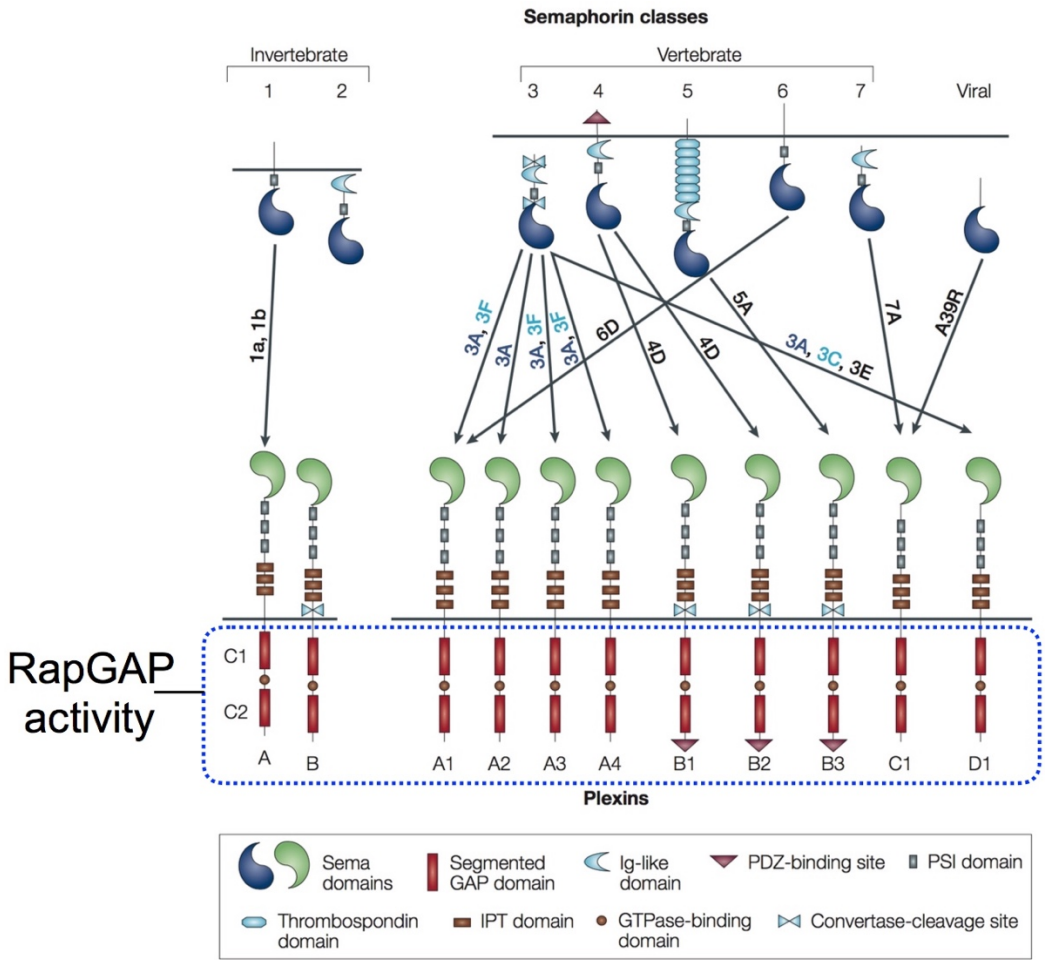

Figure 1-1. Semaphorins and Plexins.

Semaphorins are grouped into eight classes while Plexins are grouped into four classes according to their structural elements and sequence similarity. Domains of each Semaphorin and Plexin are shown. The intracellular region of Plexins is highly conserved among all Plexins; it has RapGAP activity. This figure is modified from (Kruger et al., 2005).

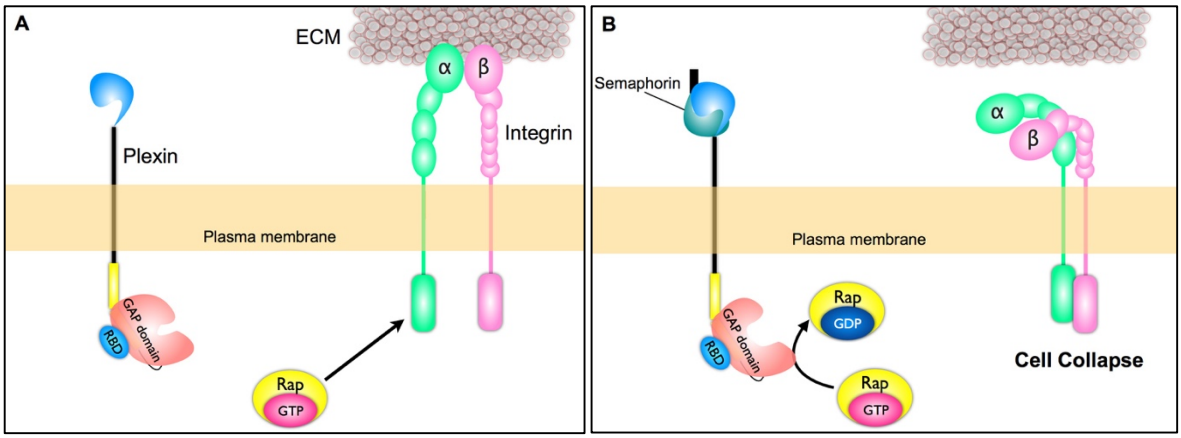

Figure 1-2. Intracellular signaling of Semaphorin-Plexin signaling.

(A) In the absence of Semaphorin, cytoplasmic RapGAP domain of Plexin is inactive. GTP-bound Rap maintain the activation of integrin.

(B) Semaphorin binding to Plexin extracellular domain stimulates the cytoplasmic RapGAP activity. Plexin GAP domain facilitates the GTP hydrolysis of GTP-bound Rap to GDP form. GDP-bound Rap is unable to maintain the adhesion of integrin to extracellular matrix (ECM). Cells shrink and collapse.

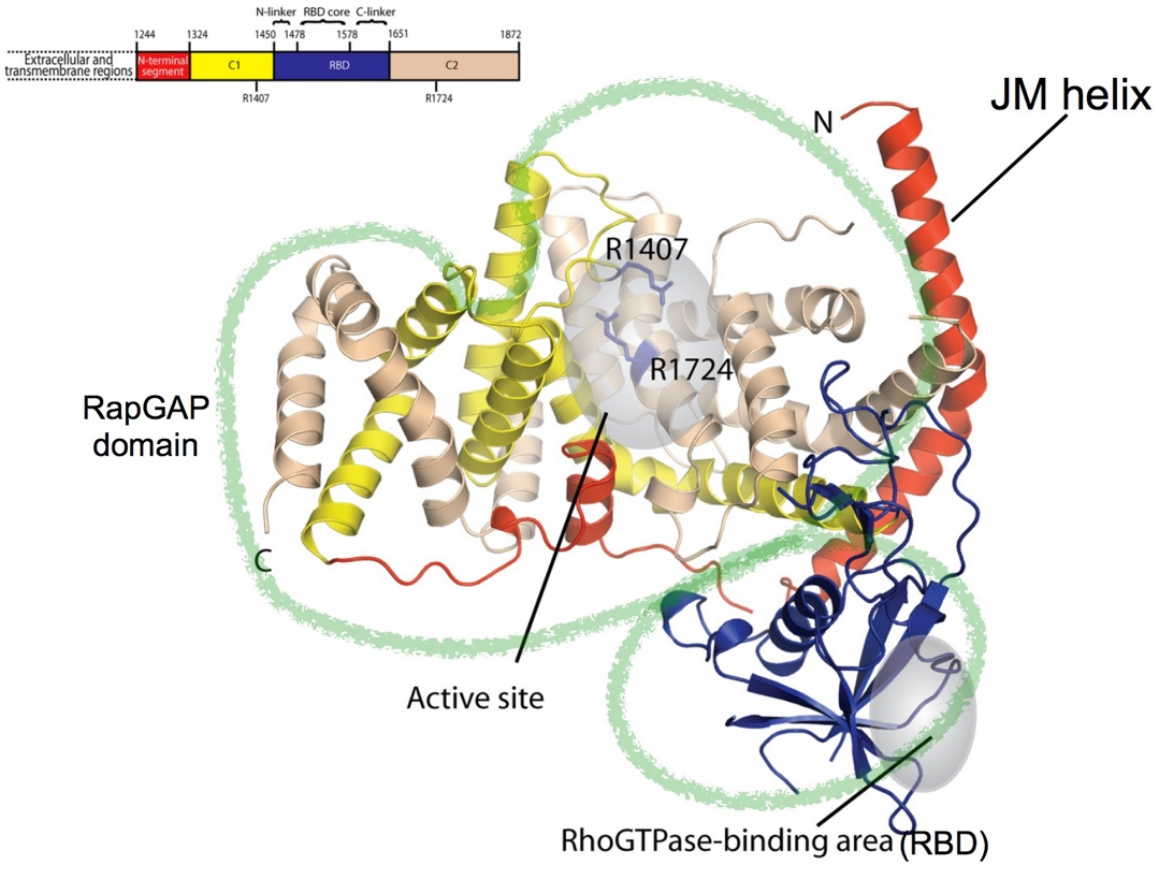

Figure 1-3. The crystal structure of the intracellular region of Plexin.

The intracellular region of Plexin is divided to three portions including the JM helix, the RBD, and the enzymatic RapGAP domain. This figure is modified from (He et al., 2009).

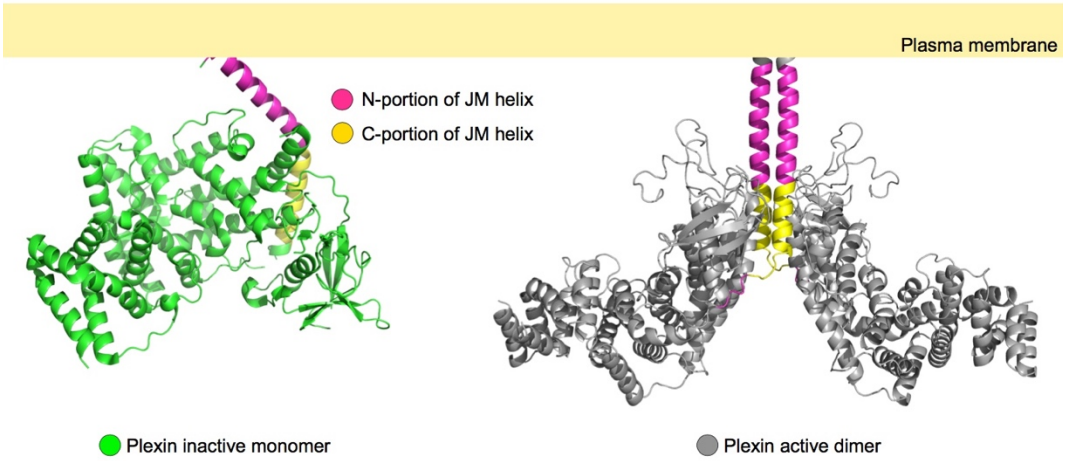

Figure 1-4. Conformational change between Plexin inactive monomer and active dimer. Dimerization of Plexin induces a large-scale conformational change. JM helix attaches to Plexin GAP domain in the inactive monomer state with a kink in the middle while it straightens and rotate to dimerize with the JM helix from another Plexin molecule. The C-terminal portion of JM helix (shown in yellow) is important for the formation of Plexin active dimer.

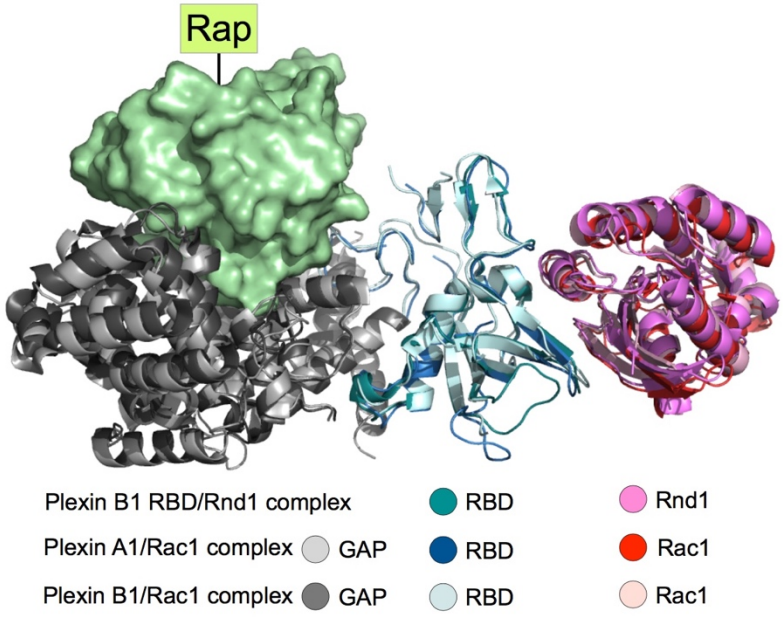

Figure 1-5. Interaction between the RhoGTPases and the Plexin RBD.

The structures of the Plexin A1/Rac1 complex (PDB ID: 3RYT), the Plexin B1/Rac1 complex (PDB ID: 3SUA) and the Plexin B1 RBD/Rnd1 complex (PDB ID: 2REX) are superimposed. Rap is docked based on the structure of the Plexin C1/Rap1B complex (PDB ID: 4M8N) to indicate the active site of the GAP domain. RhoGTPases binding to RBD does not induce significant conformational change of the GAP domain. Moreover, RBD-bound RhoGTPases are far away from the GAP active site.

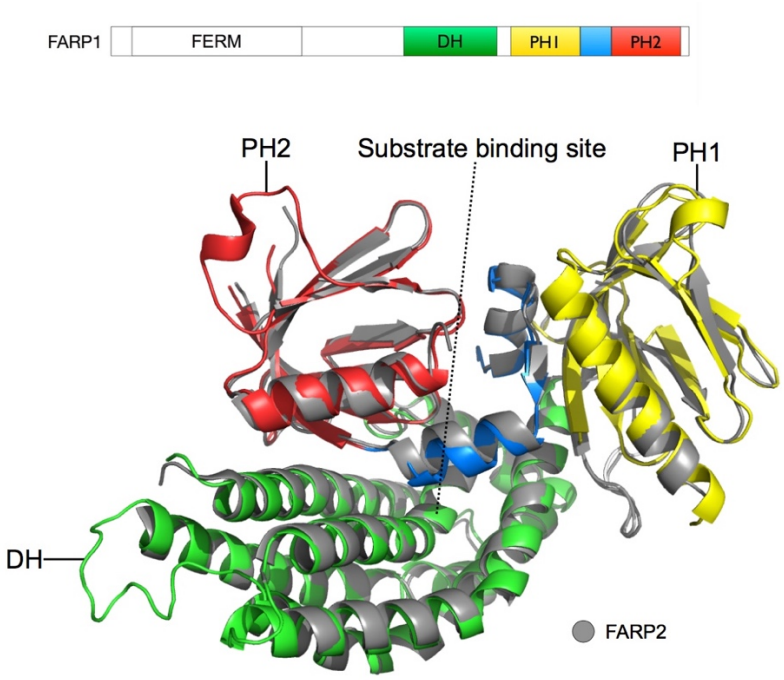

Figure 1-6. The crystal structures of DH-PH1-PH2 domains of FARP1 and FARP2.

The structures of DH-PH1-PH2 domains of both FARP1 and FARP2 adopt auto-inhibited conformation where the C-terminal portion of the last helix in the DH domain, the two PH domains, and two inter-domain linkers (shown in blue) occlude substrate binding.

CHAPTER TWO :

COMPLEX STRUCTURE OF RIF/FARP1 AND ITS IMPLICATION

SIGNALING SCAFFOLD ROLE OF FARP1 THROUGH RIF

Summary

FARP1 is essential for synapse formation and dendrite extension through its potential role as a RhoGTPase GEF. However, the substrate for FARP1 remains elusive. We have solved the crystal structure of the FARP1 DH (Dbl-homology) domain followed by tandem PH (pleckstrin homology) domains (DH-PH1-PH2 hereafter). The DH-PH1-PH2 adopts an auto-inhibition conformation where the substrate binding site is occupied by the second PH domain. To elucidate the substrate for FARP1, we examined the GEF activity of purified wild-type or auto-inhibition disrupting mutants of DH-PH1-PH2 against all types of RhoGTPases. *In vitro* measurement of fluorescent GTP incorporation demonstrates that none of the FARP1 variants showed GEF activity towards any of the RhoGTPases examined. In addition, sequence comparison with other GEFs indicates that the key catalytic residue in the DH domain is replaced in FARP1. These observations prompt us to propose that FARP1 is a pseudo-GEF which functions as a signaling scaffold. Later discovery using an unbiased yeast two-hybrid screen, Harry Mellor's group at the University of Bristol identified that FARP1

interacts with Rif (RhoF), a RhoGTPase promoting actin polymerization and synapse formation. To investigate the regulation between FARP1 and Rif, I determined the crystal structure of DH-PH1-PH2 of FARP1 in complex with Rif. Inspiringly, this complex structure perfectly endorses our signaling scaffold model. Upon binding to Rif, the DH-PH1-PH2 adopts the same auto-inhibitory conformation as the apo-structure. Moreover, this structure uncovers an unforeseen binding mode for RhoGTPases. Unlike other RhoGTPases binding to their effectors through switch I and II, Rif interacts with FARP1 via the insert helix, leaving the switch I and II available. Insert helix is a unique feature of RhoGTPases with unknown function before my study; this structure exemplifies the first case that the insert helix of a RhoGTPase is utilized to interact with an upstream regulator to bridge the extracellular and intracellular signals. Rif is known to induce filopodia formation through binding to the actin polymerization regulator–mDia via switch I and II. Our Rif/FARP1 structure explains how FARP1 promotes dendrite extension and synapse formation: upon stimulation, the Plexin-bound FARP1 recruits Rif via its insert helix, leaving the switch I and II regions of Rif available to interact with mDia to induce actin polymerization.

Introduction

FARP1 and FARP2 were reported essential for Semaphorin-Plexin mediated dendrite extension and axon repulsion respectively (Toyofuku et al., 2005; Zhuang et al., 2009). Harboring the DH domain implied that the function of FARPs is contributed from their GEF activity. The substrate specificity of FARP2 is under debate; some studies suggested Rac1

(Kubo et al., 2002; Toyofuku et al., 2005) while others indicated Cdc42 (Fukuhara et al., 2004; Fukuyama et al., 2005; Miyamoto et al., 2003; Murata et al., 2006) was the substrate for FARP2. Only one report suggested FARP1 was a RhoA GEF (Koyano et al., 2001). Our laboratory solved the crystal structures of the functional domains–DH-PH1-PH2 of FARPs. Both DH-PH1-PH2 of FARP1 and FARP2 exhibit auto-inhibition structures. The PH2 domain together with PH1 and the last helix of the DH domain occluded the substrate-binding site (He et al., 2013). With the structure information, I together with a previous postdoctoral researcher in our laboratory performed an *in vitro* GEF activity to monitor GEF activity of FARP2 after introducing truncations or mutations to the auto-inhibition elements. None of the FARP2 variants showed activity towards Rac1, Cdc42, or RhoA. To test the possibility that FARP2 acts on other RhoGTPases, I also examined GEF activity of FARP2 towards all types of RhoGTPases and detected no activity. We did not measure the *in vitro* GEF for FARP1's DH-PH1-PH2 since sequence alignment of the DH domain of FARPs with other RhoGEFs showed that the critical catalytic residue in FARP1 is mutated. Lack of GEF activity of FARPs made us propose that FARPs execute their functions as signaling scaffolds.

Two years after our structural study of FARPs was published, Harry Mellor's group in the University of Bristol performed a yeast two-hybrid screen and identified that FARP1 but not the close homolog FARP2 interacts with their protein of interest, Rif (RhoF), a RhoGTPase promoting actin polymerization and synapse formation. Their further yeast two-hybrid assay indicated that PH1-PH2 domains are essential for this interaction. The yeast

two-hybrid drew our interest because in the auto-inhibition structure of FARPs, PH1-PH2 especially PH2 blocks the substrate entry. Does binding of Rif release the auto-inhibition of FARP1? How does Rif binding with FARP1 regulate Semaphorin-Plexin signaling? We began to tackle these questions through structural perspective.

Results

GEF activity assay of FARP1 in the presence of Rif

According to the DH-PH1-PH2 structure we published (He et al., 2013), PH2, the linker between PH1-PH2, and the last helix of the DH domain together occlude the substrate-binding site of FARPs. Since the interaction detected in yeast two-hybrid showed that Rif interacts with the PH1-PH2 domains of FARP1, we firstly hypothesized binding of Rif to PH1-PH2 may unwind the autoinhibition structure of DH-PH1-PH2 and activate the GEF activity of FARP1. I employed the *in vitro* assay to examine the GEF activity of purified DH-PH1-PH2 against reported RhoGTPase substrates, Rac1 and RhoA, in the presence of Rif by measuring fluorescent N-methylanthraniloyl-GTP (MANT-GTP) incorporation. DH-PH1-PH2 of FARP1 showed no GEF activity towards these two reported GTPases in the presence of Rif (Figure 2-1).

Crystal structure of Rif in complex with DH-PH1-PH2

To obtain the structural insights how Rif may regulate DH-PH1-PH2, I opted to co-crystallize this protein complex. I expressed and purified DH-PH1-PH2 of FARP1 and Rif,

respectively. Rif was then subjected to exchange the bound nucleotide to non-hydrolysable GTP analog, 5'-Guanylyl imidodiphosphate (GMP-PNP). GMP-PNP exchanged Rif was mixed with DH-PH1-PH2 in 1:1 molar ratio and subjected to crystallization. The crystal structure of Rif bound DH-PH1-PH2 of FARP1 was determined at 2.6 Å. (Table 2-1) (Figure 2-2) In the crystal structure, DH-PH1-PH2 adopts the same autoinhibitory conformation as the apo-structure. The surface formed by this autoinhibitory conformation is utilized to seize Rif. Unlike other GTPases binding to effectors, Rif does not bind DH-PH1-PH2 through the switch I and II region. Instead, the insert helix in the back side of Rif relative to switch regions packs against the linker between two PH domains of DH-PH1-PH2. (Figure 2-2) Bulky residues Val925 and Ile929 in the linker between two PH domains are encompassed by two positive-charged residues Lys139 and Arg146 on the insert helix of Rif, forming the first interface (Figure 2-3). These two bulky hydrophobic residues are only conserved in FARP1. In FARP2, Val925 and Ile929 of FARP1 are replaced by Ala923 and Ala927. This observation is consistent with the finding that Rif only interacts with FARP1 but not FARP2. (Fan et al., 2015) The second interface of the Rif/DH-PH1-PH2 complex is majorly constituted by hydrophobic interactions. Cys700, F710, and Leu717 on the DH domain of DH-PH1-PH2 form a hydrophobic patch to bind the hydrophobic patch formed by Tyr155, Met156, and Leu159 on Rif (Figure 2-4).

Insight from this novel binding mode

Rif employs a novel binding mode to pack against DH-PH1-PH2. The switch regions of Rif are available for interacting with effectors. Rif was shown to induce filopodia formation through promoting actin polymerization via mDia1 and mDia2 (Goh et al., 2011; Pellegrin and Mellor, 2005). The complex structure of Rif bound DH-PH1-PH2 suggests that Rif is still able to interact with the effectors such as mDia1 or mDia2 through the available switch regions. As functional mDia is dimeric, I analyzed the compatibility of mDia dimer with our Rif/DH-PH1-PH2 structure. Superimposition of the structures of mDia1 dimer (PDB ID: 3OBV) with the active RhoC-bound mDia1 (PDB ID: 1Z2C) on the basis of mDia1 revealed how two copies of RhoGTPases interact with GTPase-binding domain (GBD) of the mDia1 dimer. Alignment of our Rif bound DH-PH1-PH2 structure with the above superimposition on the basis of RhoGTPases indicated Rif abound DH-PH1-PH2 structure is compatible with the RhoGTPase bound mDia dimer structure, supporting our FARP1/Rif/mDia three-way complex hypothesis. (Figure 2-5)

Validation of the structure of Rif bound DH-PH1-PH2 using *in vitro* pull-down assay

To validate this novel binding mode seen the crystal structure, we applied Strep-tag pull-down assay. I first examined the first interface. I mutated the two bulky residues Val925 and Ile929 to alanines (V925A/I929A) or arginines (V925R/I929R) in the linker between tandem PH domains. Using Strep-Tactin beads to pull down strep-tagged wild-type Rif, I compared the pull-down amount of wild-type DH-PH1-PH2 with V925A/I929A and V925R/I929R variants. Strep-tagged Rif pulled down the half amount of DH-PH1-PH2

harboring V925A/I929A mutations. DH-PH1-PH2 with V925R/I929R showed little binding to Strep-tagged Rif (Figure 2-6). Pull-down result suggested the first interface is important for constituting this complex. As I mentioned, V925R and I929R are encompassed by two positive-charged residues, Lys139 and Arg146 on the insert helix of Rif. However, when I mutated these two encompassed residues of Rif to alanines, binding of Rif to DH-PH1-PH2 was not affected. Since Arg143 and Lys144 on the insert helix of Rif seemed to interact with negative-charged residues, Glu849 and Asp850 of DH-PH1-PH2, I also mutated Arg143 and Lys144 to glutamates and inspected the interaction. Same as the result of Lys139/Arg146 mutant, binding to DH-PH1-PH2 was not affected even after charge-reversal mutations of Arg143/Lys144 were applied to Rif (Figure 2-6). The flexibility of the insert helix of Rif might account for the unaffected binding between DH-PH1-PH2 and Rif carrying mutations on the insert helix. In order to further validate this complex structure, I opted to examine the second interface using pull-down assay. Tyr155, Met156, and Leu159 of Rif are critical residues responsible for forming the second interface. I applied double mutations including Y155S/L159S and M156S/ L159S to Rif and performed Strep-tag pull-down assay. Neither mutation caused decreased binding of Rif to DH-PH1-PH2. Strangely, Y155S/L159S increased the interaction of Rif and DH-PH1-PH2 obviously (Figure 2-7). I later employed a collection of mutations in the hydrophobic patch of the DH domain which packs against Rif to form the second interface. These mutations include C700Q, C700E, F710A, L717R, and L717S. All these mutations increased the binding of DH-PH1-PH2 with Rif except for F710A (Figure 2-8). To test whether these mutations made the DH-PH1-PH2 stickier, I

checked the binding of these DH-PH1-PH2 variants against the negative control RhoGTPase, Rac1, which showed no interaction with DH-PH1-PH2 in the yeast two-hybrid performed by Mellor's group (Fan et al., 2015). Pull-down results showed that mutations of the DH domain in the second interface made the DH-PH1-PH2 stickier. Rac1 pulled down more DH-PH1-PH2 mutation variants except for F710A (Figure 2-8).

Since mutations of the interface increased the stickiness of the DH-PH1-PH2 protein and might contribute to non-specific binding to mask the real interaction in the pull-down assay, I next worked on decreasing non-specific binding of DH-PH1-PH2. Because both PH domains possess potential phosphoinositide (PtdInsP(s))-binding pockets and unknown electron density is found in the PtdInsP(s)-binding pocket of FARP2's DH-PH1-PH2 structure (He et al., 2013), I suspected the positive-charged pockets in tandem PH domains are the causes for non-specific binding. To shield these positive-charged pockets and mimic PtdInsP(s)-binding, I re-performed the pull-down experiments in phosphate buffer. Indeed, the interaction between wild-type Rif and DH-PH1-PH2 is barely detectable in the presence of phosphate (Figure 2-8). This result made me re-consider the applicability of pull-down assay for detecting the interaction. I decided to employ more sophisticated biophysical binding experiments in phosphate buffer.

Searching for methods to reliably detect the interaction of Rif and DH-PH1-PH2

Isothermal titration calorimetry

The first method that I tried is isothermal titration calorimetry (ITC) which is executed by Dr. Hua Chen with the help of Dr. Chad Brautigam from Macromolecular Biophysics Resource on campus. We reciprocally titrated DH-PH1-PH2 or Rif in the syringe into Rif or DH-PH1-PH2 in the cell, respectively. No interaction was detected between wild-type Rif and wild-type DH-PH1-PH2 in ITC experiments with neither direction of titration (Figure 2-9).

Fluorescence anisotropy

Next, I employed a more sensitive assay, fluorescence anisotropy. I decided not label lysine residues as there are several lysine residues in the first interface deemed required for the interaction. Labeling cysteines may also be an issue since there are four cysteines in the core of Rif responsible for the structural integrity. I opted to introduce a cysteine mutation, E66C to Rif. Glu66 is at the junction of a flexible loop turning to a β-strand and is far away from the interfaces. Besides, E66C seems static enough to detect the change of fluorescence anisotropy. I labeled Rif with Alexa Fluor-488 C_5 maleimide which labels the cysteine residue(s) of Rif. To prevent from labeling the core cysteines, I labeled Rif with Alexa Fluor-488 at 1:1 molar ratio. Despite sacrificing the labeling efficiency (~ 30 %), the Alexa Fluor-488 labeled Rif behaved well in the size exclusion chromatography. I titrated different concentrations of DH-PH1-PH2 to Alexa Fluor-488 labeled Rif and measured the fluorescence anisotropy in the fluorometer (Horiba, PTI QuantaMater 8000) with the help of Rashmi Voleti from Dr. Rizo-Rey's laboratory. Wild-type DH-PH1-PH2 caused an apparent

change in fluorescence anisotropy of Rif and bovine serum albumin (BSA) only resulted in little difference. I then went on to expressed and purified DH-PH1-PH2 mutant with V925R/I929R and performed the anisotropy experiment. However, V925R/I929R caused the similar extent of anisotropy change as the wild type. (Figure 2-10) We are not confident whether the anisotropy change of Rif resulted from DH-PH1-PH2 addition reflects the binding or not. The fact that V925R/I929R variant resulted in the anisotropy change indistinguishable from that of wild-type DH-PH1-PH2 suggested this method might not be a good choice.

Microscale thermophoresis

Taking advantage of the same Alexa Fluor-488 labeled Rif in the above section, microscale thermophoresis (MST, NanoTemper) was exploited to measure the interaction of Rif and DH-PH1-PH2 with the help of Dr. Chad Brautigam from Macromolecular Biophysics Resource on campus. Unfortunately, I could not detect the interaction between wild-type Rif and wild-type DH-PH1-PH2 through MST measurement (Figure 2-11).

Lipid-vesicle based FRET assay

In cells, both full-length FARP1 and Rif are localized on the plasma membrane. Since we could not detect any interaction between them in solution, it is reasonable to consider whether membrane environment can boost the interaction by simply increasing the local concentrations of both Rif and DH-PH1-PH2. For anchoring both Rif and DH-PH1-PH2 on

the membrane, I adopted a system utilizing Nickel-NTA (Ni-NTA) containing lipid vesicles (Zhang et al., 2006). Since there is no enzymatic activity I can rely on as my readout, I decided to apply a fluorescence resonance energy transfer (FRET) system to capture the interaction between Rif and DH-PH1-PH2. I fused enhanced cyan fluorescence protein (ECFP) to the C-terminus of His_6-tagged DH-PH1-PH2 and purified this His_6-DH-PH1-PH2–ECFP fusion. Also, I expressed and purified His_6-tagged Rif E66C and labeled it with Alexa Fluor-594 C_5 maleimide. I then made 5 % Ni-NTA containing lipid vesicles. By applying His_6-Rif and His_6-DH-PH1-PH2–ECFP with concentrations way above the Kd (dissociation constant) of His_6-tag to Nickel, both His_6-Rif and His_6-DH-PH1-PH2–ECFP were assumed attached to the Ni-NTA lipid on the lipid vesicles. Here, His_6-DH-PH1-PH2–ECFP served as the donor and His_6-Rif-Alexa Fluor-594 was the acceptor. If interaction happened, the donor emission would be quenched by the acceptor. We could examine the interaction by recording the donor quenching. With the increasing amount of acceptor titrated into the reaction, more donor quenching would be measured if there was an interaction between donor and acceptor as described in the study (Kadamur and Ross, 2016). With the addition of the highest concentration of acceptor, His_6-Rif-Alexa Fluor-594, the donor quenching efficiency was only about 10 % while mutation of K139E/R146E on the insert helix of Rif showed a similar effect. (Figure 2-12) Therefore, I concluded that lipid vesicle-based FRET did not detect the interaction of Rif and DH-PH1-PH2.

Cell-based confocal microscopy

Since the above *in vitro* binding assays failed to detect the interaction between Rif and DH-PH1-PH2 neither in solution nor on the membrane, I suspected that there might be some cellular factors necessary for this interaction. To bypass the unknown cellular factors and catch the binding of Rif and DH-PH1-PH2, I employed confocal microscopy imaging to observe the co-localization of these two proteins in cells with the help of Dr. Yu-Ju Chen from Dr. Jen Liou's laboratory. I transfected full-length Rif and DH-PH1-PH2 to HeLa cells and did immunofluorescence using antibodies against FLAG tag and HA tag of DH-PH1-PH2 and Rif, respectively. Rif localized on the plasma membrane because of the C-terminal lipid modification whereas DH-PH1-PH2 localized in the cytosol. I attempted to inspect whether membrane-localized Rif recruits cytosolic DH-PH1-PH2 to the cell membrane. Confocal images showed that Rif could not promote membrane localization of DH-PH1-PH2 (Figure 2-13).

Missing components required for forming the Rif/DH-PH1-PH2 complex

Since no interaction was detected using above methodologies, I started thinking whether something was missing in the crystal structure. Previous studies reported some cases where flexible regions in some proteins contribute to binding affinity to promote their interaction with binding partners (Korennykh et al., 2009; Shang et al., 2017). Moreover, the C-terminus of DH-PH1-PH2 is very close to the insert helix of Rif in the complex structure. Besides, sequence alignment of FARP1 from a variety of species showed that flexible residues at the C-terminus are fairly conserved (Figure 2-14). I hence hypothesized that the

last twelve residues of DH-PH1-PH2 excluding from the crystallization construct might be crucial for the complex formation. I expressed and purified the DH-PH1-PH2 harboring the last twelve residues (DH-PH1-PH2$_{tail}$). DH-PH1-PH2$_{tail}$ did not display stronger binding to Rif compared to tail-less DH-PH1-PH2 in the strep-tagged pull down and MST measurement (Figure 2-14). To see whether this twelve-residue flexible tail made any contact with Rif, I grew crystals of Rif with DH-PH1-PH2$_{tail}$ according to the condition growing the Rif/DH-PH1-PH2 crystals. I solved the crystal structure of Rif bound DH-PH1-PH2$_{tail.}$ The structure represented the same binding mode as that of Rif bound DH-PH1-PH2. No density was observed for the twelve residues in the C-terminus of DH-PH1-PH2. (data not shown)

Yeast two-hybrid assay

Since all above methods failed to detect the interaction between wild-type Rif and DH-PH1-PH2, I decided to employ the yeast two-hybrid method utilized in the original publication identifying the interaction of Rif and DH-PH1-PH2 (Fan et al., 2015). According to the designs in this study, I fused the Rif with the DNA-binding domain (DNA-BD; bait) and DH-PH1-PH2 with the activation domain (AD; prey). After transforming these two plasmids to the reporter yeast strain, Y2HGold, the interaction will be selected based on the histidine production. If bait protein interacts with prey protein, the HIS3 reporter gene will be transcribed and produced, and then the yeast can grow on the histidine-deficient plate. I also added the competitive inhibitor of HIS3 gene, 3-Amino-1,2,4-triazole (3-AT) to select for interaction stronger than a certain threshold.

As Fan et al. mentioned in the report (Fan et al., 2015), DH-PH1-PH2 did not show interaction with Rif; only co-transformant of PH1-PH2 with Rif had colonies survived on the selection plate. Indeed, I observed similar results. (Figure 2-15) This yeast two-hybrid result did not agree with our Rif/DH-PH1-PH2 structure as DH provides the hydrophobic patch for constituting the second interface in the crystal structure. To examine whether both DH-PH1-PH2 and PH1-PH2 were expressed in Y2HGold, I checked the protein expression by western blotting using antibodies against HA-tag built in the activation domain vector. Both DH-PH1-PH2 and PH1-PH2 were expressed in Y2HGold. It is worth noting that expression of PH1-PH2 was much lower than that of DH-PH1-PH2, presumably due to degradation.

The interaction of PH1-PH2 with Rif was specific since PH1-PH2 did not bind the control RhoGTPase, Rac1. To examine whether our complex structure is still valid to a certain extent, I introduced V925R/I929R mutation to the linker of PH1-PH2 and performed yeast two-hybrid against Rif. PH1-PH2 with V925R/I929R showed significantly weaker binding to Rif, suggesting that the linker of PH1-PH2 contributed to the binding. However, mutation of the corresponding residues on the insert helix of Rif did not affect binding in the yeast two-hybrid assay. (Figure 2-15).

The undetectable interaction of Rif with DH-PH1-PH2 in yeast two-hybrid experiment could be due to two reasons. First, DH domain sterically hinders the interface for Rif; PH1-PH2 needs to dislodge from the DH domain as a whole in order to seize Rif. (See Discussion section "*Expression of PH1-PH2*" below). The second possibility is that the current fusion designs resulted in the unfavorable geometry for DH-PH1-PH2 to interact with

Rif. To test this hypothesis, I swapped the DH-PH1-PH2 and PH1-PH2 to DNA-BD and Rif to AD. Surprisingly, neither DH-PH1-PH2 nor PH1-PH2 was able to bind Rif after swapping (Figure 2-15).

Discussion

Expression of PH1-PH2

Yeast two-hybrid assays suggested that crystal structure of the Rif/DH-PH1-PH2 complex might be a snapshot of the priming state. In cells, PH1-PH2 may need to be released from the DH domain to grab Rif after receiving specific stimuli. Based on this hypothesis, I attempted to crystallize and solve the structure of Rif-bound PH1-PH2. I firstly expressed and purified the His_6-tagged PH1-PH2 and SUMO-tagged PH1-PH2, respectively. Both constructs had extremely low yield and severe degradation issue. Poor expression results prompted me to try the co-expression system. I co-expressed PH1-PH2 either with Rif or DH domain. Unfortunately, neither of them improved PH1-PH2 expression in terms of yield and degradation.

As previously mentioned, PH1-PH2 might be dislodged from the DH domain under some cellular stimuli. Post-translational modification such as phosphorylation might account for this type of conformational change event. Since DH-PH1-PH2 is the only protein I could obtain, I decided to work on the idea to dislodge PH1-PH2 from the DH. I observed that Tyr675 in a loop region of the DH domain positioned its side chain into a hydrophobic pocket formed between DH and PH2 domains. I then opted to mutate this tyrosine residue to

either alanine (Y675A) or glutamate (Y675E) and tested their binding to Rif in pull-down and yeast two-hybrid assays. In pull-down assay, both Y675A and Y675E showed similar binding to Rif as compared to wild-type DH-PH1-PH2. In yeast two-hybrid assay, neither Tyr675Ala or Tyr675Glu made DH-PH1-PH2 capable of interacting with Rif. (data not shown)

Possible missing components for binding

Failed expression of PH1-PH2 in bacteria and remarkably low expression in yeast implied that PH1-PH2 might not exist stably in cells. In other words, PH1-PH2 dislodging from the DH domain could only be transient. As I previously mentioned, both PH domains of DH-PH1-PH2 harbor potential PtdInsP(s)-binding pockets. In the apo-structure of the DH-PH1-PH2 of FARP2, strong difference density appeared at the potential PtdInsP(s) binding site in PH1, suggesting binding of a particular small molecule compound. Previous attempts at determining the identity of the compound by mass spectrometry failed. In cells, the tandem PH domains may bind to specific PtdInsP(s), leading to a slight rotation of the PH1-PH2 relative to the DH domain. Our future direction is to identify potential PtdInsP(s) that can bind DH-PH1-PH2 and investigate whether the interaction between Rif and DH-PH1-PH2 is enhanced in the presence of that PtdInsP(s).

The increased binding of DH-PH1-PH2 to Rif after mutations introduced to the second interface may not be entirely due to non-specific binding. Instead, this observation may imply that both interfaces are sub-optimal. Mutation of an interface made the other

interface easier to access and bind. It will be interesting to solve the structure of the Rif-bound DH-PH1-PH2 harboring the mutation that enhanced the binding.

Materials and Methods

Site Directed QuikChange mutagenesis

The primers are designed according to the QuikChange manual (Stratagene). The PCR is done with Phusion DNA polymerase in the thermocycler in 25 μL volume. After PCR, add 1 μL DpnI to digest template DNA at 37°C for 1~2 hours. Transform 5 μL to DH5α cells. Inoculate colonies to liquid culture. Extract plasmids and send sequencing to obtain the mutated variants.

Protein Expression and Purification

Expression and purification of DH-PH1-PH2 of human FARP1

The coding regions of DH-PH1-PH2 domains (residues 538–1034) of human FARP1 was cloned into a modified pET-28(a) vector (Novagen) that encodes an N-terminal His_6-tag followed by a recognition site for human rhinovirus 3C protease (referred as pSKB2 herein). Point mutations were introduced by QuikChange reactions (Stratagene). The plasmids were transformed into the *E. coli* strain BL21 (DE3). BL21 (DE3) carrying individual expression plasmid was cultured at 37°C to reach OD_{600}=2.0 in TB. Protein expression was induced by 0.2 mM IPTG at 16°C overnight.

After centrifugation, the bacteria cells were resuspended in the lysis buffer containing 10 mM Tris (pH 8.0), 500 mM NaCl, 5 % glycerol (v/v), 20 mM Imidazole, and 3 mM β-mercaptoethanol. The bacteria resuspension was passed through the cell disruptor (Avestin) for 3~4 times on ice, and then the lysates were subjected to centrifugation. The supernatant was then filtered by 0.45 μM PVDF membrane to get rid of debris. The proteins were purified using a 1 mL HisTrap column (GE Healthcare) and treated with recombinant human rhinovirus 3C protease at 4°C overnight to remove the N-terminal tag.

The protein was further purified by using Resource Q (GE Healthcare) anion-exchange chromatography with a 10 mM to 500 mM NaCl gradient elution. Fractions were examined by SDS-PAGE electrophoresis and Coomassie blue staining. Fractions containing DH-PH1-PH2 were pooled together and subjected to Superdex 200 HiLoad 16/60 (GE Healthcare) to remove ~70 kD impurity. The size exclusion chromatography was equilibrated with the buffer containing 20 mM Tris (pH 8.0), 150 mM NaCl, 10 % glycerol (v/v), and 2 mM DTT. Fractions were examined by SDS-PAGE electrophoresis and Coomassie blue staining. Fractions containing pure proteins were pooled together, concentrated, and stored at −80°C.

Expression and purification of human Rif

The coding regions of human Rif (residues 12–194) was cloned into pSKB2 vector. Point mutations were introduced by QuikChange reactions. The plasmids were transformed into the *E. coli* strain BL21 (DE3). BL21 (DE3) carrying individual expression plasmid was

cultured at 37°C to reach OD_{600}=2.0 in TB. Protein expression was induced by 0.2 mM IPTG at 16°C overnight.

After centrifugation, the bacteria cells were resuspended in the lysis buffer containing 10 mM Tris (pH 8.0), 500 mM NaCl, 5 % glycerol (v/v), 20 mM Imidazole, 2 mM $MgCl_2$, and 3 mM β-mercaptoethanol. The bacteria resuspension was passed through the cell disruptor for 3~4 times on ice, and then the lysates were subjected to centrifugation. The supernatant was then filtered by 0.45 μM PVDF membrane to get rid of debris. The proteins were passed through a 1 mL HisTrap column and washed with 3 column-volume (CV) Ni-A buffer containing $MgCl_2$. The recombinant human rhinovirus 3C protease was diluted in 1 mL $MgCl_2$-containg Ni-A buffer and injected to this 1 mL HisTrap column and incubated at 4°C overnight. One day after, the digested Rif protein was washed off from the HisTrap column using $MgCl_2$-containg Ni-A. Since Rif seemed sensitive to high concentration of imidazole thus I did in-column digestion instead of direct elution using Ni-B buffer.

The protein was further passed though the Resource Q anion-exchange chromatography. Rif protein did not bind Resource Q and was in the flow-through. The flow-through was concentrated using the Amicon centrifugal filters with 3 kD cutoff. Concentrated Rif was subjected to Superdex 200 HR 10/30 (GE Healthcare) equilibrated with the buffer containing 20 mM Tris (pH 8.0), 250 mM NaCl, 10 % glycerol (v/v), 2 mM $MgCl_2$, and 2 mM DTT to exchange buffer. Purified proteins were concentrated and stored at −80°C.

Exchange of GMP-PNP or GTP to Rif protein

5 mg Rif protein was incubated with ~ 20-fold molar concentration of GMP-PNP (for crystallization) or GTP (for binding assay) in the exchange buffer containing 20 mM Tris (pH 8.0), 250 mM NaCl, 5 % Glycerol (v/v), 7.5 mM EDTA, and 1 mM DTT at RT for 2 hr. After 2 hr incubation, 20 mM $MgCl_2$ was added to stop exchange reaction. The protein was then subjected to Superdex 75 GL 10/30 (GE Healthcare) equilibrated with the buffer containing 20 mM Tris (pH 8.0), 250 mM NaCl, 10 % glycerol (v/v), 2 mM $MgCl_2$, and 2 mM DTT to remove excessive GMP-PNP or GTP.

Crystallization and Structure Determination of Rif in complex with DH-PH1-PH2 of FARP1

The Rif protein was purified and exchanged with non-hydrolysable GTP analogue, GMP-PNP (detailed procedure described in "*Exchange of GMP-PNP or GTP to Rif protein*"). The total protein concentration for crystallization was 8.5 mg/mL. DH-PH1-PH2 of FARP1 and Rif were mixed at 1:1 molar ratio thus the concentration of DH-PH1-PH2 domains of FARP1 was 6.4 mg/mL and that of GMP-PNP-exchanged Rif was 2.1 mg/mL. The two proteins were mixed in the buffer containing 10 mM Tris (pH=8.0), 150 mM NaCl, 10 % Glycerol (v/v), 2 mM $MgCl_2$, 2 mM TCEP, and 100 μM GMP-PNP. The protein mixture was subjected to crystallization trials. The complex crystals crystallized initially at 20 °C in 0.2 M $(NH_4)_2SO_4$ and 30 % PEG8000 (w/v) in sitting-drop 96-well plates. Larger crystals were grown by sitting-drop vapor diffusion or hanging drop vapor diffusion at 20°C in 0.1 M $(NH_4)_2SO_4$, 24 % PEG8000 (w/v), and 100 mM MMT (containing DL-malic acid,

MES, and Tris base at the 1:2:2 molar ratio and adjusted to pH 6.2). The crystals were only reproduced and grown at the 2:1 volume ratio of protein to crystallization solution. Crystals were cryo-protected using the crystallization solution supplemented with 30 % glycerol and flash cooled in liquid nitrogen. Diffraction data were collected at −173°C on beamline 19ID at the Advanced Photon Source (Argonne National Laboratory). Data were indexed, integrated and scaled by using HKL2000 (Otwinowski and Minor, 1997). A 2.6 Å dataset in the $P2_12_12_1$ space group was collected and then converted to the mtz format by using the Reflection file editor module in the Phenix package (Adams et al., 2002; McCoy et al., 2007). The structure of DH-PH1-PH2 of FARP1 (PDB ID: 4H6Y) and Rac1 (PDB ID: 3RYT, chain C) were used as the molecular replacement search model using the Phaser module in the Phenix package.

Iterative model building and structure refinement were performed by using the programs Coot and Phenix, respectively (Adams et al., 2002; Emsley and Cowtan, 2004). Detailed statistics of data collection and refinement are listed in Table XX. Molecular structure figures were rendered by the program Pymol (the PyMOL Molecular Graphics System, Schrödinger). Sequences were aligned by using MAFFT (Katoh et al., 2017) and rendered with ESPript (Gouet et al., 1999).

In Vitro GEF Activity Assay

The *in vitro* GEF assays were based on (Eberth and Ahmadian, 2009). 1 μM DH-PH1-PH2 of FARP1 was pre-incubated with 1 μM GTP-loaded Rif at 25 °C for 5 min. The

GEF activity buffer contains 50 mM HEPES (pH 7.5), 100 mM NaCl, 5 % Glycerol (v/v), 5 mM $MgCl_2$, and 2 mM DTT. 5 μM Rac1 or RhoA was added into 6 μM N-methylanthraniloyl-GTP (mant-GTP) in the GEF activity buffer. The pre-incubated mixture of DH-PH1-PH2 and Rif was then added into the solution containing RhoGTPase and mant-GTP. The increase of the fluorescence signal at 440 nm with 360 nm excitation upon mant-GTP binding to the GTPases was monitored by a Fluorolog-3 spectrofluorometer at 25°C.

Strep pull-down assay

20 μg of Strep-tagged Rif and its mutants were pull downed by 30 μL (50 %) Strep-Tactin resins (IBA) in the Strep-binding buffer containing 20 mM HEPES (pH=7.5), 150 mM NaCl, 5 % Glycerol (v/v), 2 mM $MgCl_2$, 0.5 % NP-40 (v/v), 10 μM GTP, and 2 mM DTT. Wild-type DH-PH1-PH2 and mutants were incubated with Strep-Rif at 3:1 molar ratio at 4°C for 1 hr on the end-over-end rotator. The Strep-Tactin resins were then spin down and washed with 1 mL Strep-binding buffer for 3 times. Each wash was incubated at 4°C for 5 min on the end-over-end rotator. The buffer was removed after the last wash and 2X SDS sample buffer was added to beads. The sample was heated at 95°C for 5 min, and half of the supernatant was loaded for SDS gel electrophoresis. The gel was stained by Coomassie blue and then destained to reveal the results.

FLAG pull-down assay

20 μg of FLAG-tagged Rif and its mutants were pull downed by 20 μL (50 %) anti-FLAG M2 affinity gel (Sigma) in the FLAG-binding buffer containing 20 mM HEPES (pH=7.5), 150 mM NaCl, 5 % Glycerol (v/v), 2 mM $MgCl_2$, 0.5 % NP-40 (v/v), 10 μM GTP. Wild-type DH-PH1-PH2 and mutants were incubated with FLAG-Rif at 3:1 molar ratio at 4°C for 1 hr on the end-over-end rotator. The anti-FLAG M2 affinity gel was then spin down and washed with 1 mL FLAG-binding buffer for 3 times. Each wash was incubated at 4°C for 5 min on the end-over-end rotator. The following procedures were the same as that described in the previous section "*Strep pull-down assay*".

Labeling of Rif for fluorescence anisotropy, MST, and FRET experiments

Prior to labeling, purified Rif with Glu66Cys was exchanged with buffer containing 1 mM TCEP. Rif protein with Glu66Cys mutation was then incubated with Alexa Fluor 488 C_5 Maleimide or Alexa Fluor 594 C_5 Maleimide (Invitrogen) at 1:1 molar ratio in the buffer containing 20 mM Tris (pH 8.0), 250 mM NaCl, 10% glycerol (v/v), 2 mM $MgCl_2$, 1 mM TCEP, and GTP at the same molar concentration as protein at room temperature in dark for 2 hr. Labeled Rif was then subjected to Superdex 200 GL 10/30 (GE Healthcare) equilibrated with the buffer containing 20 mM Tris (pH 8.0), 250 mM NaCl, 10% glycerol (v/v), 2 mM $MgCl_2$, 1 mM TCEP, and 100 μM GTP. This size exclusion chromatography could help remove the aggregated protein and check the protein quality after labeling. Fractions containing labeled Rif was pooled together and concentrated and stored at −80°C.

The concentration of the labeled Rif and the labeling efficiency were measured and calculated as described below. Here I took the Alexa 488 Fluor-labeled Rif as the example. Basically, measure the absorbance at wavelength 280 nm (A_{280}) and 494 nm (A_{494}) of labeled Rif. Fluorophore concentration was obtained through dividing the A_{494} read by the extinction coefficient (ε) of Alexa Fluor 488 dye at 494 nm (Can find it in Invitrogen manual). A_{280} is constituted of absorbance of protein and fluorophore at wavelength 280 nm. The extinction coefficient (ε) of Alexa Fluor 488 dye at 280 nm could be calibrated by the correction factor (Can find it in Invitrogen manual). A_{280} contributed from Alexa Fluor 488 dye can be calculated through multiplying the fluorophore concentration by the extinction coefficient of Alexa Fluor 488 dye at 280 nm. Now the A_{280} contributed by the protein can be derived from subtracting A_{280} of Alexa Fluor 488 from A_{280} read. Protein concentration can be obtained through dividing A_{280} of protein by its extinction coefficient. Now the labeling efficiency can be calculated via dividing the fluorophore concentration by protein concentration.

Isothermal titration calorimetry (ITC)

All ITC experiments were conducted using a MicroCal ITC200 instrument (GE Healthcare). Purified and concentrated proteins (DH-PH1-PH2 and Rif) were dialyzed overnight at 4°C against 1 L of buffer containing 10 mM Tris (pH 8.0), 150 mM NaCl, 10% glycerol (v/v), 2 mM $MgCl_2$, and 1 mM TCEP. All proteins were thoroughly degassed before titration. DH-PH1-PH2 proteins (500 μM) were placed in the syringe, and Rif proteins (50 μM) were placed in the cell. Reciprocally, titrations of Rif into DH-PH1-PH2 were also

carried out by using 300 and 30 μM protein solutions, respectively. The DH-PH1-PH2 was titrated into the cell over the course of 18 injections of 2 μL. All titrations were conducted at 20 °C with continuous stirring at 1,000 rpm and 2-min intervals between injections. Data were integrated by using NITPIC (Keller et al., 2012).

Microscale thermophoresis (MST)

The interaction of Rif and DH-PH1-PH2 was also examined by changes in the thermophoretic movement of Rif- labeled with Alexa Fluor 488 C_5 Maleimide (Lableing procedure was described in "*Labeling of Rif for fluorescence anisotropy, MST, and FRET experiments*") by means of the microscale thermophoresis binding assay (NanoTemper Technologies) (Wienken et al., 2010). For all thermophoretic experiments, Premium treated capillary tubes were used (NanoTemper, LLC). All data sets were collected at ambient temperature. For the study of the interaction between DH-PH1-PH2 and Alexa Fluor 488-labeled Rif, usually a concentration series of DH-PH1-PH2 was prepared using a 1:1 serial dilution of the protein into MST-binding buffer containing 10 mM $NaHPO_4$ (pH=7.5), 150 NaCl, 5% Glycerol (v/v), 2 mM $MgCl_2$, 3 μM GTP, and 0.1 % Tween 20 (v/v), with the top concentration of DH-PH1-PH2 equals 965 μM; sixteen 10-μL samples were thus prepared ranging in concentration from 965 μM to 29.5 nM. The association was initiated by the addition of an equal volume of 400 nM labeled Rif in the MST-binding buffer without Tween 20 to each reaction mixture, resulting in a final concentration of labeled Rif of 200 nM and also halving all of the DH-PH1-PH2 concentrations. The mixtures were incubated in

the dark at room temperature for 20 min before being loaded into capillary tubes and inserted into the apparatus (NanoTemper Monolith.NT115 in this study) for data acquisition. The LED power was set to 20 %, and the MST power was 20 %, 40 %, and 60 %. The pre-MST period was 5 s, the MST-acquisition period was 60 s, and the post-MST period was 5 s. All the MST raw data was passed to PALMIST (Scheuermann et al., 2016) for fitting and global analysis.

Fluorescence anisotropy

The fluorescence anisotropy (FA) assays were performed on a PTI (Photon Technologies International) fluorimeter equipped with automated polarizers (Horiba, PTI QuantaMater 8000 in this study) at 25 °C. Rif was labeled by Alexa Fluor 488 C_5 Maleimide (See "*Labeling of Rif for fluorescence anisotropy, MST, and FRET experiments*"). Titrations were conducted by monitoring FA as a function of increasing amounts of proteins added to 50 nM Alexa 488-labeled Rif in buffer containing 10 mM $NaHPO_4$ (pH=7.5), 150 NaCl, 5% Glycerol (v/v), 2 mM $MgCl_2$, 3 μM GTP, 1 mM TCEP, and 1 μM Bovine Serum Albumin (BSA). When DH-PH1-PH2 was limited, the highest concentration of DH-PH1-PH2 was mixed with 50 nM Alexa 488-labeled Rif in the above buffer and the FA was measured. After the first FA was measured, the DH-PH1-PH2 was diluted to half through mixing the first mixture with equal volume of 50 nM Alexa 488-labeled Rif in buffer. Similar procedures were repeated several times to obtain enough data points to fit. FA was calculated according to this equation, $FA = (F_{//} - F_{\perp})/(F_{//} + 2F_{\perp})$, where $F_{//}$ = fluorescence intensity

parallel to the excitation plane; $F_{\perp}$ = fluorescence intensity perpendicular to the excitation plane. The dissociation constants (K_d) were determined by fitting the titration curves to the equation, $F = F_0 + (F_\infty - F_0)*(x/(K_d + x)$, where x is the protein concentration at each measurement point, F is the observed FP value at the given protein concentration, F_0 is the FP value of Alexa 488-Rif alone, and F_∞ is the maximal FP value saturated with protein.

Fluorescence resonance energy transfer with lipid vesicle

Equilibrium fluorescence measurements were performed on a Fluorolog-3 spectrofluorometer (Horiba Jobin Yvon) using a 3 mm cuvette with both excitation and emission slits set at 1 nm (depending on the donor signal). FRET assay buffer contains 20 mM HEPES, 150 mM NaCl, 5 % Glycerol (v/v), and 5 mM $MgCl_2$. Large unilamellar vesicles were added to FRET buffer to make the final concentration 12.5 μM. Protein concentration in the reaction must be way above the Kd of His_6 to Ni-NTA so that all donors and acceptors are on the lipid vesicles. Here, 1 μM His_6-tagged DH-PH1-PH2-CFP was added in the reaction. After incubated at 25°C for 10 min, fluorescence was recorded between 450 nm and 650 nm with excitation at 432 nm. 1 μM, 2 μM, 4 μM, and 8 μM of Alexa 594-labeled His_6-tagged Rif was gradually added to the cuvette. After adding each concentration of acceptor, the mixture was incubated at 25 °C for 10 min, fluorescence was then recorded for each concentration of acceptor. FRET was measured as the decrease of DH-PH1-PH2-CFP fluorescence at 475 nm in the presence of various concentration of Alexa594-labeled Rif. Two factors were calibrated during FRET efficiency calculation. The

volume change was corrected since a serial concentration of Alexa594-labeled Rif was titrated into the same cuvette. The difference of Alexa Fluor 594 labeling efficiency for wild-type Rif and mutant Rif was calibrated as well.

Lipid vesicle preparation

DOPC and DOGS-NTA-Ni lipids in chloroform (Avanti Polar Lipids, Inc) were mixed at 95 % to 5 % ratio in a glass tube. A lipid film was formed upon removing chloroform under a stream of nitrogen gas, followed by putting the tube under vacuum for at least 1 hr. FRET assay buffer was added to rehydrate the lipid film and incubated for at least 1 hr. Intermittent vigorous vortexing during the incubation was applied to convert the lipid film into large, multilamellar vesicles. These mutilamellar vesicles were then forced through a polycarbonate filter (pore size: 200 nm) 21–41 times using a mini-extruder (Avanti Polar Lipids, Inc) to yield homogenous large unilamellar vesicles.

Yeast two hybrid

Human Rif-QL (residue 1-207 with Gln77Leu mutation) cDNA was cloned into pGBKT7 (Clontech). Human FARP1 DH-PH1-PH2 (residue 538-1045) and PH1-PH2 (residue 735-1045) cDNA were cloned into pGADT7 (Clontech). Point mutations were introduced by QuikChange reactions. The detailed procedures of yeast two hybrid was performed according to the manufacturer's instructions (Clontech). Basically, Co-transform pGBKT7 Rif-QL with pGADT7 DH-PH1-PH2 or PH1-PH2 of FARP1 to Y2HGold yeast

strain (Clontech) and plate the transformants on –Trp-Leu SCD plate to select the yeast cells carrying both plasmids. After the colonies were grown, a colony was picked up to –Trp-Leu liquid SCD culture overnight. The culture was then spotted on three different SCD plates, –Trp-Leu, –Trp-Leu-His, and –Trp-Leu-His with 10 mM 3-Amino-1,2,4-triazole (3-AT) with a serial dilution of yeast cells. His gene product will be produced if interaction between bait and prey happens and then the yeast can grow on the –Trp-Leu-His SCD plate. 3-AT is a competitive inhibitor of His gene product thus it can prevent leakage of gene expression and select interaction stronger than certain threshold.

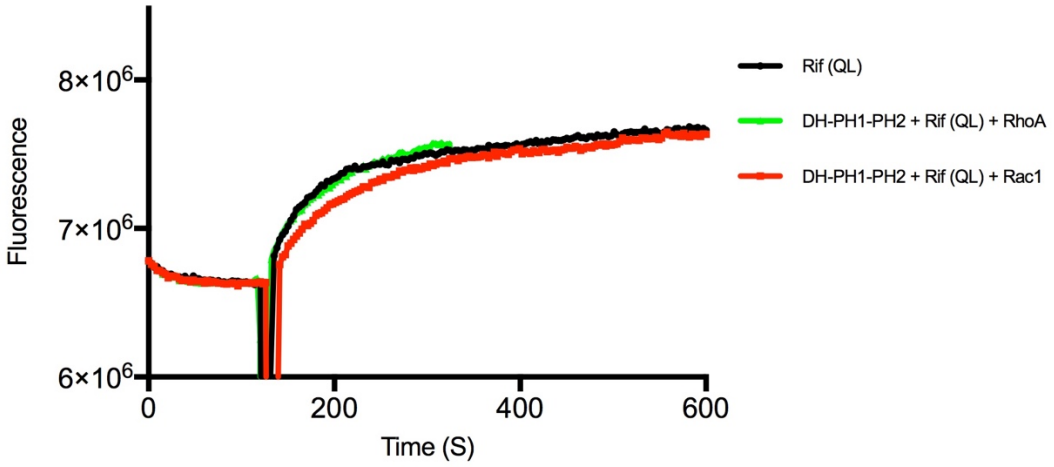

Figure 2-1. GEF activity of DH-PH1-PH2 of FARP1 towards Rac1 and RhoA in the presence of Rif.

Mant-GDP was present in the reaction buffer and its binding to the RhoGTPases was measured by monitoring the increase of the fluorescence signal. The DH-PH1-PH2 protein displayed no GEF activity to either RhoGTPases. The intrinsic GTP/GDP exchange rate of Rif was high enough to be captured.

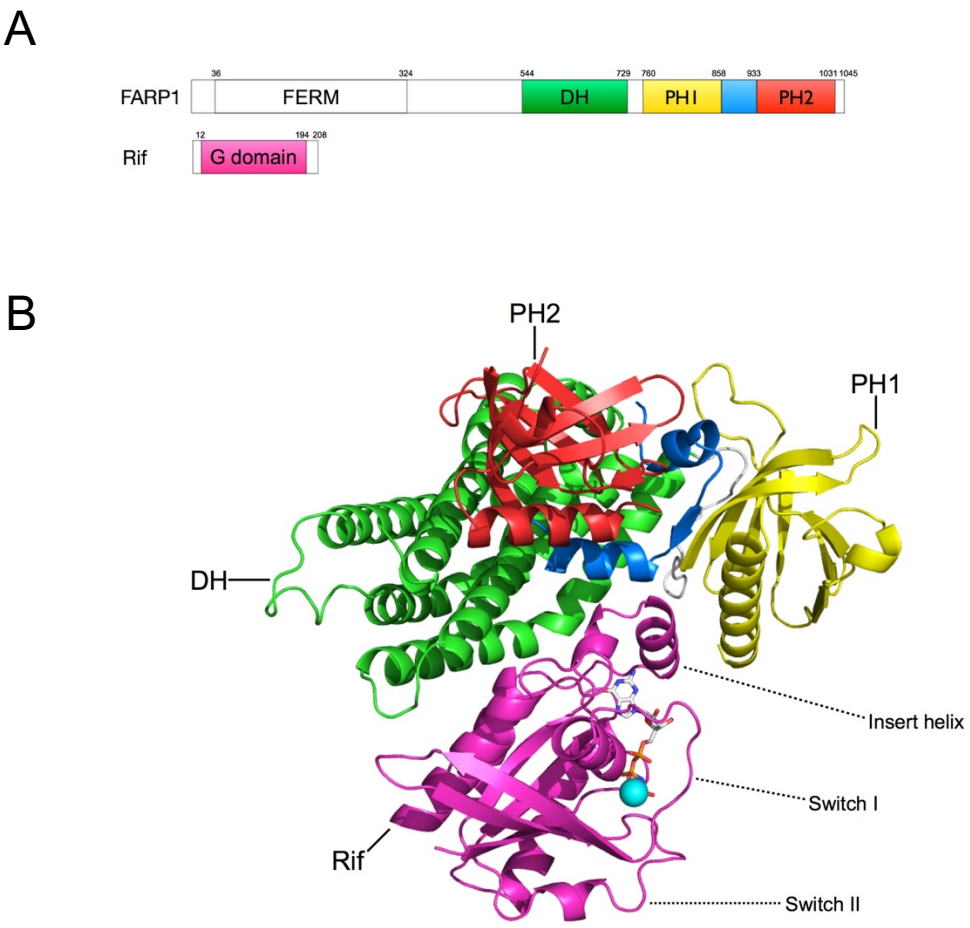

Figure 2-2. Crystal structure of Rif in complex with DH-PH1-PH2 of FARP1.

(A) Domain architecture of FARP1 and Rif. Residues numbers are based on human FARP1 and human Rif, respectively. DH: Dbl-homology domain; PH: pleckstrin-homology domain. (B) Overall structure of the Rif/DH-PH1-PH2 complex. The color scheme is the same as in A. Sticks represents the Rif-bound GMP-PNP. Sphere represents Mg^{2+} ion.

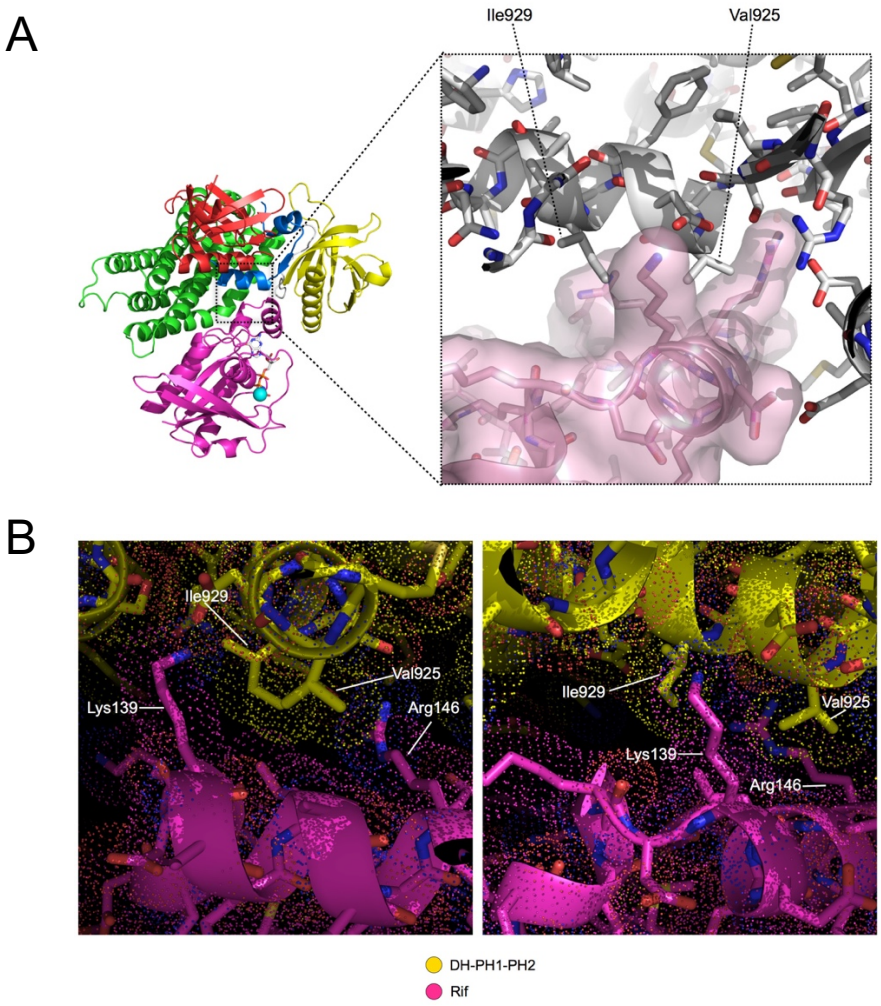

Figure 2-3. The first interface in the crystal structure of Rif/DH-PH1-PH2 complex.

(A) The first interface in the complex crystal structure of Rif/DH-PH1-PH2. Val925 and Ile929 are embedded in the first interface.

(B) Dots representation shows the positive-charged cage formed by Lys139 and Arg146 on the insert helix of Rif encompasses Val925 and Ile929 of DH-PH1-PH2. structure of the Rif/DH-PH1-PH2 complex.

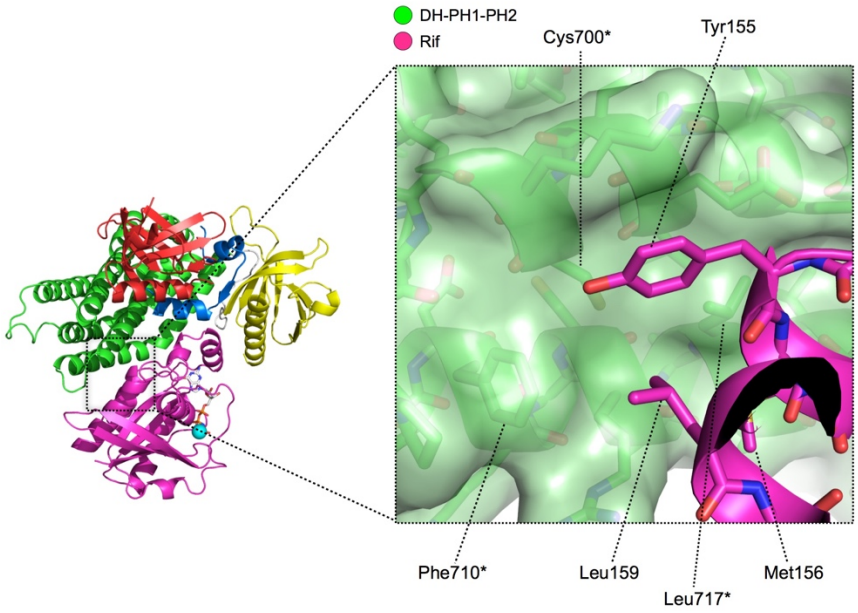

Figure 2-4. The second interface in the crystal structure of Rif/DH-PH1-PH2 complex.

In the second interface, Tyr155, Met156, and Leu159 of Rif pack against Cys700, Phe710, and Leu717 of DH domain to form hydrophobic interactions. * represents the residues of DH-PH1-PH2.

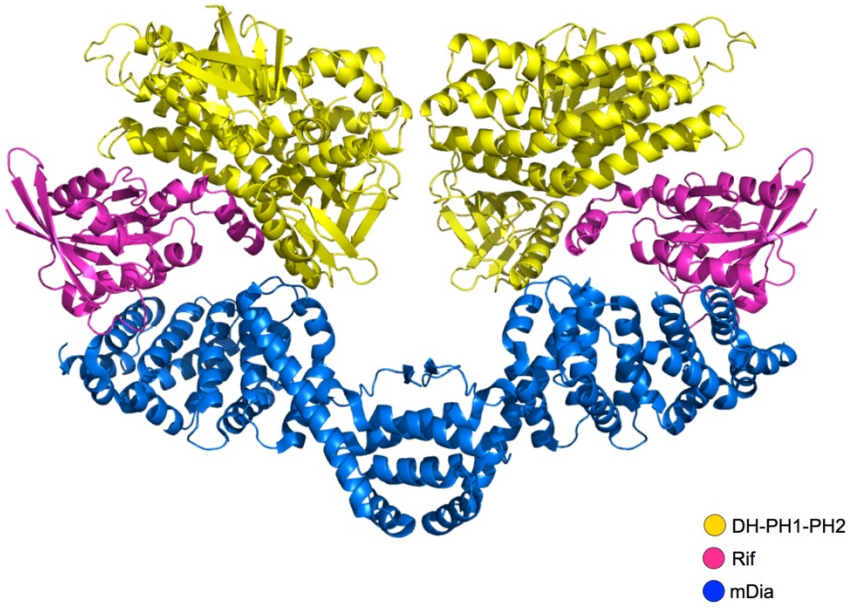

Figure 2-5. Modeling of the Rif/DH-PH1-PH2 structure with the RhoGTPase-bound mDia.

Active RhoC-bound mDia1 structure (PDB ID: 1Z2C) was first superimposed with the dimer structure of Formin mDia1 (PDB ID: 3OBV) on the basis of mDia1. Rif bound DH-PH1-PH2 structure was then aligned with RhoC on the basis of RhoGTPases.

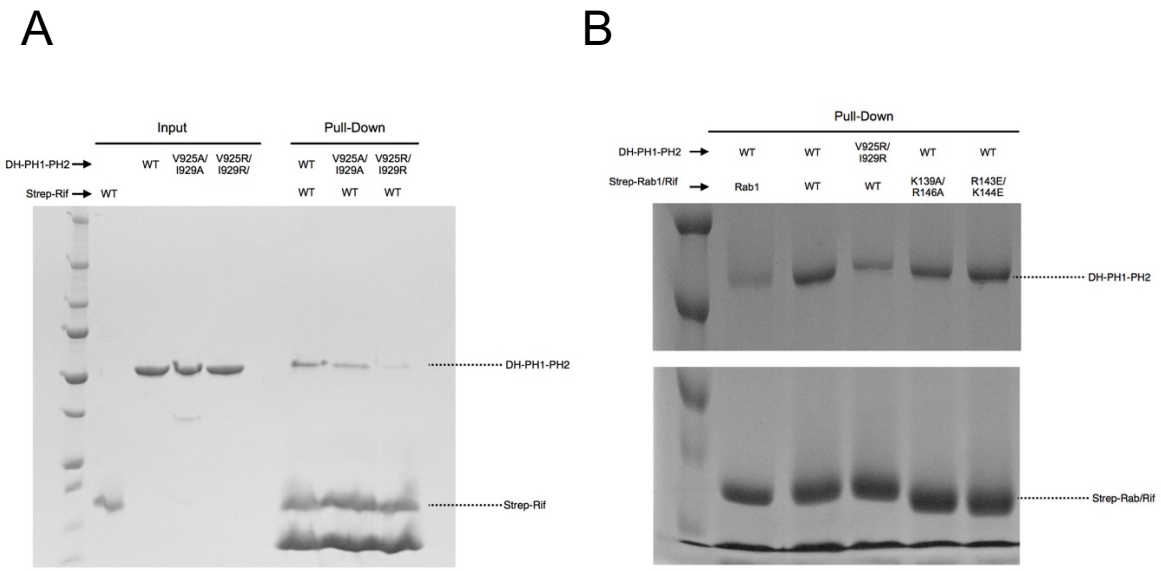

Figure 2-6. Strep-tag pull down to examine the first interface of the Rif/DH-PH1-PH2 structure.

(A) DH-PH1-PH2 wild type (WT), V925A/I929A, or V925R/I929R was incubated with strep-Rif which was then pulled down by Strep-Tactin beads, and the amount of pulled-down DH-PH1-PH2 variants was examined.

(B) DH-PH1-PH2 wild type (WT) or V925R/I929R was incubated with strep-Rif wild type (WT), K139A/K146A, or R143E/K144E. Strep-Rab1 or Rif was then pulled down by Strep-Tactin beads, and the amount of pulled-down DH-PH1-PH2 variants was examined. Strep-Rab1 served as a negative control.

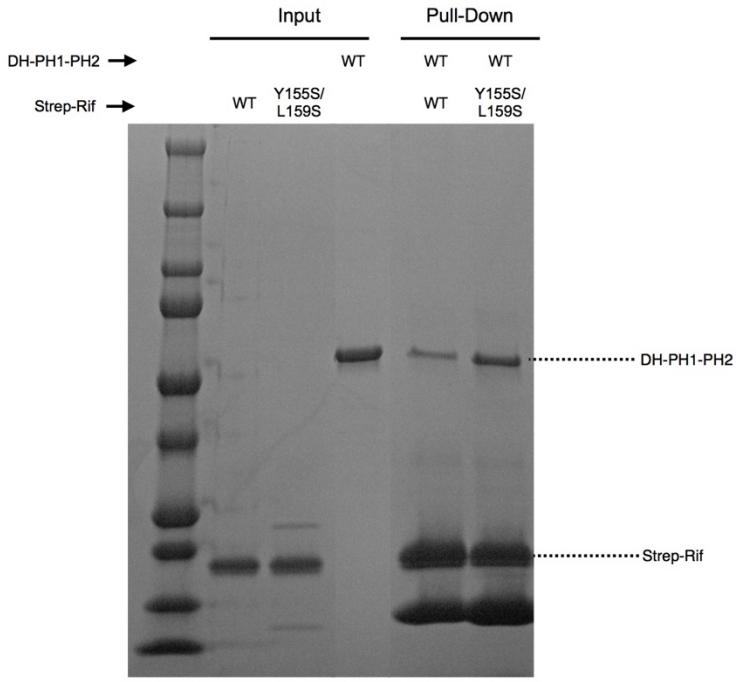

Figure 2-7. Strep-tag pull down to examine the second interface of the Rif/DH-PH1-PH2 structure.

DH-PH1-PH2 wild type (WT) was incubated with strep-Rif wild type (WT) or Y155S/L159S. Strep-Rif was then pulled down by Strep-Tactin beads, and the amount of pulled-down DH-PH1-PH2 was examined.

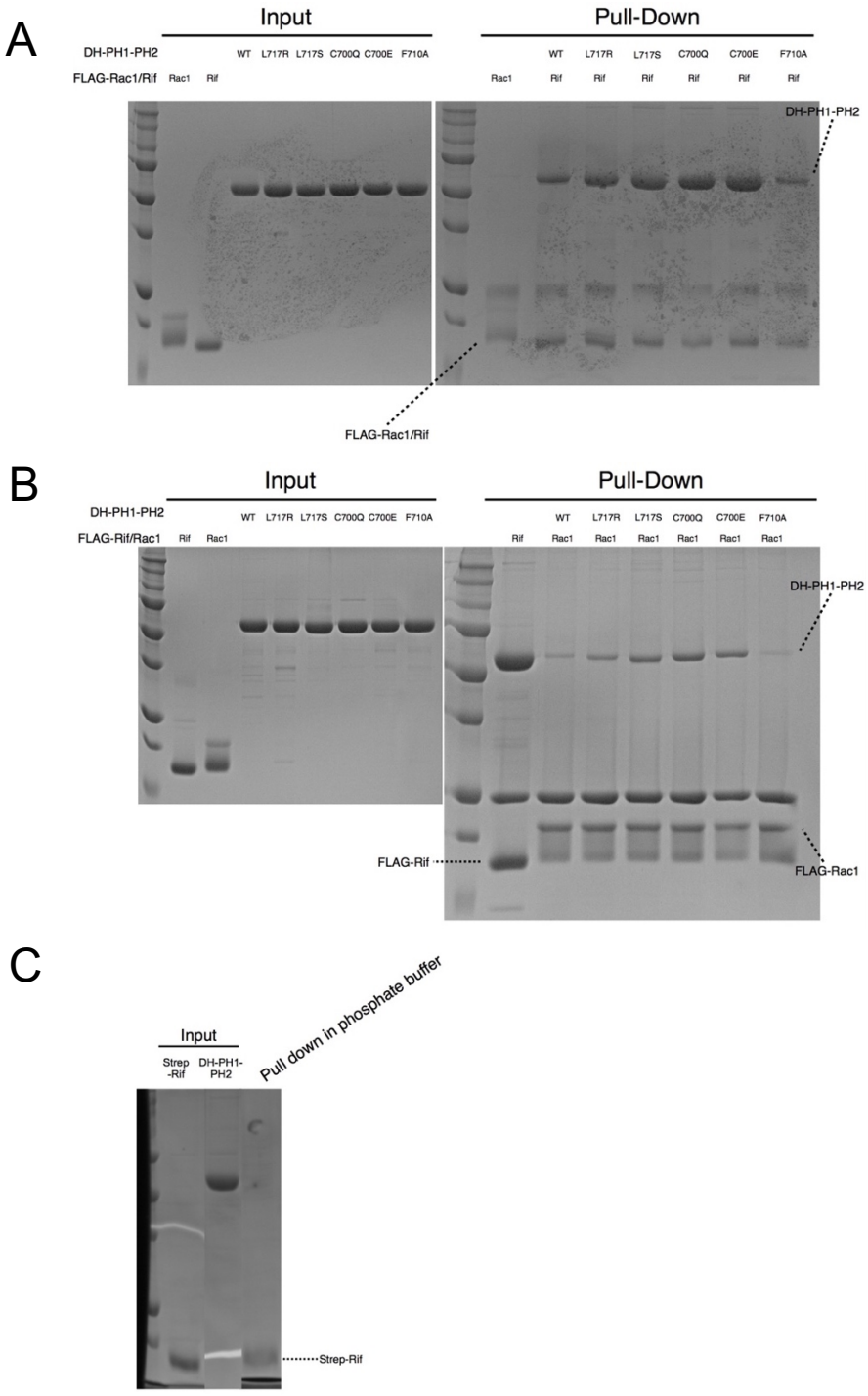

Figure 2-8. FLAG-tag pull down to examine the second interface of the Rif/DH-PH1-PH2 structure.

(A) DH-PH1-PH2 wild type (WT), L717R, L717S, C717Q, C700E, or F710A was incubated with FLAG-Rif which was then pulled down by anti-FLAG beads, and the amount of pulled-down DH-PH1-PH2 variants was examined. FLAG-Rac1 served as a negative control.
(B) DH-PH1-PH2 wild type (WT), L717R, L717S, C717Q, C700E, or F710A was incubated with FLAG-Rac1 which was then pulled down by anti-FLAG beads, and the amount of pulled-down DH-PH1-PH2 variants was examined. FLAG-Rif served as a positive control.
(C) DH-PH1-PH2 was incubated with strep-Rif in phosphate-buffer saline, and then strep-tag pull down was performed.

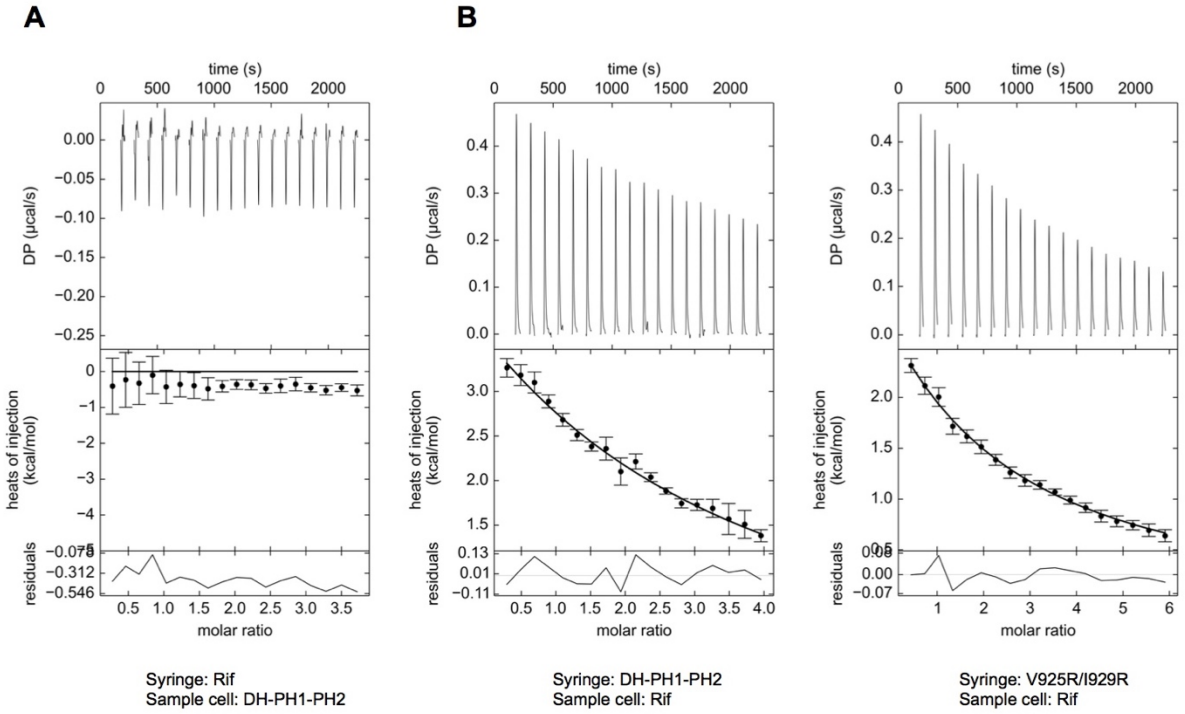

Figure 2-9. ITC experiments to examine the interaction of Rif and DH-PH1-PH2.

Interaction examination between Rif and DH-PH1-PH2 by ITC. Top: Representative baseline-subtracted ITC thermograms. Middle: integrated titration heats (circles) with fits shown (lines). Bottom: residuals plots.

(A) Titration of Rif to DH-PH1-PH2.

(B) Titration of DH-PH1-PH2 or DH-PH1-PH2 with V925R/I929R to Rif. Note: the decrease of heat flow spikes was due to dilution effect instead of binding event.

Note: The ITC experiments were performed by Dr. Hua Chen with the help of Dr. Thomas Scheuermann at MBR in UTSW.

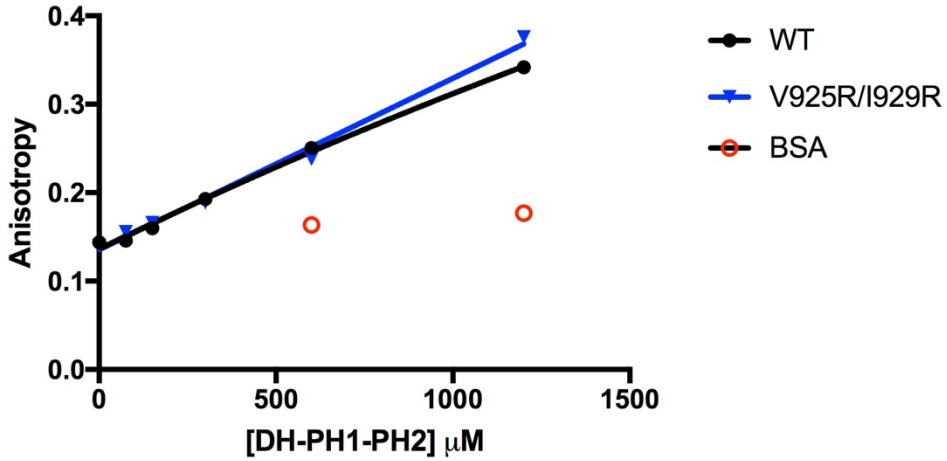

Figure 2-10. Fluorescence anisotropy experiments to examine the interaction of Rif and DH-PH1-PH2.

Alexa488-Rif was titrated with increasing concentrations of DH-PH1-PH2 wild type (WT) or V925R/I929R. BSA titration served as a control.

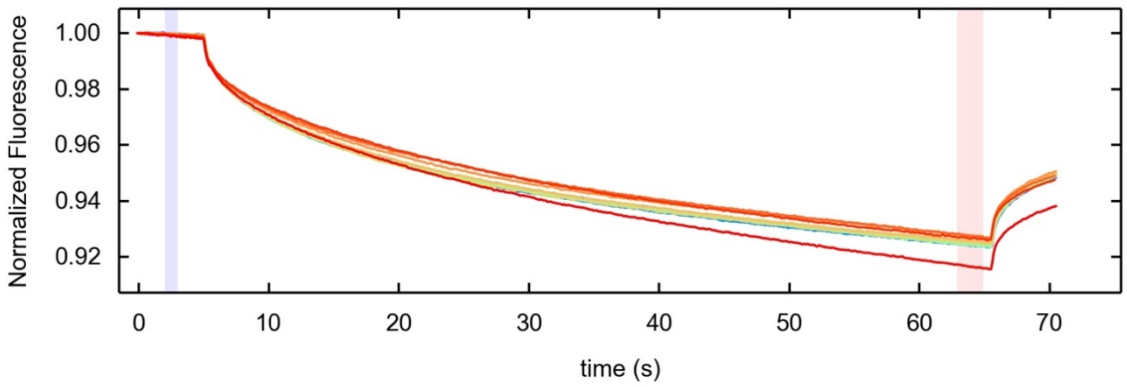

Figure 2-11. MST experiments to examine the interaction of Rif and DH-PH1-PH2.

Alexa488-Rif was titrated with 16 increasing concentrations of DH-PH1-PH2. Representative titration traces in PALMIST were shown here.

A

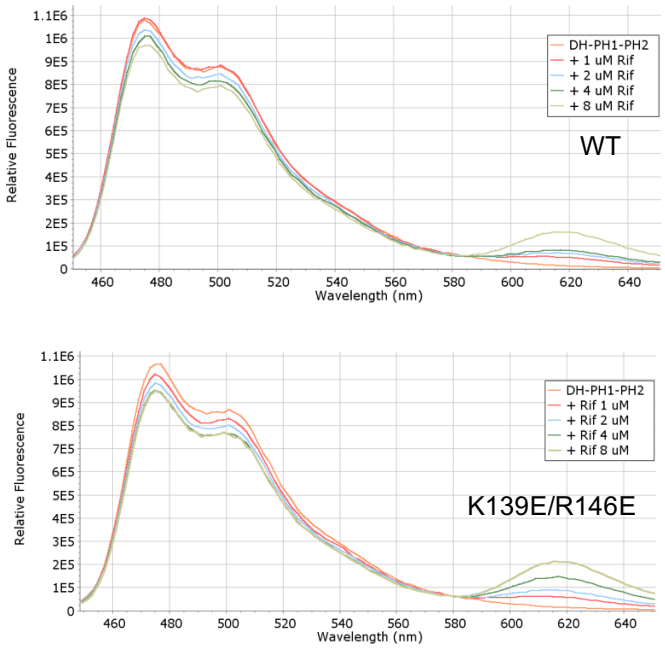

B

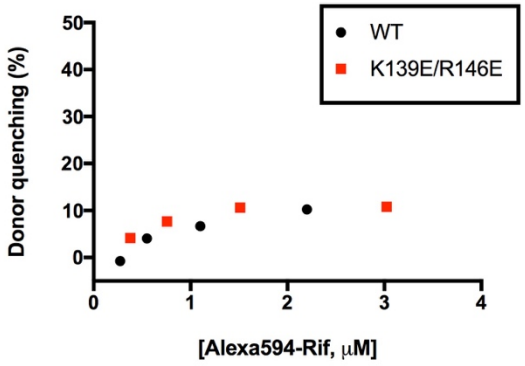

Figure 2-12. Vesicle-based FRET experiments to examine the interaction of Rif and DH-PH1-PH2.

(A) DH-PH1-PH2-ECFP was titrated with increasing concentrations of Alexa594-Rif wild type (WT), Upper or K139E/R146E, Lower. FRET between the two fluorophores in DH-PH1-PH2-ECFP and Alexa594-Rif is demonstrated by donor quenching and acceptor enhancement. 1 μM DH-PH1-PH2-ECFP was incubated in the presence of the indicated concentrations of Alexa594-Rif in buffer as described under "Materials and Methods". Data

show decrease of DH-PH1-PH2-ECFP fluorescence at 475 nm and enhancement of PH-Alexa594 fluorescence at 617 nm. Fluorescence from direct excitation of Alexa594 is subtracted from each spectrum.

(B) Equilibrium binding of Rif to DH-PH1-PH2. Fluorescence of 1 μM DH-PH1-PH2-ECFP was measured as described in (A) at increasing concentrations of Alexa594-Rif. Data show the percent of ECFP fluorescence that is quenched at 475 nm.

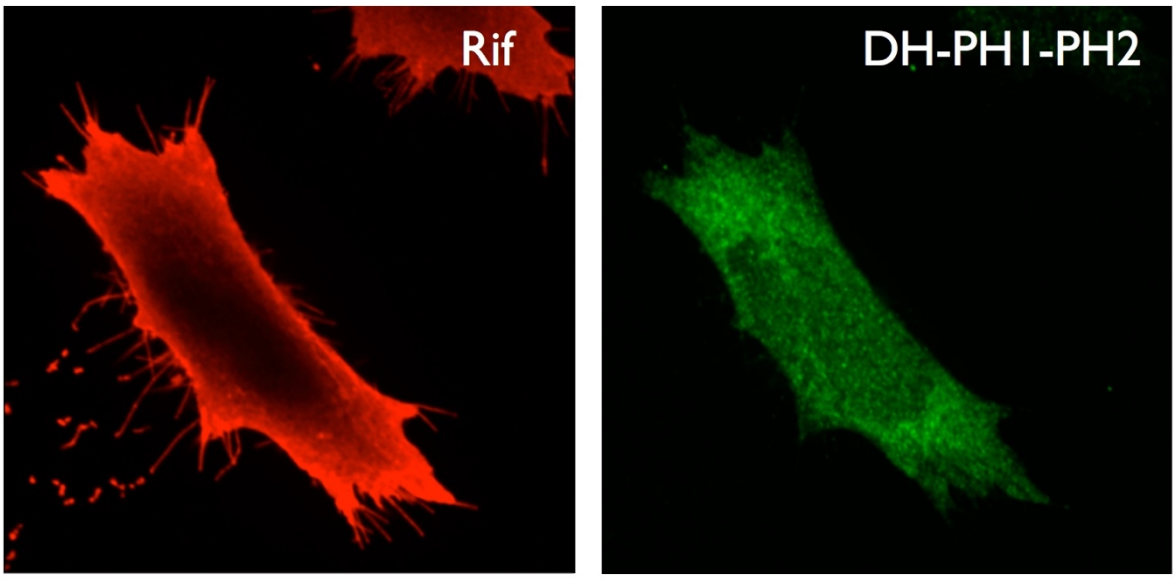

Figure 2-13. Confocal microscopy to examine whether membrane-localized Rif recruits DH-PH1-PH2 to plasma membrane.

FLAG-tagged Rif and HA-tagged FARP1 DH-PH1-PH2 were transfected to HeLa cells. 16 hr after transfection, the cells were fixed, and immunofluorescence was performed with anti-FLAG and anti-HA primary antibodies and then Alexa555- and Alexa488-conjugated secondary antibodies. Confocal microscope imaging was further executed.

Note: The confocal microscopy imaging was performed by Dr. Yu-Ju Chen in Dr. Jen Liou's laboratory at UTSW.

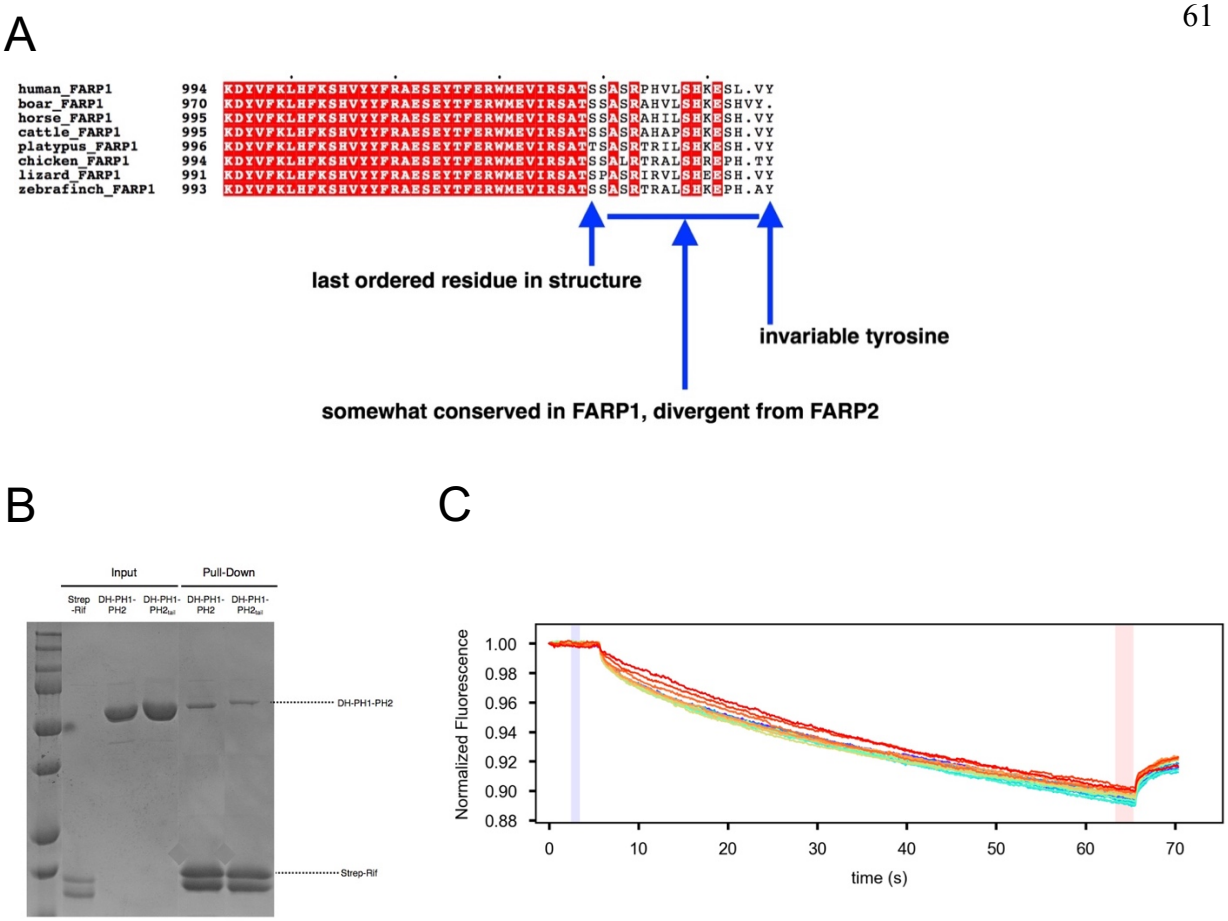

Figure 2-14. Investigation of the last 12 residues at the C-terminus of FARP1.

(A) Sequence alignment of the C-terminus of FARP1 among different species.

(B) Strep-tag pull down to compare the binding of Rif to DH-PH1-PH2 with (DH-PH1-$PH2_{tail}$) or without (DH-PH1-PH2) the last 12 residues.

(C) MST measurement to compare the binding of Rif to DH-PH1-PH2 with (DH-PH1-$PH2_{tail}$) or without (DH-PH1-PH2) the last 12 residues.

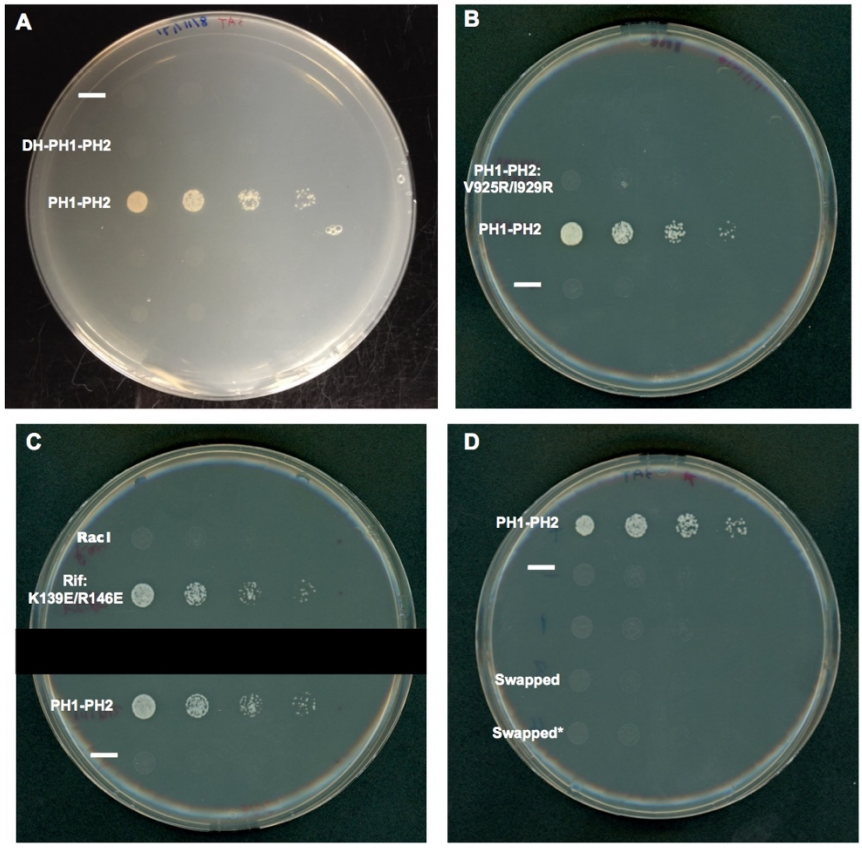

Figure 2-15. Yeast two-hybrid experiments to examine the interaction of Rif and DH-PH1-PH2.

Interaction of Rif with FARP1 variants was measured in a yeast two-hybrid assay by growth on Trp/Leu/His-deficient medium in the presence of 10 mM 3-amino-1,2,4-triazole (3-AT). Plasmids encoding activated (QL) Rif fused to the Gal4-DNA binding domain (DBD) were transformed into Y2HGold yeast cells together with the respective FARP1 variants fused to the Gal4 activation domain (AD) except for Swapped and Swapped* in (D). Swapped: Rif was fused to AD, PH1-PH2 was fused to DBD; Swapped*: Rif was fused to AD, DH-PH1-PH2 was fused to DBD.

Table 2-1. Data collection and refinement statistics of Rif/DH-PH1-PH2

Data collection	
Space group	P 21 21 21
Cell dimensions	
a, *b*, *c* (Å)	58.139, 96.838, 247.164
a,*b*,*g* (°)	90, 90, 90
Resolution (Å)	47.52-2.604 (2.697-2.604)*
*R*sym (%)	11.7 (58.8)
I/σ*I*	21.1 (1.8)
Completeness (%)	98.7 (94.5)
Redundancy	5.1 (2.8)
Refinement	
Resolution (Å)	2.6
No. reflections	42636
*R*work/ *R*free (%)	21.6 (29.2)/26.6 (33.3)
No. atoms	8856
Protein	8758
Ligand/ion	58
Water	40
B-factors	
Protein	80.6
Ligand/ion	86.7
Water	60.9
R.m.s deviations	
Bond lengths (Å)	0.003
Bond angles (°)	0.65
Ramanchandran plot	
Favored (%)	96
Allowed (%)	3.81
Disallowed (%)	0.19

*Highest resolution shell is shown in parenthesis.

CHAPTER THREE :

STRUCTURE OF THE FERM DOMAIN OF FARPS AND ITS INTERACTION WITH PLEXINS

BINDING OF FERM TO THE JM HELIX OF PLEXIN

Summary

FARPs was shown to be immunoprecipitated with Plexins through the N-terminal FERM domain. To investigate how FARP's FERM binds to Plexin and how this interaction regulates Semaphorin-Plexin signaling, I attempted to co-crystallize the complex of FERM and Plexin. Previously, our laboratory has elucidated the activation mechanism of Plexin through determining its inactive monomer and active dimer structures. Intriguingly, I found FERM preferentially interacts with Plexin active dimer but not inactive monomer. Elucidating the binding mode of FERM to Plexin active dimer will advance the mechanistic understanding. During the attempts to co-crystallize the FERM/Plexin complex, we encountered difficulties obtaining complex crystals due to the transient interaction. I hence established a high-throughput native gel electrophoresis assay to search for the best combinations of FERMs and Plexins either with different truncations or from different species that can co-crystallize. Unfortunately, none of the FERM/Plexin complexes crystallized.

Further experiments indicated that the C-terminal half of Plexin juxtamembrane helix (JM-C) is the region for FERM domain of FARPs to bind. Crystallization trials of JM fused to various FERMs failed. In order to further characterize the interaction between FERM and JM, JM was fused to GST. GST pull-down assays confirmed that JM-C is sufficient to pull down FERM. Consistently, mutations of several conserved residues in JM-C abolished its interaction with FERM. Since Plexin JM-C is located at the dimer interface of Plexin active dimer and important for active dimer formation, binding of FERM to JM-C suggests that FARPs may inhibit GAP activity of Plexins via N-terminal FERM domain binding.

During the process of FERM/Plexin co-crystallization, I solved two apo-structures of FERM domain from zebrafish FARP1 and zebrafish FARP2. Superimposition of these two structures with the previously solved FERM of mouse FARP2 revealed identical oligomerization patterns formed by residues highly conserved among all FARPs from different species, suggesting a conserved oligomerization-regulated mechanism inherited in FARPs.

Introduction

FARP2 interacts with Plexin through the N-terminal FERM domain whereas FARP1 interacts with Plexin through both the N-terminal FERM and C-terminal tandem PH domains detected by immunoprecipitation (Toyofuku et al., 2005; Zhuang et al., 2009). Toyofuku et al. showed that FARP2 dissociated from Plexin after Semaphorin binding whereas Zhuang et al. indicated FARP1 constitutively interacted with Plexin before and after Semaphorin

stimulation. Sequence alignment of FERM domains between FARP1 and FARP2 showed significant conservation (65 % identity), suggesting the binding mode of FARPs to Plexin should be similar. The inconsistent occasions for FARP1 and FARP2 to interact with Plexin brought an important question: what types of Plexin FARPs bind, inactive monomer (before Semaphorin stimulation) or active dimer (after Semaphorin stimulation)? Resolving the binding mode will also imply the regulation of FERM on Plexin: whether FERM binding boosts or inhibits Plexin activation, or Plexin just provides the anchoring site for FERM domain of FARPs.

Results

Crystal structure of FERM domain

Structural features of FARP2 FERM

Previously, our laboratory has solved the crystal structure of mouse FARP2 FERM domain (Figure 3-1). FERM domain represents a clover-shaped structure containing three lobes. The charge distribution on the surface of FERM is intriguing; one side of the FERM protein carries negative charge while the other side harbors positive charge. In crystal lattice, FERM domains form infinite oligomers. The endless chain is a result of the packing of the positive-charged surface against the negative-charged surface. Those interacting residues in the oligomerization interfaces are highly conserved between FARP1, FARP2, and among all species (Figure 3-2).

FERM renders FARP1 to localize on the plasma membrane

FERM domains of both FARP1 and FARP2 contain a positive-charged patch presumably essential for plasma membrane anchoring. I over-expressed C-terminally FLAG-tagged FARP1 in HeLa cells and investigated cellular localization of FARP1 protein through immunofluorescence using the antibody against FLAG-tag. I performed confocal microscopy to take pictures of the Z-stack slices with the help of Dr. Yu-Ju Chen from Dr. Jen Liou's laboratory. Confocal images revealed that full-length FARP1 is mainly localized on the plasma membrane while DH-PH1-PH2 lacking the FERM domain is localized in the cytosol. In order to further characterize essential residues required for membrane targeting, we looked at the structure of FERM and found a potential positive-charged patch in the third lobe of the clover structure. Charge-reversal mutation of two positive-charged residues, Arg273 and Lys274, in full-length FARP1 completely abolished the membrane localization of FARP1. (Figure 3-3)

Difficulties in establishing a reliable binding assay to dissect the interaction of FERM/Plexin

Several difficulties hindered us and others to establish a reliable binding assay to dissect the interaction between FERM and Plexin. FERM proteins are not easy to express and purify. We solved the expression problem of FARP2 FERM by SUMO-tag fusion. After we determined the crystal structure of FARP2 FERM, we realized that FERM domain forms infinite oligomers in the crystal lattice. I mutated a critical residue in the oligomerization

interface, Asp212 in FARP1 and Asp216 in FARP2 both to asparagines. Expression of FARP1's FERM domain was initially infeasible. The inclusion of a long flexible loop following the FERM domain (FERM adjacent region, FA as the abbreviation) was the prerequisite for expressing FARP1's FERM. After the oligomerization nature and interface was revealed by the FARP2 structure, FARP1's FERM domain was then able to be expressed and purified. Since we saw the charge-charge interactions constitute the interfaces for the infinite oligomers in the crystal lattice, we hypothesized that FERM domain has to be kept in buffer conditions containing high salt. Following this assumption, I found most purified FERM domains from different species precipitated when the salt concentration was decreased to below 500 mM. This precipitation process is reversible upon tuning up the salt concentration.

Native gel electrophoresis

As I mentioned in the previous section, the protein expression and stability difficulties have been solved. The next goal is to establish an assay that can detect the interaction between FERM and Plexin reliably. Since our goal is to solve the complex structure of FERM bound Plexin to reveal how they interact, high throughput platform would be the better choice. Since our laboratory has developed the expression and purification system for the intracellular region of Plexin, I took this advantage to start examining the interaction with the proteins that I could obtain. Native gel electrophoresis is a suitable assay system for my purpose because of the easy readout and simple manipulation. FERM domain

is positively charged in net and can form oligomers according to our structure. In native gel electrophoresis, instead of running to the opposite direction as other positive-charged proteins did, FERM stuck in the edges of the well. Plexin ran as a condensed band on the native gel, and its intensity was gradually depleted as the FERM amount was increased in the mixture. In classical native gel electrophoresis, if the interaction happens between two purified proteins, the intensity of individual proteins would be decreased while the new band of the complex would be formed. In our system, I suspected the complex band was stuck in the edges of the well as FERM domain behaved thus I only observed depletion but no extra band. The observation that Plexin B2 was not depleted by the FARP2 FERM suggested the specificity of this interaction and the authenticity of this native gel system. (Figure 3-4)

FERM preferentially interacts with dimeric Plexin

Previously our laboratory identified that fusion of the coiled-coil (CC) from GCN4 transcription factor with Plexin intracellular region induced Plexin dimerization and activation (Wang et al., 2013). Out of curiosity, I performed native gel electrophoresis with CC-fused Plexin against a series of increasing amount of FERM. The result brought me two surprises. FERM not only depleted CC-Plexin but also caused an extra band formation which was assumed as the complex of FERM/CC-Plexin (Figure 3-4 and 3-5). Interestingly, comparison of the binding of FERM towards Plexin monomer and dimer showed that FERM preferentially interacted with Plexin dimer (Figure 3-4).

Imidazole negative staining to verify the identity of the extra band and determine the stoichiometry of the complex

In order to verify the identity of the extra band, I employed a staining method named imidazole-SDS-zinc reverse staining (Ortiz et al., 1992). This technique primarily stained SDS-PAGE but not proteins on it. Unlike Coomassie blue staining, proteins on the imidazole-SDS-zinc stained gel are still mobile. Taking advantage of this staining method, I cut the extra band from the native gel and re-ran this extra band in the conventional SDS-PAGE and stained it by Coomassie blue. The extra band ran as two separate bands with molecular weight same as Plexin and FERM respectively. (Figure 3-6) The method clearly demonstrated that FERM interacted with Plexin to form the extra complex band on native gel electrophoresis. Moreover, the extra band from the native gel was mobilized and ran on the SDS-PAGE together with the known amount of Plexin and FERM as standards. The SDS-PAGE was further stained by Coomassie blue. Intensity comparison of the two bands from the extra band with standard bands revealed that FERM and Plexin formed a 1:1 complex. (Figure 3-6)

Choices of FERM and Plexin from different species

By the native gel electrophoresis platform, I examined the interaction of Plexins and a collection of FERM domains of FARP1 and FARP2 from different species. The criteria for choosing the species was according to their sequence identity. My purpose was to select the species whose sequence identity is close enough so that the chance for them to interact with

Plexin is high. Meanwhile, I needed to filter out those with too close sequence identity because I expected the sequence diversity to increase the probability of crystallization. The most divergent species that I chose has about 20 % difference of sequence identity while the most related species has about 10 % difference. For FARP2's FERM, these species include mouse FARP2, human FARP2, and zebrafish FARP2; For FARP1's FERM, these species include human FARP1, Xenopus FARP1, and zebrafish FARP1. Plexins are highly conserved among different species. I opted to adopt A family of Plexin since it was reported to bind FARPs in previous studies (Toyofuku et al., 2005; Zhuang et al., 2009). I performed native gel electrophoresis to investigate the interaction between Plexins and FERMs from the species that I chose and then set up crystallization trials for those combinations showing strong interaction.

Crystal screenings

Table 3-1 showed the combinations of FERMs and Plexins that I have tried for crystallization. Because native gel results showed that FERM preferentially interacted dimeric Plexin, I initially crystallized all the dimeric Plexin A family that I could express and purify with FERM domains. I started crystallizing monomeric Plexins with FERM domains after most combinations of Plexin dimers and FERM failed to crystallize.

FERM tends to crystallize by itself presumably due to self-oligomerization. In order to reduce the chance crystallizing FERM domain alone, I also applied oligomerization-disrupting mutations, D212N of FARP1 and D216N of FARP2, to set up crystal trials with

various Plexins. Unfortunately, all the trials failed to grow complex crystals. More FERM domain structures from different species were solved during this process. Mouse FARP2 FERM domain carrying D216N mutation was still crystallized through different packing. The structure of zebrafish FARP2 FERM was determined as well; it adopts the same conformation and packing mode as the mouse FARP2 FERM (Figure 3-1).

Mapping the binding region of Plexins for FERM domain

FERM interacts with the JM helix of Plexin

I divided the intracellular region of Plexins into JM portion and GAP-RBD portion and fused the JM portion with GST. I expressed and purified GST-tagged JM and GAP-RBD, and ran native gel electrophoresis with increasing amount of FERM domain. Native gel electrophoresis results showed that FERM domain depleted GST-JM at 4:1 molar ratio (FERM:GST-JM=4:1) but not GAP-RBD. (data not shown)

Since previously I have shown that FERM preferentially interacted with CC-Plexin dimers, I suspected FERM interacts better with dimeric JM. I expressed and purified CC-JM and ran native gel electrophoresis. The results showed that FERM interacted with CC-JM. The JM helix in the Plexin A3 structure (PDB ID: 3IG3) can be divided into two portions based on the kink in the middle. The C-terminal part of the JM forms several interactions with the GAP domain in Plexin A3 monomer structure. Semaphorin binding to Plexin induces dislodgment of the JM from the GAP domain, and the JM undergoes a conformational change to dimerize with the JM helix from another Plexin molecule (Wang et

al., 2013). I further constructed N-terminal and C-terminal portion of JM and fused them with CC. Native gel electrophoresis showed that FERM interacted with the C-terminal portion of JM but not the N-terminal portion (Figure 3-7). I next crystallized the FERM domains of FARP1 and FARP2 with the C-terminal portion of CC-JM. Unfortunately, the FERM domain from FARP2 crystallized by itself. We did not see any extra electron density from CC-JM.

GST pull down to confirm and characterize the interaction of FERM and Plexin JM helix

In order to verify that above finding in native gel electrophoresis: FERM interacts with the C-terminal portion of the JM helix, I chose to apply GST pull-down assay to examine the interaction. I fused the JM helix to GST and performed GST pull-down assay to determine whether this GST pull-down system can detect this interaction. I pulled down GST-fused JM and detected its binding with FERM domains from FARP1 and FARP2. The GST pull-down result clearly showed that FARP1 FERM was pulled down by GST-JM but not GST control (Figure 3-8). Since the molecular size of FARP2 FERM is very close to GST-fused JM, the interaction could not be concluded yet.

To further characterize this interaction, I fused a series of JM helix variants to GST, including full-length JM helix (JM), the N-terminal portion of JM (JC-N), the C-terminal portion of JM (JM-C), and mutation of a highly conserved Phe residue located at the C-terminal portion of JM (F1292A). GST pull-down assay was employed to detect the binding between FERM and these GST-fused JM variants. GST pull-down results showed that

FERM domain interacted with JM, specifically the C-terminal portion. The finding that mutation of the highly conserved Phe abolished the interaction not only indicated the critical residue essential for binding but also reinforced the idea that C-terminal portion of JM is the binding region for FERM (Figure 3-9). GST pull-down results pointed towards the same conclusion as native gel electrophoresis did.

In the following section, I will describe my crystallization efforts for the JM helix with FERM. Since all the crystallization trials failed to reveal the electron density of JM helix, I mutated a few more conserved residues of the GST-JM-C and performed GST pull-down assay trying to identify the residues essential for this interaction. GST pull-down results indicated that F1292A had the most significant, A1291Q, A1293Q, and L1295R had modest whereas I1299R had the least effect in abrogating the interaction (Figure 3-10).

Fusion of FERM with JM helix of Plexin

GST pull-down results suggested that the binding between FERM domain and JM was really weak; a vast amount of GST-JM bait could only pull down a tiny bit of FERM. I opted to fuse the C-terminal portion of JM (JM-C) with FERM domains, express and purify the fusions and crystallize them. In order to examine whether my fusion design works and search for the best linker length between FERM and JM-C, I employed the GST pull down as my platform. I pulled down GST-fused JM-C bait protein and tested its binding to FERM domain. Working FERM–JM-C fusions would not be able to be pulled down by GST-bait as the binding pocket of FERM is occupied by the fused JM-C. The results showed that fusions

remarkably blocked the binding to GST-JM bait. Fusions with different linker length including 5, 10, and 15 residues displayed similar blocking effects (Figure 3-11). I hence went on to crystallize the fusion with the shortest linker length. I tried mouse FARP2 fusion, mouse FARP2 D216N fusion, zebrafish FARP2 fusion, human FARP1 D212N fusion, and zebrafish FARP1 fusion. I solved the structures from mouse FARP2 and zebrafish FARP1 fusions. Unfortunately, none of them revealed the JM-C density. Crystal structure of zebrafish FARP1 was the first FERM domain structure of FARP1; it adopts the same conformation as the FARP2 FERM. (Figure 3-1)

Discussion

The C-terminal portion of JM helix is important for the formation of Plexin active dimer (Wang et al., 2013). Binding of FERM domain to Plexin implies that FERM blocks the Plexin activation. FERM domain of FARP1 and FARP2 adopts the same conformation, suggesting the binding mode of both FERM to JM-C is the same. However, there might be some differences in terms of the respective binding affinity. FARP2 is reported to interact with Plexin in the absence of Semaphorin stimuli. Semaphorin binding to Plexin induces the dissociation of FARP2 from Plexin (Toyofuku et al., 2005). Conversely, FARP1 interacts with Plexin constitutively regardless of Semaphorin (Zhuang et al., 2009).

Modeling of the JM helix bound FERM

Although I have mapped JM-C as the binding region for FERM domain, the modeling for the JM bound FERM is still challenging. FERM domains among different proteins represent various binding modes for interacting proteins. The established GST binding assay platform prompted me to pursue the binding surface of FERM domain. However, FERM expression is the main obstacle for this purpose. Mutation of a Trp residue in the canonical binding pocket of FERM of both FARP1 and FARP2 flubbed the expression. An *in vivo* binding approach such as yeast two-hybrid without protein purification needs to be implemented in order to grasp the interface of FERM for future modeling.

Dimeric or monomeric Plexin

We do not have clear-cut evidence indicating whether FERM domain interacts with monomeric or dimeric Plexins except for the native gel results. The native gel result showing that FERM depleted CC-induced Plexin active dimer and formed the complex does not solely mean FERM interacts with Plexin active dimers. Because JM interacts with the GAP domain in the monomer state and CC-fusion induces its dislodgment, one can argue that the interaction shown in native gel electrophoresis is simply resulted from exposure of the JM helix induced by CC fusion.

Inhibition of Plexin GAP activity

According to our GST pull-down results, FERM binds to the essential elements for Plexin dimerization. I attempted to examine whether the GAP activity of dimeric Plexin is

abrogated *in vitro*. However, the high-salt dependence of FERM and low-salt condition of GAP assay made this *in vitro* measurement difficult. The future direction can be focused on cell-based collapse assay. Taking advantage of the Plexin-expressing stable COS7 cells that I established, I can explore whether FERM domain overexpression abolishes Semaphorin-induced COS7 collapse.

What FERM apo-structures tell us

In several crystal structures of FERM domain that we solved, we noticed a head-to-tail packing. This packing, if exists in solution, could lead FERM to form large oligomers. The charge-charge interactions found in the oligomerization interfaces suggest that high salt environment could stabilize FERM protein. Two observations indicated that FERM oligomers exist in solution. As I described in the previous section, buffer containing salt concentration below 500 mM led to FERM precipitation while increasing the salt concentration immediately reversed the precipitation. In addition, a previous postdoctoral researcher in our laboratory found that FARP2 FERM domain migrated together with the salt peak in size exclusion chromatography when running buffer only contains 150 mM NaCl. The residues responsible for forming such charge-charge interactions are highly conserved in all FERM domains of FARPs among different species. Whether this oligomerization plays a regulation function for FARPs is worth further pursuing.

Materials and Methods

Protein Expression and Purification

Expression and purification of FERM domains from FARP1 and FARP2

The coding regions of the FERM domain of mouse FARP2 (residues 44–324), human FARP2 (residues 44–324), zebrafish FARP2 (residues 49–335), human FARP1 (residues 36–329), xenopus FARP1 (residues 37–324), and zebrafish FARP1 (residues 38–326) were cloned into a modified pET-28(a) vector that encodes an N-terminal His_6-tag followed by a SUMO-tag, and a recognition site for Ulp SUMO protease (This vector is referred as ppSUMO herein). The cDNAs of FERM domain of mouse and human FARP2, and human FARP1 were from OpenBiosystem; the cDNAs of the rest were synthesized from Genscript with codon optimization. Point mutations were introduced by QuikChange reactions. The plasmids were transformed into the *E. coli* strain BL21 (DE3). BL21 (DE3) carrying individual expression plasmid was cultured at 37°C to reach OD_{600}=2.0 in TB. Protein expression was induced by 0.2 mM IPTG at 16°C overnight.

After centrifugation, the bacteria cells were re-suspended in the Ni-lysis buffer containing 10 mM Tris (pH 8.0), 1 M NaCl, 5 % glycerol (v/v), 20 mM Imidazole, and 3 mM β-mercaptoethanol. The bacteria resuspension was passed through the cell disruptor for 3~4 times on ice, and then the lysates were subjected to centrifugation. The supernatant was then filtered by 0.45 μM PVDF membrane to get rid of debris. The proteins were passed through a 1 mL HisTrap column and washed with 3 CV Ni-A buffer. The recombinant SUMO protease was diluted in 1 mL Ni-A buffer and injected to this 1 mL HisTrap column and incubated at 4°C overnight. One day after, the digested FERM protein was washed off from the HisTrap

column using Ni-A. Re-pass the flow-through through a 5 mL HisTrap column (GE Healthcare) to remove excessive SUMO in the flow-through.

The protein was further purified by Superdex 200 HiLoad 16/60 chromatography equilibrated with the buffer containing 20 mM Tris (pH 8.0), 500 mM NaCl, 10% glycerol (v/v), and 2 mM DTT. Purified proteins were concentrated and stored at −80°C. All FERM domains need to be kept in the buffer where the concentration of NaCl is at least 500 mM.

Expression and purification of intracellular region of mouse Plexins and CC-fused Plexins

The coding regions of the intracellular region of mouse Plexin A1 (residues 1288–1912), A2 (residues 1289–1922), A4 (residues 1264–1893), zebrafish C1 (residues 552–1147), and CC-fused A1, A2, and A4 were cloned into pSKB2 vector. The CC is the colied-coil dimerization motif of GCN4 and its sequence can be found in this publication (Wang et al., 2013). I adopted the CC register creating the most active Plexins to make the fusion constructs here. CC was fused to the intracellular regions of Plexins through multiple steps of PCR reaction. The C CC-fused mouse A2, zebrafish A3 (residues 1268–1892) and C1 were cloned into ppSUMO vector. Point mutations were introduced by QuikChange reactions. The plasmids were transformed into the *E. coli* strain ArcticExpress (Stratagene). ArcticExpress carrying individual expression plasmid was cultured at 37°C in 100~120 mL LB in the presence of Gentamycin overnight. The bacteria cells were scaled up at 30°C to reach OD_{600}=2.0 in TB. Protein expression was induced by 0.2 mM IPTG at 10°C overnight.

After centrifugation, the bacteria cells were re-suspended in the Ni-lysis buffer containing 10 mM Tris (pH 8.0), 500 mM NaCl, 5 % glycerol (v/v), 20 mM Imidazole, and 3 mM β-mercaptoethanol. The bacteria resuspension was passed through the cell disruptor for 3~4 times on ice, and then the lysates were subjected to centrifugation. The supernatant was then filtered by 0.45 μM PVDF membrane to get rid of debris. The proteins were purified using a 1 mL HisTrap column, eluted by Ni-B buffer and treated with recombinant human rhinovirus 3C protease or SUMO protease for His-tagged or SUMO-tag Plexins at 4°C overnight to remove the N-terminal tag.

The protein was further purified by using Resource Q anion-exchange chromatography with a 10 mM to 300 mM NaCl gradient elution. Fractions were examined by SDS-PAGE electrophoresis and Coomassie blue staining. Fractions containing Plexins were pooled together. For pSKB2 constructs, Plexins were subjected to exchange buffer to 20 mM Tris (pH 8.0), 150 mM NaCl, 10% glycerol (v/v), and 2 mM DTT through Superdex 200 GL 10/30 chromatography. For ppSUMO constructs, Plexins were subjected to Superdex 200 HiLoad 16/60 (GE Healthcare) to remove excessive SUMO-tag. Purified proteins were concentrated and stored at −80°C.

Expression and purification of CC-fused and GST-fused JM helix constructs

I employed the JM helix sequence from mouse Plexin A4 throughout this study. Three CC-fused JM constructs including CC-fused full-length JM (residues 1263–1301), JM-N (residues 1263–1285), and JM-C (residues 1286–1301) were cloned into ppSUMO vector.

For GST-fused JM constructs, the full-length JM helix containing the membrane proximal 3 positive-charged residues (named +KRK, residues 1260–1301), full-length JM helix (residues 1263–1301), JM-N (residues 1263–1285), and JM-C (residues 1286–1301) were cloned into pGEX-6P-1 (GE Healthcare) vector. Point mutations were introduced by QuikChange reactions. The plasmids were transformed into the *E. coli* strain BL21 (DE3). BL21 (DE3) carrying individual expression plasmid was cultured at 37°C to reach OD_{600}=2.0 in TB. Protein expression was induced by 0.2 mM IPTG at 16°C overnight.

For SUMO-tagged CC-fused JM purification, after centrifugation, the bacteria cells were re-suspended in the Ni-lysis buffer containing 10 mM Tris (pH 8.0), 500 mM NaCl, 5 % glycerol (v/v), 20 mM Imidazole, and 3 mM β-mercaptoethanol. The bacteria resuspension was passed through the cell disruptor for 3~4 times on ice, and then the lysates were subjected to centrifugation. The supernatant was then filtered by 0.45 μM PVDF membrane to get rid of debris. The proteins were passed through a 1 mL HisTrap column and washed with 3 CV Ni-A buffer. The recombinant SUMO protease was diluted in 1 mL Ni-A buffer and injected to this 1 mL HisTrap column and incubated at 4°C overnight. One day after, the digested FERM protein was washed off from the HisTrap column using Ni-A. Re-pass the flow-through through a 5 mL HisTrap column (GE Healthcare) to remove excessive SUMO in the flow-through. For GST-fused JM purification, the lysed supernatant was passed through a 1 mL GSTrap column (GE Healthcare) and eluted by 10 mM glutathione-containing buffer. Both CC-JM and GST-JM were further subjected to Superdex 200 GL

10/30 equilibrated with the buffer containing 20 mM Tris (pH 8.0), 150 mM NaCl, 10% glycerol (v/v), and 2 mM DTT. Purified proteins were concentrated and stored at −80°C.

Crystallization and Structure Determination of FERM domains of FARPs

The total protein concentration for crystallization was 6 mg/mL. The intracellular region of Plexins and the FERM domain of FARP1 or FARP2 were mixed at 1:1 molar ratio thus the concentration of Plexin was 4.1 mg/mL and that of FERM domain was 1.9 mg/mL. The two proteins were mixed in the buffer containing 10 mM Tris (pH=8.0), 150 mM NaCl, 10 % Glycerol (v/v), and 2 mM TCEP. The protein mixture was subjected to crystallization trials. FERM domain proteins of FARP1 from human, xenopus, and zebrafish were not stable at 20 °C so that crystallization trials for those proteins have to set up at 4 °C. No FERM/Plexin complex crystallized.

The zebrafish FARP2 crystals crystallization trials were initially set at 20 °C in sitting-drop 96-well plates. Larger crystals were found in a well of these sitting-drop 96-well plates at 20°C in 0.2 M potassium sodium tartrate tetrahydrate and 20 % PEG3350 (w/v). Crystals were cryo-protected using the crystallization solution supplemented with 30 % glycerol and flash cooled in liquid nitrogen. Diffraction data were collected at −173°C on beamline 19ID at the Advanced Photon Source (Argonne National Laboratory). Data were indexed, integrated and scaled by using HKL2000 (Otwinowski and Minor, 1997). A 2.0 Å dataset in the $P2_12_12_1$ space group was collected and then converted to the mtz format by using the Reflection file editor module in the Phenix package (Adams et al., 2002; McCoy et

al., 2007). The structure of mouse FARP2 FERM (Solved by a previous postdoctoral researcher in our laboratory) was used as the molecular replacement search model using the Phaser module in the Phenix package.

The construct of zebrafish FARP1 FERM was originally fused with JM-C of Plexin and designed to crystallize and solve the structure of the complex. The fusion protein was crystallized initially at 4°C in 0.1 M Bicine and 10 % MPD (v/v) in sitting-drop 96-well plates. Larger crystals were grown by sitting-drop vapor diffusion or hanging drop vapor diffusion at 4 °C in Bicine and 16 % MPD (v/v). The crystals were reproduced and grown at the 1:1 volume ratio of protein to crystallization solution. Crystals were cryo-protected using the crystallization solution supplemented with 30 % glycerol and flash cooled in liquid nitrogen. Diffraction data were collected at −173°C on beamline 19ID at the Advanced Photon Source (Argonne National Laboratory). Data were indexed, integrated and scaled by using HKL2000 (Otwinowski and Minor, 1997). A 3.0 Å dataset in the $P2_12_12_1$ space group was collected and then converted to the mtz format by using the Reflection file editor module in the Phenix package (Adams et al., 2002; McCoy et al., 2007). The structure of mouse FARP2 FERM (Solved by a previous postdoctoral researcher in our laboratory) was used as the molecular replacement search model using the Phaser module in the Phenix package.

Iterative model building and structure refinement were performed by using the programs Coot and Phenix, respectively (Adams et al., 2002; Emsley and Cowtan, 2004). Detailed statistics of data collection and refinement are listed in Table 3-2 and 3-3. Molecular structure figures were rendered by the program Pymol (the PyMOL Molecular Graphics

System, Schrödinger). Sequences were aligned by using MAFFT (Katoh et al., 2017) and rendered with ESPript (Gouet et al., 1999).

Native gel electrophoresis

15 μg Plexin protein was incubated with FERM domain at 1:1, 1:2, and 1:4 molar ratio. Native gel running buffer containing 25 mM Tris and 192 mM glycine was pre-cooled at 4°C. 2 mM DTT was added freshly to the running buffer to prevent unwanted cysteine-mediated cross-linking. The native gels were purchased from Bio-Rad. Native sample buffer containing 20 mM Tris (pH8.0), 150 mM NaCl, 5 % Glycerol (v/v), and 4 % bromophenol blus was added to protein mixture before running. The native gel electrophoresis was performed at constant 80 Volt for 13 hr in 4°C on ice bath. The gel was stained by Coomassie blue and then destained to reveal the results.

Imidazole-SDS-zinc staining

After native electrophoresis, the gel was rinsed in distilled water for 30 to 60 s and then soaked in 100 mL solution containing 0.2 M imidazole and 0.1% SDS for 15 min. The solution was discarded, and the gel was immersed in 50–100 mL solution containing 0.2 M zinc sulfate or zinc chloride for 15 to 60 s until gel background became deep white. The staining was stopped by discarding the zinc solution and rinsing the stained gel with distilled water. (Three times, 5 s for each)

In the experiment determining the stoichiometry of FERM/Plexin complex on native gel, the complex band was cut out from the imidazole-SDS-zinc stained gel. This gel piece was soaked in mobilization buffer containing 25 mM Tris and 192 mM glycine for 5 to 10 min until the gel pierce became completely transparent.

GST pull-down assay

20 μg of GST-JM baits were pull downed by 40 μL (50 %) glutathione sepharose (GE Healthcare) in the GST-binding buffer containing 20 mM HEPES (pH=7.5), 500 mM NaCl, 5 % Glycerol (v/v), 5 mM EDTA, 0.5 % NP-40 (v/v), and 2 mM DTT. FERM domains were incubated with GST-JM baits at 3:1 molar ratio at 4°C for 1 hr on the end-over-end rotator. The glutathione sepharose was then spin down and washed with 1 mL GST-binding buffer for 3 times. Each wash was incubated at 4°C for 5 min on the end-over-end rotator. The buffer was removed after the last wash and 2X SDS sample buffer was added to beads. The sample was heated at 95°C for 5 min, and half of the supernatant was loaded for SDS gel electrophoresis. The gel was stained by Coomassie blue and then destained to reveal the results.

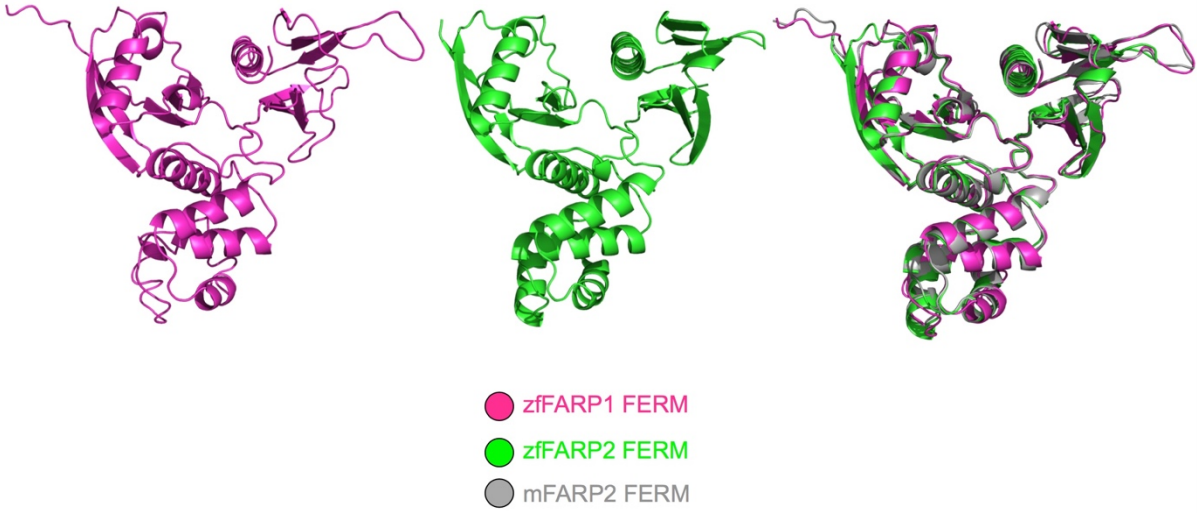

Figure 3-1. Crystal structures zebrafish FARP1 and FARP2 FERM domain.

Left, crystal structure of FERM domain of zebrafish FARP1. Middle, crystal structure of FERM domain of zebrafish FARP2. Right, superimposition of FERM domain structures of zfFARP1, zfFARP2, and mFARP2.

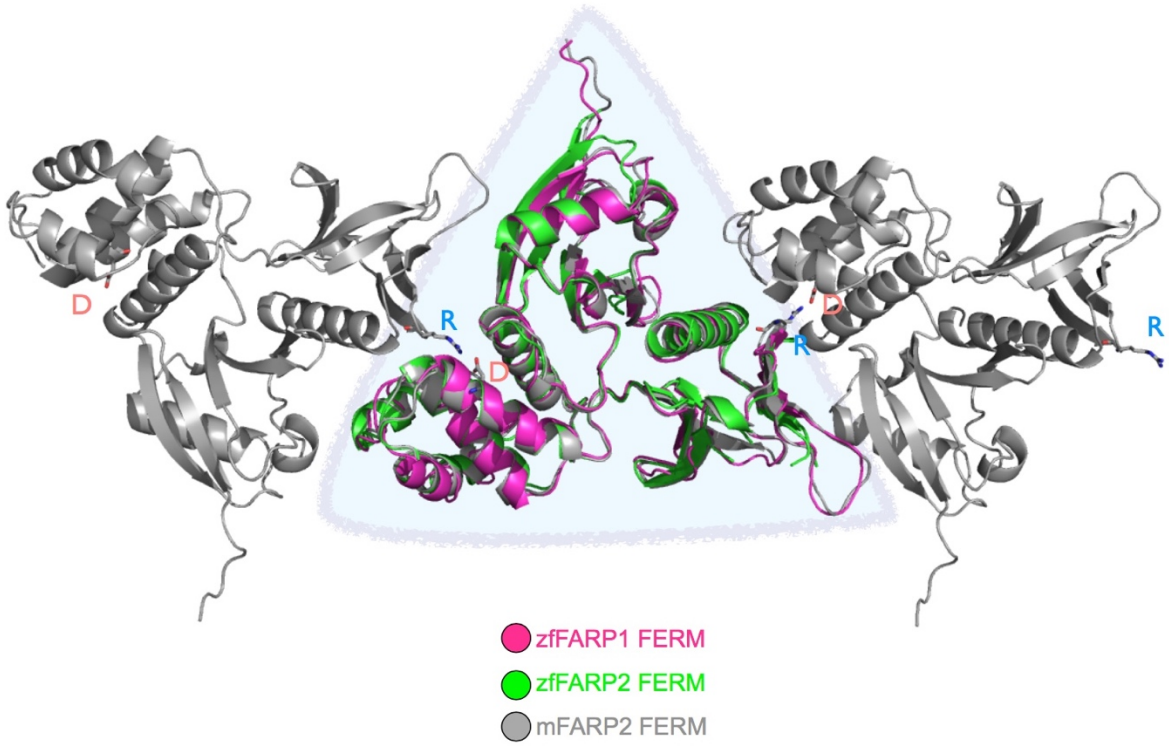

Figure 3-2. Head-to-tail oligomerization pattern is found the FERM crystal lattice.

Highly conserved residues of FERMs among different species form charge-dependent oligomerization interfaces observed in crystal lattices. R: Arg residue; D: Asp residue.

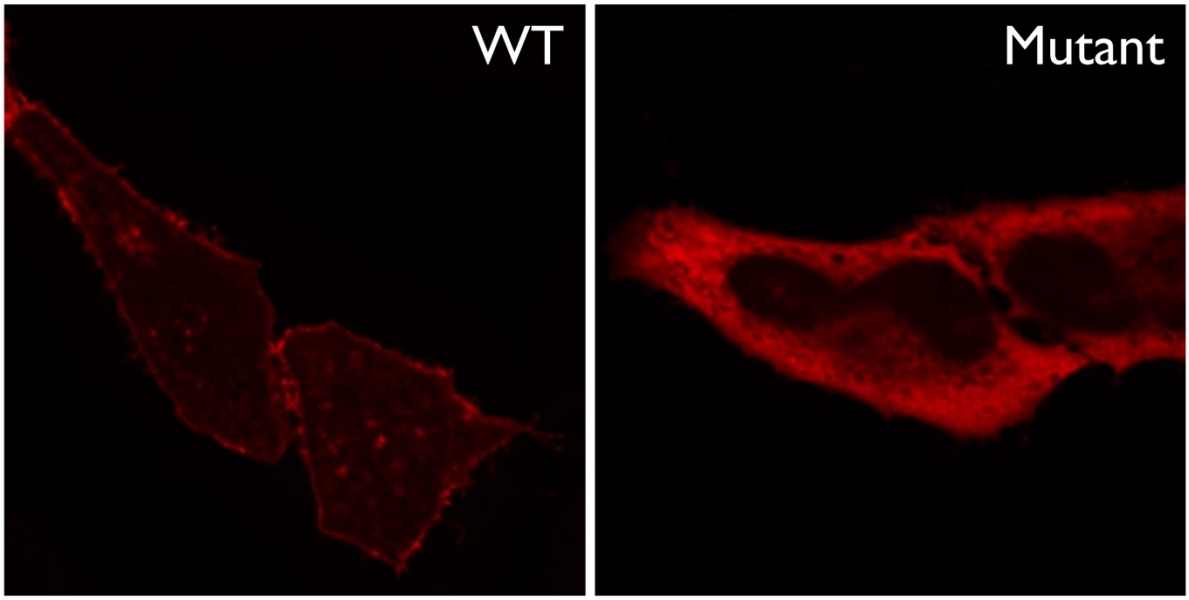

Figure 3-3. Confocal microscopy showed the membrane location of FARP1.

FLAG-tagged FARP1 wild type (WT) or R273E/K274E (Mutant) was transfected to HeLa cells. 16 hr after transfection, the cells were subjected to immunofluorescence with anti-FLAG tag and confocal microscope imaging.

Note: The confocal microscopy imaging was performed by Dr. Yu-Ju Chen in Dr. Jen Liou's laboratory at UTSW.

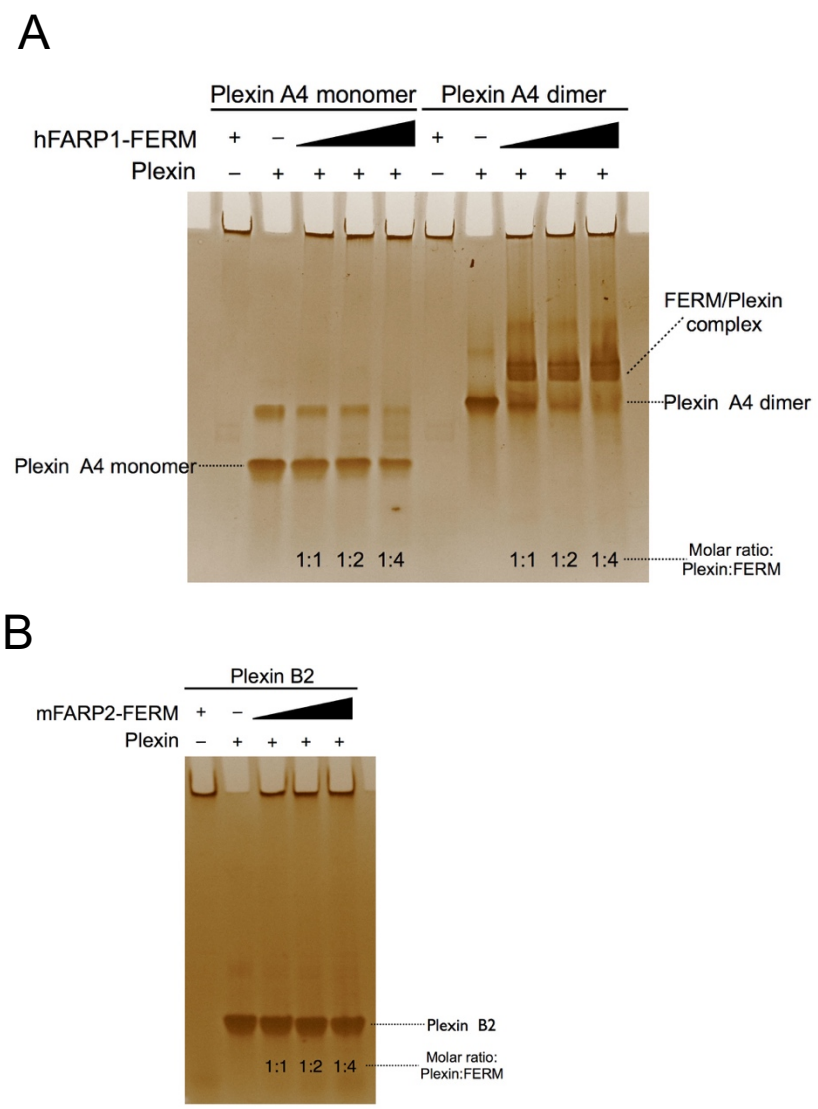

Figure 3-4. Native gel electrophoresis to detect the interaction of FERM and Plexin.

(A) Left, native gel electrophoresis result of Plexin A4 monomer with increasing amount of hFARP1-FERM. Right, native gel electrophoresis result of Plexin A4 dimer with increasing amount of hFARP1-FERM. The gel was stained with Coomassie blue staining.

(B) Native gel electrophoresis result of Plexin B2 with increasing amount of hFARP1-FERM. The gel was stained with Coomassie blue staining.

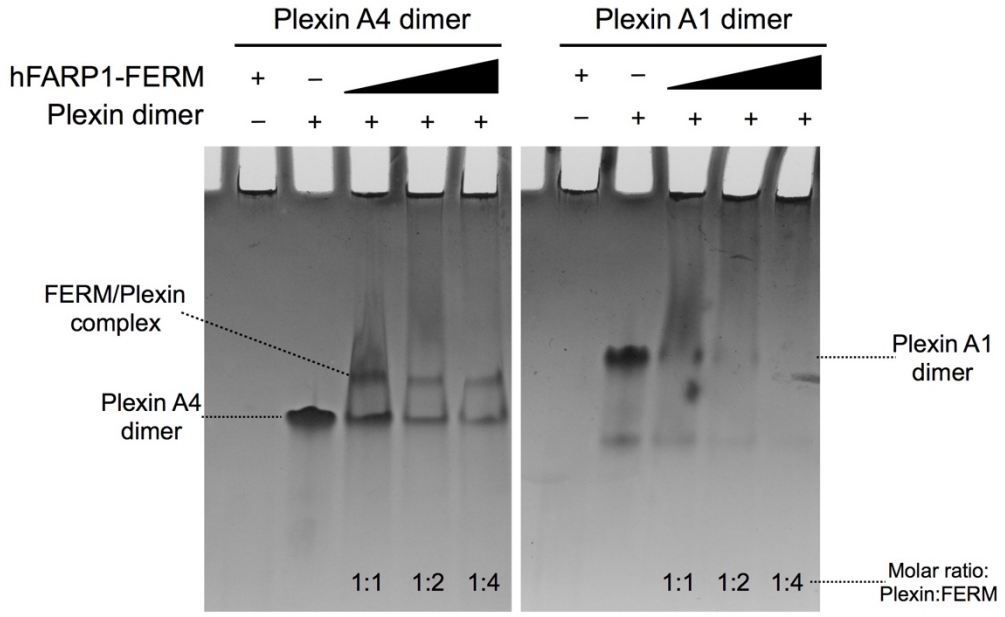

Figure 3-5. Some FERM formed extra band with Plexin dimer whereas some depleted Plexin on native gel electrophoresis.

Left, native gel electrophoresis result of Plexin A4 dimer with increasing amount of hFARP1-FERM. Right, native gel electrophoresis result of Plexin A1 dimer with increasing amount of hFARP1-FERM. The gels were stained with Coomassie blue staining.

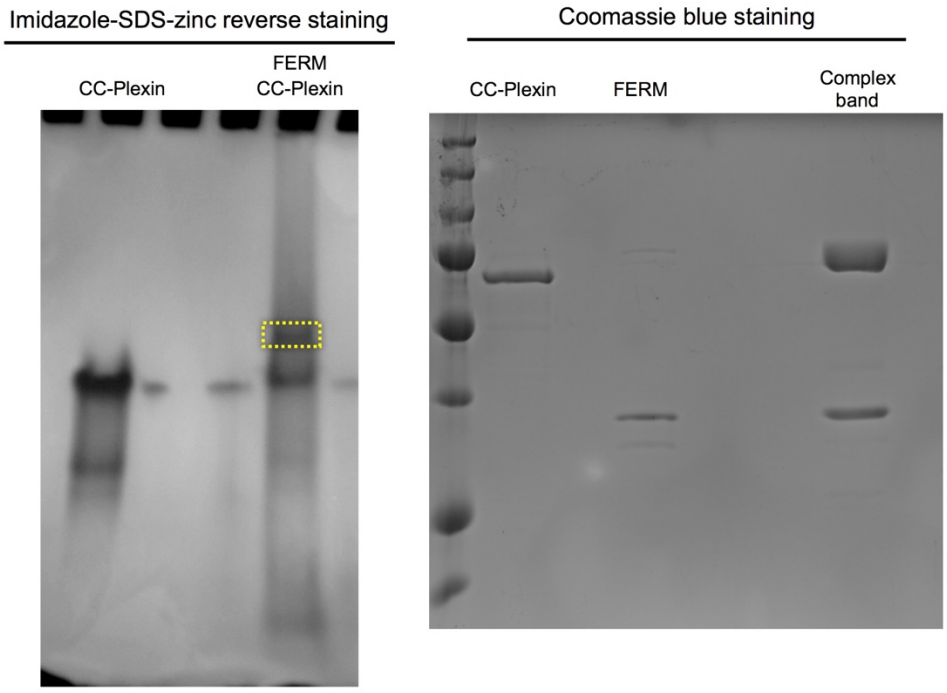

Figure 3-6. Imidazole-SDS-zinc reverse staining to identify the stoichiometry of the FERM/Plexin complex.

Left, native gel electrophoresis result of FERM from hFARP1 with CC-Plexin A4. The gel was stained with Imidazole-SDS-zinc reverse staining. Dotted rectangle indicated the complex band of FERM/Plexin.

Right, SDS-PAGE result of the complex band cut from native gel (dotted rectangle) together with CC-Plexin and FERM at 1:1 molar ratio. The intensity of bands were quantified using ImageJ (Schneider et al., 2012).

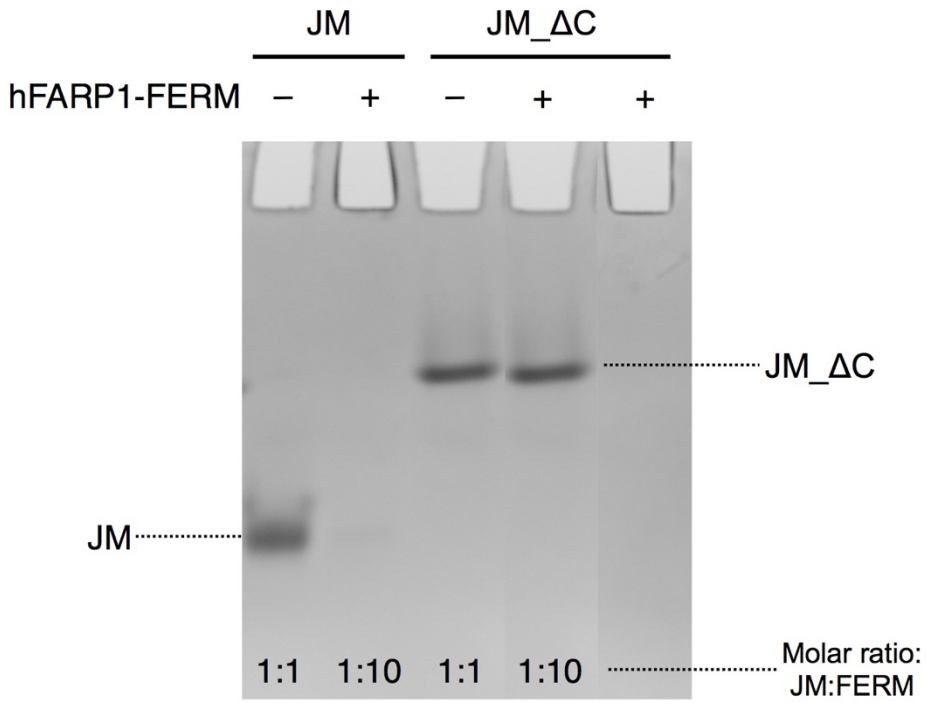

Figure 3-7. Native gel electrophoresis showed the interaction of C-terminal half of Plexin JM helix and hFARP1 FERM.

Native gel electrophoresis result of excessive hFARP1-FERM incubated with CC-JM helix (JM) or CC-JM lacking C-terminal half (JM_ΔC). The gel was stained with Coomassie blue staining.

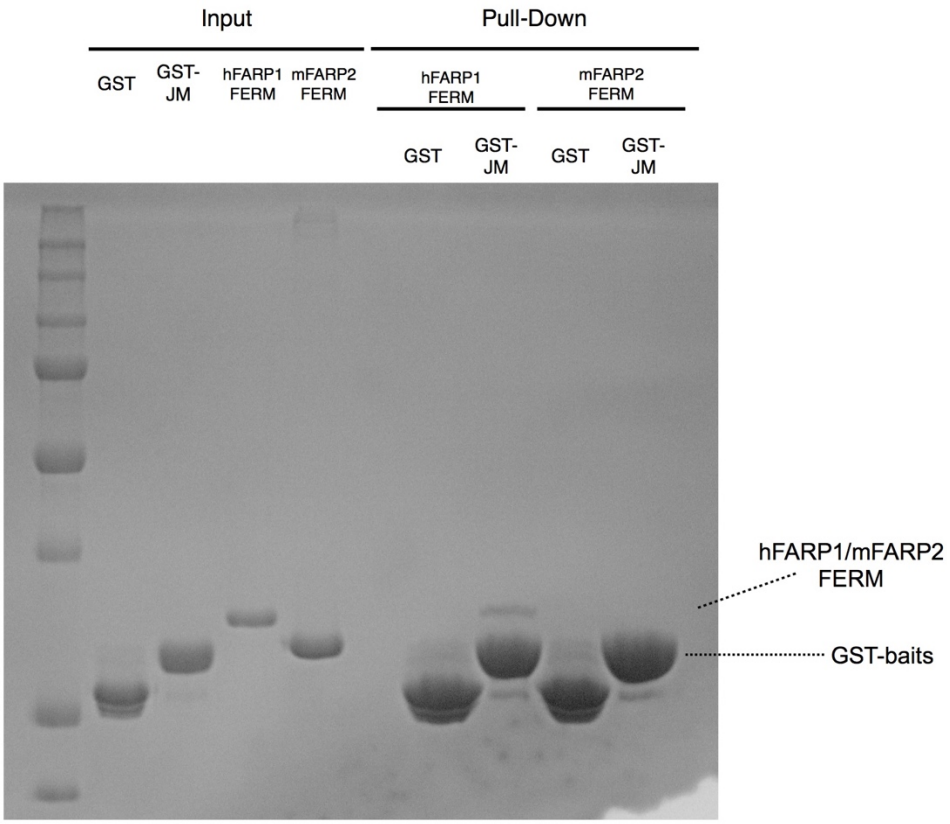

Figure 3-8. GST pull-down result to examine the interaction between Plexin JM and FERM from hFARP1 or mFARP2.

GST pull-down result of GST-JM incubated with hFARP1-FERM or mFARP2-FERM. The gel was stained with Coomassie blue staining.

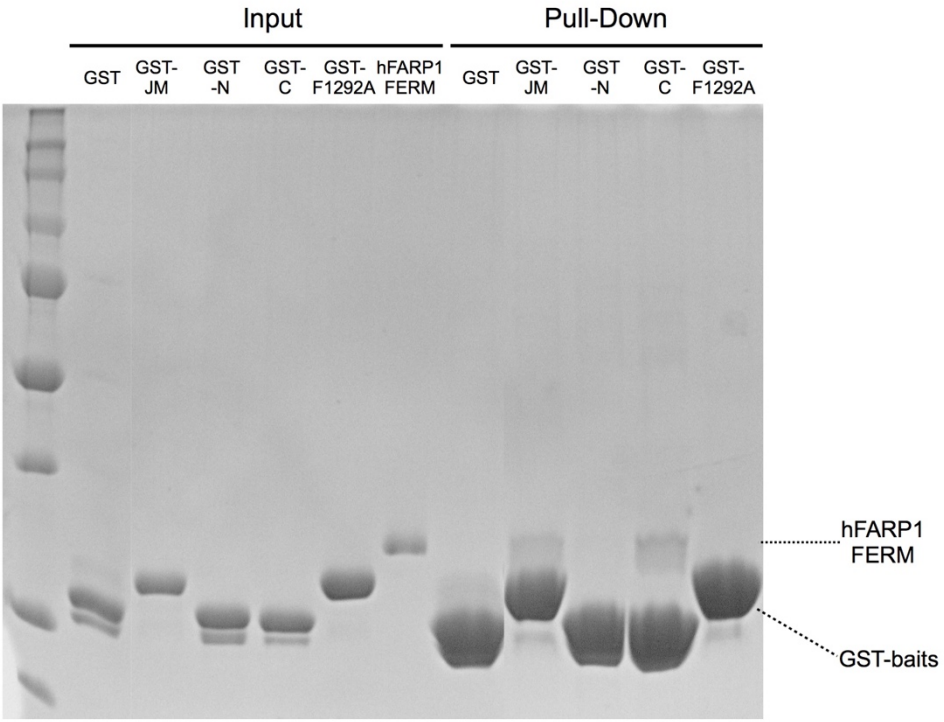

Figure 3-9. GST pull-down result to characterize the interaction between Plexin JM and FERM.

GST pull-down result of GST-JM variants incubated with hFARP1-FERM. The gel was stained with Coomassie blue staining. GST-JM: GST-fused full-length JM of Plexin; GST-N: GST-fused N-terminal half of JM; GST-C: GST-fused C-terminal half of JM; GST-F1292A: GST-fused JM harboring F1292A mutation.

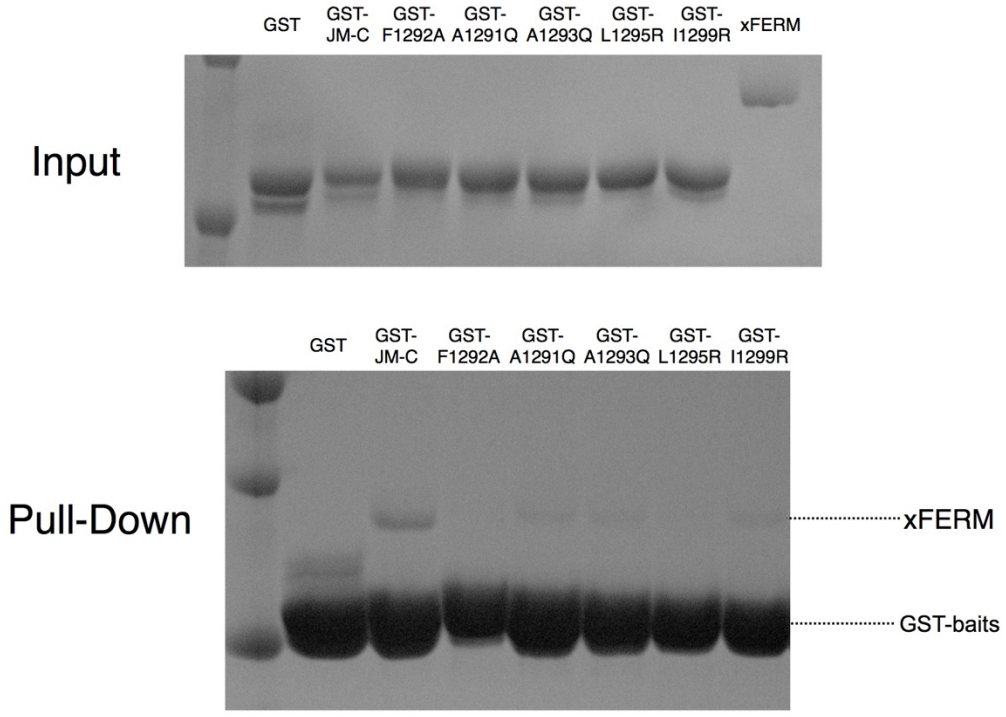

Figure 3-10. GST pull-down result to characterize the interaction between Plexin JM-C and FERM.

GST pull-down result of GST-JM-C variants incubated with xFARP1-FERM. The gel was stained with Coomassie blue staining. GST-JM-C: GST-fused C-terminal half of JM; GST-F1292A: GST-fused JM-C with F1292A mutation; GST-A1291Q: GST-fused JM-C with A1291Q mutation; GST-A1293Q: GST-fused JM-C with A1293Q mutation; GST-L1295R: GST-fused JM-C with L1295R mutation; GST-I1299R: GST-fused JM-C with I1299R mutation.

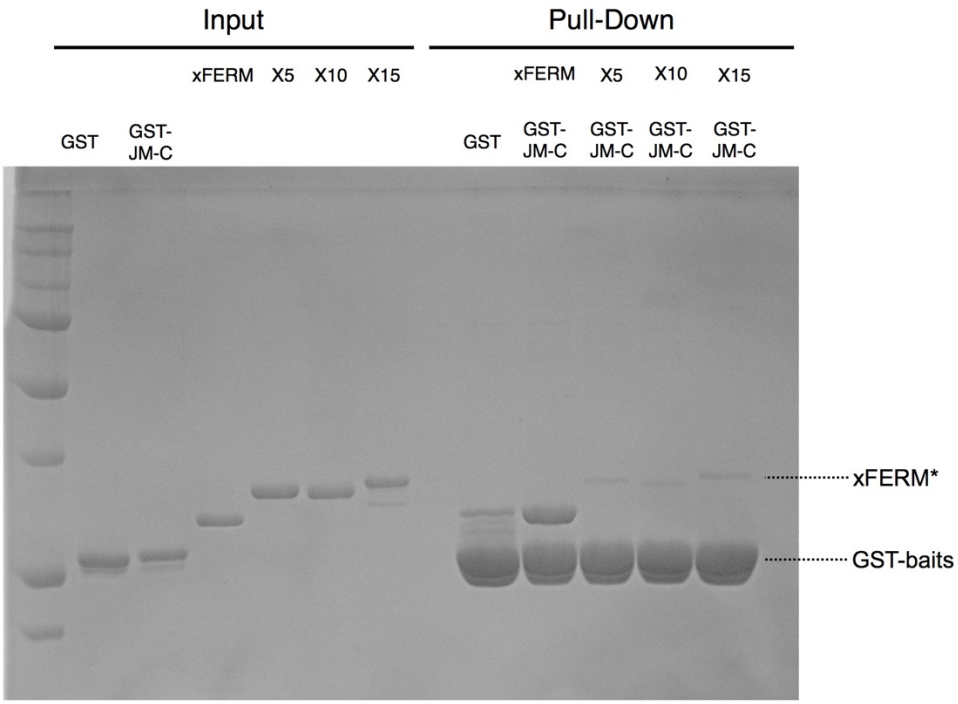

Figure 3-11. GST pull-down result to compare the intramolecular interaction of fusion proteins of JM-C/FERM with different linker length.

GST pull-down result of JM-C/xFERM fusion harboring 5- (X5), 10- (X10), or 15- (X15) residue linker to GST-JM-C. The gel was stained with Coomassie blue staining. GST-C: GST-fused C-terminal half of JM; xFERM: xenopus FARP1 FERM; xFERM*: xenopus FARP1 FERM fused with JM-C.

Table 3-1. Crystallization trials for FERM/Plexin complex

	mFARP2_324_R277E	hFARP1_FA	hFARP1_FA_R273E	zfFARP2_FA	hFARP2_FA	mFARP2_FA	FRMD7_FA	FARP1_321-381	FRMD7_281-328	zfFARP1_FA	xenoFARP1_FA	hFARP1_D212N	mFARP2_D216N	zfFARP2_D216N
A1ccLm1	X	X (4°C) FERM alone X (RT)	X	X	X		X		X	X	X (RT)			
A1ccLm1_4Δ			X (4°C)	X	X	X	X (4°C)			X (4°C)	X (RT)	X	X	X
A4ccLm1_4Δ	A4 octamer	X (4°C) FERM alone X (RT)	X	No binding	X		X A4 alone; X with pure FRMD7	X	X	X	X (RT)	X	X	X
A1ccLm4	X	X (4°C)	X (4°C)											
A4ccLm4	X some tiny crystals at pH6	X (4°C)	X (4°C)											
A2ccLm1	X													
zfA3ccLm1			X	X										
zfC1ccLm1							X							
A1	X		X	X	X		X		X				X	
A4	X	X	X	No binding	X		X	X					X	
A2					X		X						X	
zfA3				X										
A1_E1488R														
A4_E1486R		X												
Δ6_CC_A4_N-helix												X	X	X
CC_A4_N-helix													X	

h: human; m: mouse; zf: zebrafish; xeno: xenopus.

FA: FERM adjacent region

Table 3-2. Data collection and refinement statistics of zfFARP2-FERM

Data collection	
Space group	P 21 21 21
Cell dimensions	
a, *b*, *c* (Å)	35.377 82.723 96.015
a,*b*,*g* (°)	90, 90, 90
Resolution (Å)	32.53 - 1.999 (2.071 - 1.999)*
*R*sym (%)	10.4 (71.4)
I/σ*I*	31.18 (1.76)
Completeness (%)	98.9 (88.3)
Redundancy	7.2 (3.8)
Refinement	
Resolution (Å)	2.00
No. reflections	19499
*R*work/ *R*free (%)	21.8 (27.3)/26.0 (34.9)
No. atoms	2244
Protein	2107
Ligand/ion	
Water	137
B-factors	30.8
Protein	30.5
Ligand/ion	0
Water	35.8
R.m.s deviations	
Bond lengths (Å)	0.008
Bond angles (°)	1.24
Ramanchandran plot	
Favored (%)	97
Allowed (%)	1.8
Disallowed (%)	1.2

*Highest resolution shell is shown in parenthesis.

Table 3-3. Data collection and refinement statistics of zfFARP1-FERM

Data collection	
Space group	P 21 21 21
Cell dimensions	
a, *b*, *c* (Å)	56.031, 59.436, 97.462
a,*b*,*g* (°)	90, 90, 90
Resolution (Å)	40.77 - 2.994 (3.082 - 2.976)*
*R*sym (%)	13.8 (93.0)
I/σ*I*	12.25 (1.67)
Completeness (%)	99.6 (100)
Redundancy	11.6 (11.9)
Refinement	
Resolution (Å)	3.00
No. reflections	7005
*R*work/ *R*free (%)	22.67 (32.75)/28.99 (30.30)
No. atoms	2232
Protein	2232
Ligand/ion	
Water	0
B-factors	76.6
Protein	76.6
Ligand/ion	
Water	
R.m.s deviations	
Bond lengths (Å)	0.003
Bond angles (°)	0.72
Ramanchandran plot	
Favored (%)	94
Allowed (%)	5.63
Disallowed (%)	0.37

*Highest resolution shell is shown in parenthesis.

CHAPTER FOUR :

CRYSTAL STRUCTURE OF RHOD/PLEXIN COMPLEX

CANONICAL BINDING MODE WITH ROTATIONAL SHIFT

Summary

The Semaphorin–Plexin signaling is a repulsive axon guidance signal (Kruger et al., 2005). Binding of Semaphorin to the Plexin receptor induces the dimerization of Plexin and stimulates its GAP activity towards Rap (Wang et al., 2012). Plexin activity is antagonistically regulated by two types of small GTPases: Rnd1 boosts Plexin-mediated cell collapse whereas RhoD inhibits collapse (Zanata et al., 2002).

In order to understand the mechanism by which RhoD inhibits Plexin activation, we determined the crystal structure of a RhoD/Plexin-RBD complex. RhoD interacts with Plexin-RBD in the canonical mode, using the switch II region to form several hydrophobic interactions with RBD. A superimposition of our structure with the Rnd1/PlexinB1-RBD complex (PDB ID: 2REX) based on the RBDs reveals that RhoD has a slight but interesting difference to Rnd1. In the switch II region of Rnd1, the key residue interacting with the RBD domain of Plexin is a Cys, while the corresponding residue in RhoD is a Phe. This bulky Phe of RhoD pushes the switch II away from the RBD. This slight deviation in the switch II

region of RhoD is propagated to the whole protein, leading to a rotational difference in the binding mode. Modeling the structure of RhoD/Plexin-RBD with the Plexin active dimer structure (PDB ID: 4M8M) (Wang et al., 2013) implies that the rotational change pushes up RhoD towards the plasma membrane, leading to unfavorable interactions of two Glu residues with the plasma membrane. Our RhoD/Plexin structure suggests that these unfavorable interactions prevent the formation of Plexin active dimer, which underlies inhibition of Plexin by RhoD.

Introduction

The structure of the intracellular region of Plexin is divided into three portions, JM helix, GAP domain, and RBD domain. The existence of the RBD suggests the potential roles that RhoGTPases may play to regulate Semaphorin-Plexin signaling. In 2002, (Zanata et al., 2002) found that two types of RhoGTPases regulated Plexin signaling using COS7 collapse as the readout for Plexin activity: Rnd1/Rac1 overexpression boosted Plexin-mediated COS7 collapse in the absence of Semaphorin whereas RhoD overexpression inhibited Semaphorin-induced collapse. The complex structure of Rac1 bound Plexin A1 solved by our laboratory (PDB ID: 3RYT) showed that Rac1 binding to the RBD domain of Plexin did not induce a significant conformational change to enzymatic GAP domain. Besides, the addition of purified Rac1 or Rnd1 to purified Plexin in solution did not boost the GAP activity of Plexin. These observations exclude the possibility that Rac1 binding allosterically affects the GAP activity of Plexin.

After the active dimer structure of Plexin was revealed by our laboratory, the regulation of Rnd1 and RhoD on Plexin could be reconsidered in another perspective. Modeling the structures of inactive monomer and active dimer of Plexins on the plasma membrane revealed that Rnd1 binding to RBD could potentially facilitate the formation of active dimer because the backside of Rnd1 contains a positive-charged patch that favors interactions with the plasma membrane. This Rnd1/Plexin model brings another puzzling question: how come the structurally similar RhoD exerts opposite effect on Plexin activity? We interrogated this question from the structural perspective.

Results

Crystal structure of the RhoD-bound Plexin

GST pull-down assay as the platform to screen for the best pair of RhoD and Plexin

This study started from a previous student in our laboratory. I together with him designed the GST pull-down system to systemically screen for the Plexin showing the strongest binding to RhoD. We fused human RhoD with GST, expressed and purified it. Because the previous student has shown this interaction is GTP-dependent, the RhoD construct that we used has the Q75L mutation to remove the hydrolysis activity of RhoD. Meanwhile, the RhoD protein would be exchanged with GTP before subjected to test the binding with Plexins. In order to verify the detected binding is specific, we applied excessive His-tagged RhoD to compete with GST-RhoD; The pull-down Plexins would not remain with GST-RhoD if the binding is specific.

RhoD showed the strongest interaction with Plexin B2 (Figure 4-1). We further tested whether this binding depends on GTP/GDP state of RhoD by competing the GST-RhoD with GTP- or GDP-bound His-tagged RhoD. The result showed that the interaction between RhoD and Plexin B2 is GTP-dependent. (Figure 4-2) We hence set up crystallization trials with this combination. The combination of RhoD and Plexin B2 was crystallized; however, the crystals were difficult to reproduce. Diffractable crystals appeared around a month after the trays were set up. In order to reproduce and obtain diffractable crystals for data collection, I made several deletions on Plexin B2 and examined their interaction with RhoD. All the deletion constructs showed similar binding to RhoD as the wild-type Plexin B2 did (Figure 4-3); however, the diffractable crystals were still hard to reproduce.

The crystal structure of RhoD-bound Plexin B2

The resolution of the best dataset reached 3.0 Å. The complex structure was solved by molecular replacement using Plexin B2 (PDB ID: 5E6P) and RhoD (PDB ID: 2J1L) as search models. The statistics of this crystal structure is listed in Table 4. Surprisingly, the crystal structure only contains two RhoD bound RBD domains of Plexin B2 in the asymmetric unit. The GAP domain of Plexin B2 was probably chopped off and proteolyzed. RhoD interacted with the RBD domain as the canonical binding mode (Figure 4-4 and Figure 4-5). The two RBD domains in the asymmetric unit formed domain-swapping dimers; N-terminal halves of both RBD domains dimerized with C-terminal halves of the other RBD domains to assemble into intact RBD domains in the asymmetric unit. The domain-swapping

RBD domains were bolstered by two unexpected disulfide bonds formed between Cys1508 and Cys1510 from one another RBD molecule (Figure 4-5). All above facts in part explained why the crystals were so difficult to be reproduced and took a long time to grow.

In the crystal structure, RhoD interacts with Plexin B2 RBD using the switch II region as the canonical mode of RhoGTPase binding to effectors. Although this is a canonical binding mode, this binding is unanticipated before the structure. Sequence alignment of Rnd1, Rac1, and RhoD showed that the residue in switch II critical for RBD binding is a smaller residue in Rnd1 and Rac1; Cys in Rnd1 and Ser in Rac1. Bulky Phe85 in the corresponding position made us think that RhoD could not accommodate the same binding mode. Superimposition of the structure of RhoD bound RBD with Rnd1 bound RBD (PDB ID: 2REX) on the basis of RBD showed that the bulky Phe in the switch II of RhoD pushes switch II deviating from Rnd1. The switch II deviation is propagated to the rest of RhoD to rotate RhoD (Figure 4-6). This rotation of RhoD is modest but important because RhoD is leveraged by this rotation. Modeling of RhoD bound RBD on the basis of Plexin active dimer in the plasma membrane context revealed that switch II deviation pushes RhoD towards the plasma membrane. This upward RhoD leads to unfavorable interactions between Glu149/Glu158 and plasma membrane. We hypothesized that these unfavorable interactions propel RBD away from the plasma membrane and prevent Plexin from dimerization. (Figure 4-7)

Experiments for testing this hypothesis

Superimposition of Rnd1-bound and RhoD-bound RBD suggests that Rnd1 binding could perfectly fit into the space between RBD and plasma membrane. The positive-charged residues, Lys133 and Lys157, in the backside relative to switch regions of Rnd1 interact with the plasma membrane. Binding of switch regions to RBD and attaching the backside to the plasma membrane led us to propose that Rnd1 potentiates Plexin signaling through carrying Plexin to better geometry for forming the active dimer. Following this hypothesis, the mechanism by which RhoD blocks Plexin signaling could be resulted from the disadvantageous geometry for Plexin active dimer because of the unfavorable repulsion from the plasma membrane. (Figure 4-7)

In order to test this hypothesis, several strategies are ongoing to be applied. A previous study has shown RhoD shut down Semaphorin-induced CO7 collapse (Zanata et al., 2002). I will employ the COS7 cell collapse assay to record the inhibition effect by RhoD. Mutation of the bulky Phe85 in the switch II to smaller residues and charge-reversal mutation of the membrane repulsive negative-charged residues, Glu149 and Glu158, will be tested to inspect whether the inhibition effect of RhoD is destroyed by these mutations. Increasing the space between the plasma membrane and RBD of Plexin through extending the juxtamembrane helix of Plexin will also be tested to investigate whether decreasing the bumping of RhoD to the plasma membrane could break the inhibition effect. Finally, I will also examine whether I could turn Rnd1 from the signaling booster to inhibitor by mutating the potential membrane-associating residues, Lys133 and Lys157 to glutamines, perhaps combining C81F mutation, where Cys81 is the corresponding residue of Phe85 in RhoD.

Materials and Methods

Protein Expression and Purification

Expression and purification of intracellular region of mouse Plexins

The coding regions of the intracellular region of mouse Plexin A1 (residues 1269–1894), A2 (residues 1264–1894), B1 (residues 1500–2119), B2 (residues 1228–1842), B2_3Δ (residues 1228–1842; deletion of residues 1228–1274, 1613–1617, and 1839–1842), B2_4Δ (residues 1228–1842; deletion of residues 1228–1274, 1613–1617, 1839–1842, and 1578–1583), B2_4Δ* (residues 1228–1842; deletion of residues 1228–1274, 1613–1617, 1839–1842, and 1604–1608), B2_5Δ (residues 1228–1842; deletion of residues 1228–1274, 1613–1617, 1839–1842, 1578–1583, and 1604–1608), B3 (residues 1260–1902), C1 (residues 975–1571), and D1 (residues 1297–1916) were cloned into pSKB2 vector. Point mutations were introduced by QuikChange reactions; deletions were introduced by two-step PCR procedure. The plasmids were transformed into the *E. coli* strain ArcticExpress (Stratagene). ArcticExpress carrying individual expression plasmid was cultured at 37°C in 100~120 mL LB in the presence of Gentamycin overnight. The bacteria cells were scaled up at 30°C to reach OD_{600}=2.0 in TB. Protein expression was induced by 0.2 mM IPTG at 10°C overnight.

After centrifugation, the bacteria cells were re-suspended in the Ni-lysis buffer containing 10 mM Tris (pH 8.0), 500 mM NaCl, 5 % glycerol (v/v), 20 mM Imidazole, and 3 mM β-mercaptoethanol. The bacteria resuspension was passed through the cell disruptor for 3~4

times on ice, and then the lysates were subjected to centrifugation. The supernatant was then filtered by 0.45 μM PVDF membrane to get rid of debris. The proteins were purified using a 1 mL HisTrap column, eluted by Ni-B buffer and treated with recombinant human rhinovirus 3C protease at 4°C overnight to remove the N-terminal tag.

The protein was further purified by using Resource Q anion-exchange chromatography with a 10 mM to 300 mM NaCl gradient elution. Fractions were examined by SDS-PAGE electrophoresis and Coomassie blue staining. Fractions containing Plexin B2 were pooled together and subjected to exchange buffer to 20 mM Tris (pH 8.0), 150 mM NaCl, 10% glycerol (v/v), and 2 mM DTT through Superdex 200 GL 10/30 chromatography. Purified proteins were concentrated and stored at −80°C.

Expression and purification of human RhoD

The coding regions of human RhoD (residues 8–194) was cloned into pSKB2 and pGEX-6P-1 (GE Healthcare) vector, respectively. Point mutations were introduced by QuikChange reactions. The plasmids were transformed into the *E. coli* strain BL21 (DE3). BL21 (DE3) carrying individual expression plasmid was cultured at 37°C to reach OD_{600}=2.0 in TB. Protein expression was induced by 0.2 mM IPTG at 16°C overnight.

For His_6-tagged RhoD purification, after centrifugation, the bacteria cells were re-suspended in the Ni-lysis buffer containing 10 mM Tris (pH 8.0), 500 mM NaCl, 5 % glycerol (v/v), 20 mM Imidazole, 2 mM $MgCl_2$, and 3 mM β-mercaptoethanol. The bacteria resuspension was passed through the cell disruptor for 3~4 times on ice, and then the lysates

were subjected to centrifugation. The supernatant was then filtered by 0.45 μM PVDF membrane to get rid of debris. The proteins were purified using a 1 mL HisTrap column, eluted by Ni-B buffer and treated with recombinant human rhinovirus 3C protease at 4°C overnight to remove the N-terminal tag. For GST-tagged RhoD purification, the lysed supernatant was passed through a 1 mL GSTrap column (GE Healthcare) and eluted by 10 mM glutathione-containing buffer. Both His_6-tagged and GST-tagged RhoD were further subjected to Superdex 200 GL 10/30 equilibrated with the buffer containing 20 mM Tris (pH 8.0), 250 mM NaCl, 10 % glycerol (v/v), 2 mM $MgCl_2$, and 2 mM DTT. Purified proteins were concentrated and stored at −80°C.

Exchange of GMP-PNP or GTP to RhoD protein

5 mg RhoD protein was exchanged with GMP-PNP for crystallization or GTP/GDP for binding assay. The procedure is identical as that described in the section of "*Exchange of GMP-PNP or GTP to Rif protein*".

GST pull-down assay

20 μg of GST-RhoD was pull downed by 40 μL (50 %) glutathione sepharose in the GTPase-binding buffer containing 20 mM HEPES (pH=7.5), 150 mM NaCl, 5 % Glycerol (v/v), 2 mM $MgCl_2$, 0.5 % NP-40 (v/v), and 2 mM DTT. Various Plexin intracellular regions were incubated with GST-RhoD at 3:1 molar ratio at 4°C for 1 hr on the end-over-end rotator. The glutathione sepharose was then spin down and washed with 1 mL GTPase-

binding buffer for 3 times. Each wash was incubated at 4°C for 5 min on the end-over-end rotator. The buffer was removed after the last wash and 2X SDS sample buffer was added to beads. The sample was heated at 95°C for 5 min, and half of the supernatant was loaded for SDS gel electrophoresis. The gel was stained by Coomassie blue and then destained to reveal the results.

Crystallization and Structure Determination of RhoD in complex with Plexin B2

The RhoD protein was purified and exchanged with non-hydrolysable GTP analogue, GMP-PNP (detailed procedure described in "*Exchange of GMP-PNP or GTP to RhoD protein*"). The total protein concentration for crystallization was 6 mg/mL. Intracellular region of Plexin B2 and RhoD were mixed at 1:1 molar ratio thus the concentration of Plexin B2 was 4.6 mg/mL and that of GMP-PNP-exchanged RhoD was 1.4 mg/mL. The two proteins were mixed in the buffer containing 10 mM Tris (pH=8.0), 150 mM NaCl, 10 % Glycerol (v/v), 2 mM $MgCl_2$, 2 mM TCEP, and 100 μM GMP-PNP. The protein mixture was subjected to crystallization trials. The complex crystals crystallized initially at 20 °C in 0.2 M $MgCl_2$ and 20 % PEG3350 (w/v) in sitting-drop 96-well plates. Larger crystals were grown by sitting-drop vapor diffusion or hanging drop vapor diffusion at 20°C in 0.2 M $MgCl_2$, 22 % PEG3350 (w/v), and 100 mM MIB (containing sodium malonate, imidazole, and boric acid at the 2:3:3 molar ratio. These three chemicals have three different buffering curves and their ratios have been selected to keep pH variation almost linear. The desired pH is obtained by mixing high- and low-pH stock solutions. Here the pH was adjusted to 6.8.). The crystals

were reproduced and grown at the 1:1 volume ratio of protein to crystallization solution. Large crystals appeared after trays were set up more than a month. Crystals were cryo-protected using the crystallization solution supplemented with 30 % glycerol and flash cooled in liquid nitrogen. Diffraction data were collected at −173°C on beamline 19ID at the Advanced Photon Source (Argonne National Laboratory). Data were indexed, integrated and scaled by using HKL2000 (Otwinowski and Minor, 1997). A 3.0 Å dataset in the $P3_1$ space group was collected and then converted to the mtz format by using the Reflection file editor module in the Phenix package (Adams et al., 2002; McCoy et al., 2007). The structure of Plexin B2 (PDB ID: 5E6P) and RhoD (PDB ID: 2J1L) were initially used as the molecular replacement search model using the Phaser module in the Phenix package. During the progress of molecular replacement, we found only the RBD domain but not the full-length Plexin B2 was in the asymmetric unit, we hence re-executed molecular replacement using RBD domain of Plexin B2 (PDB ID: 5E6P) and RhoD (PDB ID: 2J1L) as search model.

Iterative model building and structure refinement were performed by using the programs Coot and Phenix, respectively (Adams et al., 2002; Emsley and Cowtan, 2004). Detailed statistics of data collection and refinement are listed in Table XX. Molecular structure figures were rendered by the program Pymol (the PyMOL Molecular Graphics System, Schrödinger). Sequences were aligned by using MAFFT (Katoh et al., 2017) and rendered with ESPript (Gouet et al., 1999).

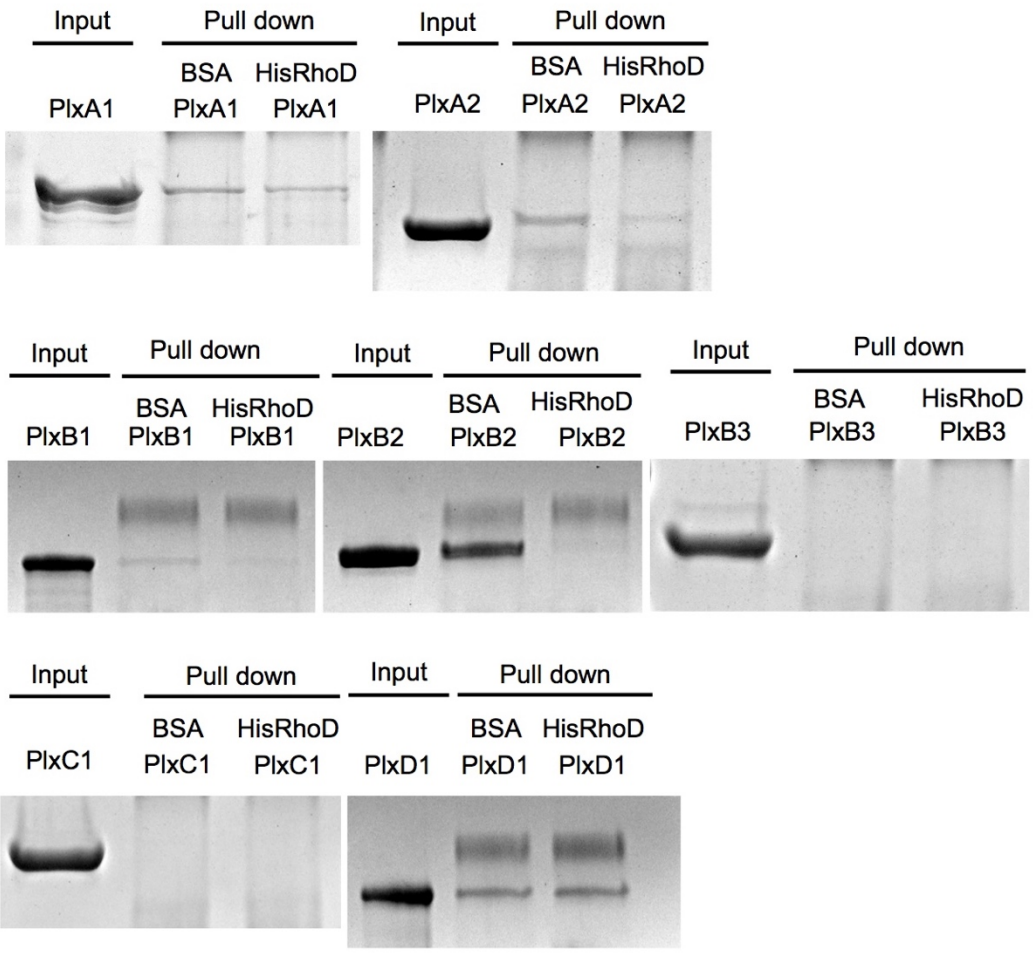

Figure 4-1. Screening for Plexins showing strong binding to RhoD using GST pull-down assay.

GST-RhoD was incubated with various Plexins in the presence of BSA or His-tagged RhoD to compete. BSA was used as a negative competitor. Detailed construct information is in Materials and Method.

Note: These pull-down assays were performed by a previous graduate student in our laboratory, Dr. Yuxiao Wang.

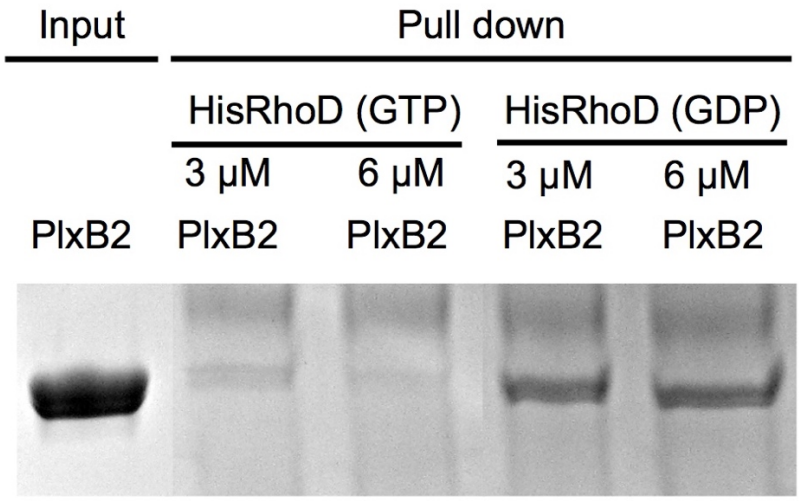

Figure 4-2. GTP/GDP dependence of RhoD binding to Plexin B2 in GST pull-down assay.

GST-RhoD was incubated with Plexin B2 in the presence of different concentrations of GTP- or GDP-bound His-tagged RhoD to compete.

Note: This pull-down assay was performed by a previous graduate student in our laboratory, Dr. Yuxiao Wang.

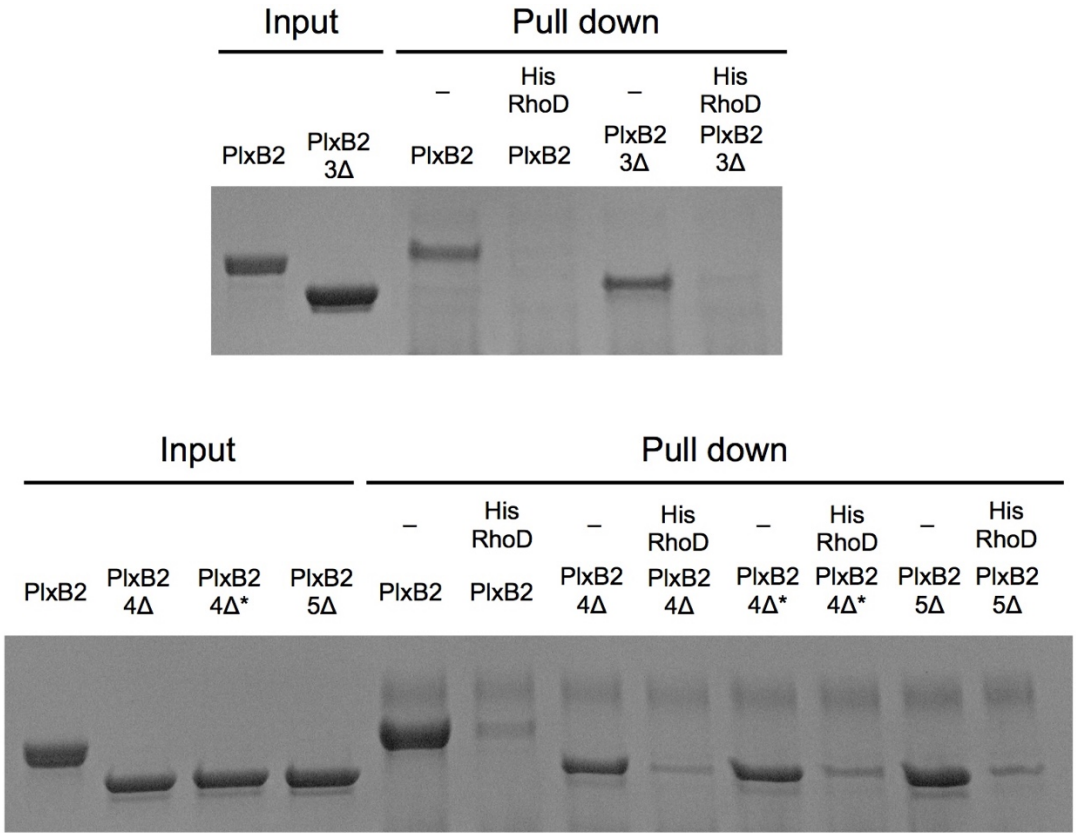

Figure 4-3. Examination of interaction of RhoD to Plexin B2 deletions variants in GST pull-down assay.

GST-RhoD was incubated with Plexin B2 with various deletions for assisting crystallization. His-tagged RhoD was incubated to compete. Detailed construct information is in Materials and Method.

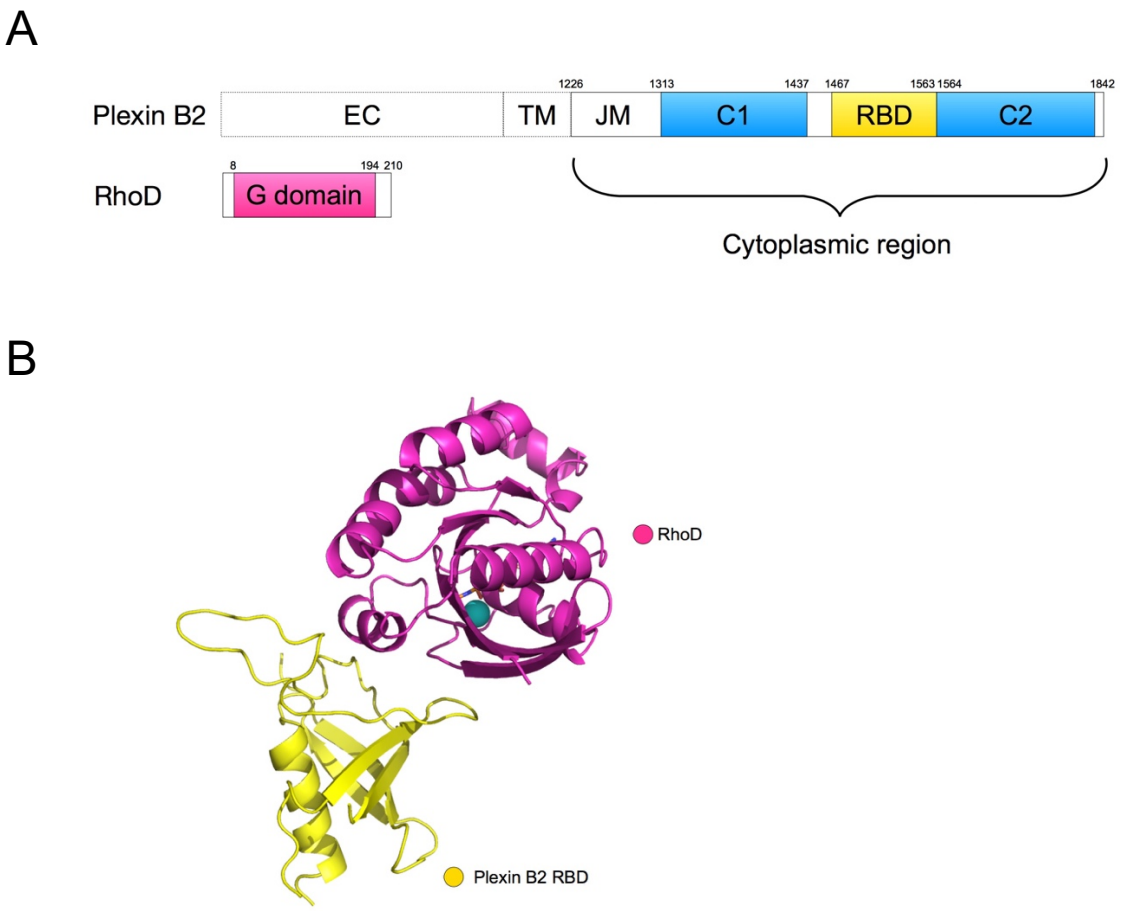

Figure 4-4. Crystal structure of RhoD in complex with Plexin B2.

(A) Domain architecture of Plexin B2 and RhoD. Residues numbers are based on mouse Plexin B2 and human RhoD, respectively. EC-region: extracellular region; TM: transmembrane region; JM: juxtamembrane segment. The C1 and C2 segments in plexin together form the GAP domain.

(B) Crystal structure of RhoD in complex with Plexin B2. Only RBD of Plexin B2 is present in the crystal to form complex with RhoD; GAP domain of Plexin B2 is degraded. Sticks represents the Rif-bound GMP-PNP. Sphere represents Mg^{2+} ion. The color scheme is the same as in A.

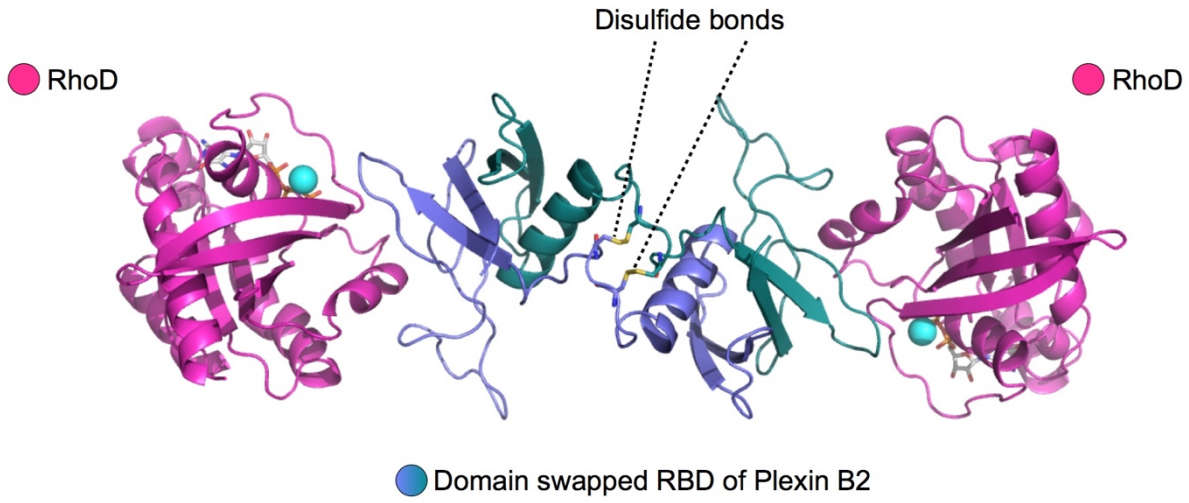

Figure 4-5. RBD domain of Plexin B2 swapped in the crystal structure.

Two RBD domains in the asymmetric unit form a domain-swapping dimer supported by inter-molecular disulfide bonds. Sticks represents the Rif-bound GMP-PNP. Sphere represents Mg^{2+} ion.

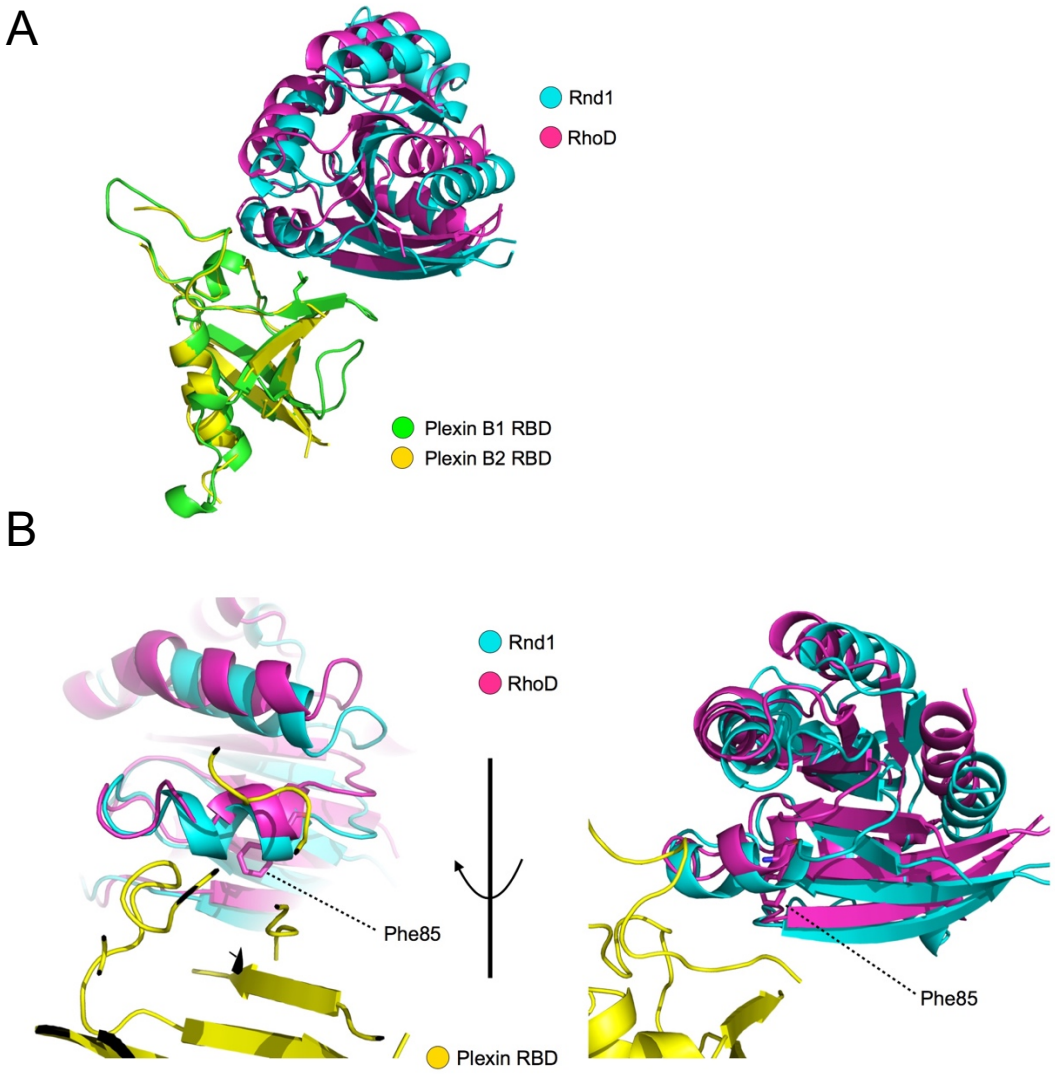

Figure 4-6. Superimposition of the structures of RhoD-RBD and Rnd1-RBD based on the RBD domain.

(A) Superimposition of the structures of RhoD-RBD and Rnd1-RBD based on the RBD domain shows a rotational movement of RhoD. (PDB ID of Rnd1-RBD: 2REX)

(B) The structure alignment of RhoD-RBD and Rnd1-RBD starts deviating from Phe85 of RhoD. This deviation is gradually propagated to the whole protein of RhoD, leading to the rotational difference.

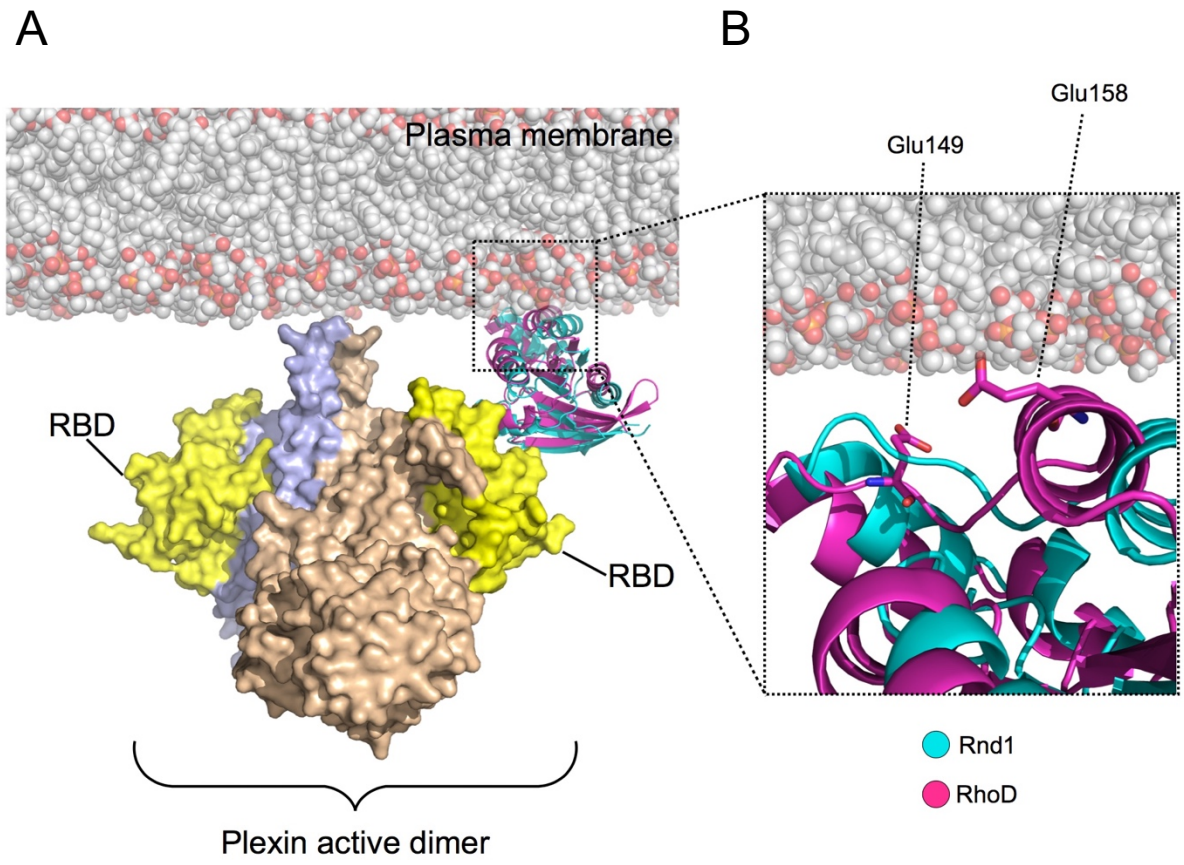

Figure 4-7. Modeling of the RhoD-RBD structure with the Plexin active dimer in the context of plasma membrane.

(A) Modeling of the RhoD-RBD structure with the Plexin active dimer shows that the rotational change pushes up RhoD towards the plasma membrane.

(B) Two negative-charged residues might prevent RhoD from associating with plasma membrane, forestalling the formation of Plexin active dimer.

Table 4-1. Data collection and refinement statistics of RhoD-Plexin B2-RBD

Data collection	
Space group	P 31
Cell dimensions	
a, *b*, *c* (Å)	82.81, 82.81, 136.761
a,*b*,*g* (°)	90, 90, 120
Resolution (Å)	39.63 - 3.101 (3.212 - 3.101)*
*R*sym (%)	12.8 (0)
I/σ*I*	18.62 (1.08)
Completeness (%)	97.0 (69.7)
Redundancy	5.3 (3.2)
Refinement	
Resolution (Å)	3.00
No. reflections	18920
*R*work/ *R*free (%)	21.11 (37.61)/26.03 (43.01)
No. atoms	4432
Protein	4356
Ligand/ion	68
Water	8
B-factors	124.5
Protein	124.7
Ligand/ion	112.5
Water	83.9
R.m.s deviations	
Bond lengths (Å)	0.003
Bond angles (°)	0.73
Ramanchandran plot	
Favored (%)	95
Allowed (%)	5
Disallowed (%)	0

*Highest resolution shell is shown in parenthesis.

CHAPTER FIVE :

CONCLUSIONS REMARKS

CONVERGENCE OF REGULATORS TO PLEXIN RECEPTORS

Dual role of FARP1 in regulating neuronal development

In this study, we dissected FARP1's function. FARP1 was previously thought to function through its GEF activity. In the apo-structure study of FARPs we reported in 2013, we have suggested FARPs might function as signaling scaffolds due to the lack of *in vitro* GEF activity and absence of the catalytic residue in the catalytic DH domain. This study corroborates the idea of signaling scaffold; the DH-PH1-PH2 adopts the same conformation as the apo-structure, and the concave surface area is utilized to interact with Rif, which can bind mDia via switch I and II to induce actin polymerization. Since FARPs were known to bind Plexin receptor, the structure of DH-PH1-PH2/Rif complex demonstrates how FARP1 bridges the extracellular and intracellular signals. Moreover, this structure also provides an explanation how FARP1 promotes dendrite extension and synapse formation: upon stimulation, the Plexin-bound FARP1 recruits Rif via its insert helix; the available switch I and II of Rif interact with mDia to induce actin

polymerization, thus resulting in dendrite outgrowth and dendritic spine formation. (Figure 5-1)

Although the complex of FERM/Plexin failed to crystallize, binding assays inspecting their interactions suggested that FERM binds to the C-terminal half of JM helix. The GAP activity of Plexin is stimulated through dimerization. Structure of Plexin active dimer shows that the C-terminal half of JM helix of Plexin is required for forming the dimer interface. Binding of FERM domain to the C-terminal half of the JM helix suggests that FERM may block Plexin dimerization. Our interaction results implied a novel function of FERM in addition to merely anchoring full-length FARP1 to Plexin receptor. More importantly, the function of the C-terminal DH-PH1-PH2 is to promote actin filament formation and cell outgrowth. Preventing Plexin from dimerization-induced activation by FERM ensures the coherent manner of cellular signaling as Plexin GAP activity induces cell collapse. (Figure 5) This study provides structural evidence supporting that FARP1 functions as a signaling regulator.

Role of RhoGTPases in regulating Plexin signaling

The existence of RBD in Plexin intracellular region suggests the important role of GTPases in regulating Plexin signaling. Revealing of the structures of Plexin inactive monomer and active dimer allows us to understand better how RhoGTPases may regulate Plexin activation in the context of the plasma membrane. Previous structural studies

showed that binding of Rac1/Rnd1 to Plexin did not induce a significant conformational change in the GAP domain. To uncover the long-standing puzzle: Rnd1 and RhoD exert the antagonistic effect in regulating Plexin activity, the missing structure of RhoD-bound Plexin is required. Our RhoD/Plexin B2 structure provides the missing piece. Modeling of our RhoD/RBD structure together with the reported Rnd1/RBD structure with the active dimer structure of Plexin in the context of membrane presents a hypothesis how structurally similar RhoD and Rnd1 achieve antagonistic regulation to Plexin. (Figure 4-7)

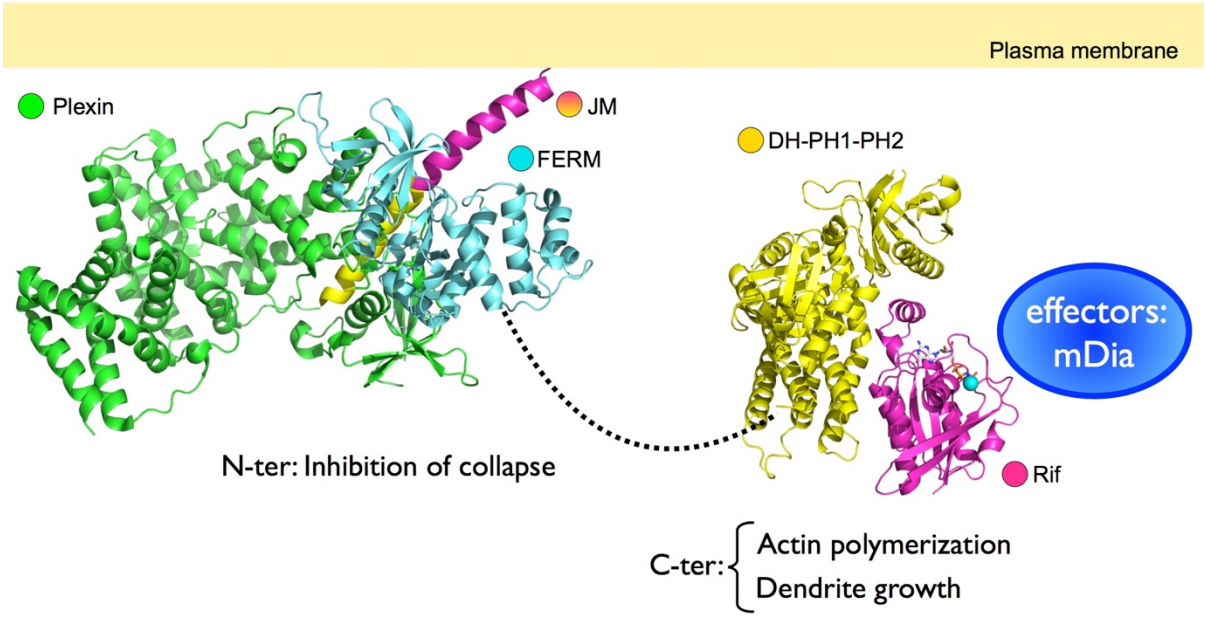

Figure 5-1. Proposed model of FARP1's function in promoting dendrite growth and synapse formation.

FARP1 switches the Semaphorin-Plexin signaling from repulsion to attraction through two mechanisms. The N-terminal FERM domain binds to the JM helix of Plexin, blocking its activation. The C-terminal DH-PH1-PH2 domains provide a docking site for recruiting Rif through the insert helix. The available switch I and switch II of Rif interact with downstream effectors such as mDia to induce actin polymerization, leading to dendrite growth and synapse formation.

BIBLIOGRAPHY

(1999). Unified nomenclature for the semaphorins/collapsins. Semaphorin Nomenclature Committee. Cell *97*, 551-552.

Adams, P.D., Grosse-Kunstleve, R.W., Hung, L.W., Ioerger, T.R., McCoy, A.J., Moriarty, N.W., Read, R.J., Sacchettini, J.C., Sauter, N.K., and Terwilliger, T.C. (2002). PHENIX: building new software for automated crystallographic structure determination. Acta Crystallogr D Biol Crystallogr *58*, 1948-1954.

Ahmad, K.F., and Lim, W.A. (2010). The minimal autoinhibited unit of the guanine nucleotide exchange factor intersectin. PLoS One *5*, e11291.

Antipenko, A., Himanen, J.P., van Leyen, K., Nardi-Dei, V., Lesniak, J., Barton, W.A., Rajashankar, K.R., Lu, M., Hoemme, C., Puschel, A.W*., et al.* (2003). Structure of the semaphorin-3A receptor binding module. Neuron *39*, 589-598.

Bell, C.H., Aricescu, A.R., Jones, E.Y., and Siebold, C. (2011). A dual binding mode for RhoGTPases in plexin signalling. PLoS Biol *9*, e1001134.

Bielnicki, J.A., Shkumatov, A.V., Derewenda, U., Somlyo, A.V., Svergun, D.I., and Derewenda, Z.S. (2011). Insights into the molecular activation mechanism of the RhoA-specific guanine nucleotide exchange factor, PDZRhoGEF. J Biol Chem *286*, 35163-35175.

Bishop, A.L., and Hall, A. (2000). Rho GTPases and their effector proteins. Biochem J *348 Pt 2*, 241-255.

Bokoch, G.M. (2003). Biology of the p21-activated kinases. Annu Rev Biochem *72*, 743-781.

Bos, J.L., Rehmann, H., and Wittinghofer, A. (2007). GEFs and GAPs: critical elements in the control of small G proteins. Cell *129*, 865-877.

Capparuccia, L., and Tamagnone, L. (2009). Semaphorin signaling in cancer cells and in cells of the tumor microenvironment--two sides of a coin. J Cell Sci *122*, 1723-1736.

Cheadle, L., and Biederer, T. (2012). The novel synaptogenic protein Farp1 links postsynaptic cytoskeletal dynamics and transsynaptic organization. J Cell Biol *199*, 985-1001.

Chen, Z., Guo, L., Sprang, S.R., and Sternweis, P.C. (2011). Modulation of a GEF switch: autoinhibition of the intrinsic guanine nucleotide exchange activity of p115-RhoGEF. Protein Sci *20*, 107-117.

Chhatriwala, M.K., Betts, L., Worthylake, D.K., and Sondek, J. (2007). The DH and PH domains of Trio coordinately engage Rho GTPases for their efficient activation. J Mol Biol *368*, 1307-1320.

Chrencik, J.E., Brooun, A., Zhang, H., Mathews, II, Hura, G.L., Foster, S.A., Perry, J.J., Streiff, M., Ramage, P., Widmer, H.*, et al.* (2008). Structural basis of guanine nucleotide exchange mediated by the T-cell essential Vav1. J Mol Biol *380*, 828-843.

Derewenda, U., Oleksy, A., Stevenson, A.S., Korczynska, J., Dauter, Z., Somlyo, A.P., Otlewski, J., Somlyo, A.V., and Derewenda, Z.S. (2004). The crystal structure of RhoA in complex with the DH/PH fragment of PDZRhoGEF, an activator of the Ca(2+) sensitization pathway in smooth muscle. Structure *12*, 1955-1965.

Driessens, M.H., Hu, H., Nobes, C.D., Self, A., Jordens, I., Goodman, C.S., and Hall, A. (2001). Plexin-B semaphorin receptors interact directly with active Rac and regulate the actin cytoskeleton by activating Rho. Curr Biol *11*, 339-344.

Eberth, A., and Ahmadian, M.R. (2009). In vitro GEF and GAP assays. Curr Protoc Cell Biol *Chapter 14*, Unit 14 19.

Emsley, P., and Cowtan, K. (2004). Coot: model-building tools for molecular graphics. Acta Crystallogr D Biol Crystallogr *60*, 2126-2132.

Fan, L., Yan, H., Pellegrin, S., Morigen, and Mellor, H. (2015). The Rif GTPase regulates cytoskeletal signaling from plexinA4 to promote neurite retraction. Neurosci Lett *590*, 178-183.

Fansa, E.K., Dvorsky, R., Zhang, S.C., Fiegen, D., and Ahmadian, M.R. (2013). Interaction characteristics of Plexin-B1 with Rho family proteins. Biochem Biophys Res Commun *434*, 785-790.

Fukuhara, T., Shimizu, K., Kawakatsu, T., Fukuyama, T., Minami, Y., Honda, T., Hoshino, T., Yamada, T., Ogita, H., Okada, M.*, et al.* (2004). Activation of Cdc42 by trans interactions of the cell adhesion molecules nectins through c-Src and Cdc42-GEF FRG. J Cell Biol *166*, 393-405.

Fukuyama, T., Ogita, H., Kawakatsu, T., Fukuhara, T., Yamada, T., Sato, T., Shimizu, K., Nakamura, T., Matsuda, M., and Takai, Y. (2005). Involvement of the c-Src-

Crk-C3G-Rap1 signaling in the nectin-induced activation of Cdc42 and formation of adherens junctions. J Biol Chem *280*, 815-825.

Gloerich, M., and Bos, J.L. (2011). Regulating Rap small G-proteins in time and space. Trends Cell Biol *21*, 615-623.

Goh, W.I., Sudhaharan, T., Lim, K.B., Sem, K.P., Lau, C.L., and Ahmed, S. (2011). Rif-mDia1 interaction is involved in filopodium formation independent of Cdc42 and Rac effectors. J Biol Chem *286*, 13681-13694.

Gouet, P., Courcelle, E., Stuart, D.I., and Metoz, F. (1999). ESPript: analysis of multiple sequence alignments in PostScript. Bioinformatics *15*, 305-308.

Gu, C., and Giraudo, E. (2013). The role of semaphorins and their receptors in vascular development and cancer. Exp Cell Res *319*, 1306-1316.

Hayashi, M., Nakashima, T., Taniguchi, M., Kodama, T., Kumanogoh, A., and Takayanagi, H. (2012). Osteoprotection by semaphorin 3A. Nature *485*, 69-74.

He, H., Yang, T., Terman, J.R., and Zhang, X. (2009). Crystal structure of the plexin A3 intracellular region reveals an autoinhibited conformation through active site sequestration. Proc Natl Acad Sci U S A *106*, 15610-15615.

He, X., Kuo, Y.C., Rosche, T.J., and Zhang, X. (2013). Structural basis for autoinhibition of the guanine nucleotide exchange factor FARP2. Structure *21*, 355-364.

Heasman, S.J., and Ridley, A.J. (2008). Mammalian Rho GTPases: new insights into their functions from in vivo studies. Nature reviews Molecular cell biology *9*, 690-701.

Hota, P.K., and Buck, M. (2009). Thermodynamic characterization of two homologous protein complexes: associations of the semaphorin receptor plexin-B1 RhoGTPase binding domain with Rnd1 and active Rac1. Protein Sci *18*, 1060-1071.

Hu, H., Marton, T.F., and Goodman, C.S. (2001). Plexin B mediates axon guidance in Drosophila by simultaneously inhibiting active Rac and enhancing RhoA signaling. Neuron *32*, 39-51.

Kadamur, G., and Ross, E.M. (2016). Intrinsic Pleckstrin Homology (PH) Domain Motion in Phospholipase C-beta Exposes a Gbetagamma Protein Binding Site. J Biol Chem *291*, 11394-11406.

Katoh, K., Rozewicki, J., and Yamada, K.D. (2017). MAFFT online service: multiple sequence alignment, interactive sequence choice and visualization. Brief Bioinform.

Kawakita, A., Yamashita, T., Taniguchi, M., Koyama, Y., Kubo, T., Tsuji, L., and Tohyama, M. (2003). Developmental regulation of FERM domain including guanine nucleotide exchange factor gene expression in the mouse brain. Brain Res Dev Brain Res *144*, 181-189.

Keller, S., Vargas, C., Zhao, H., Piszczek, G., Brautigam, C.A., and Schuck, P. (2012). High-precision isothermal titration calorimetry with automated peak-shape analysis. Anal Chem *84*, 5066-5073.

Korennykh, A.V., Egea, P.F., Korostelev, A.A., Finer-Moore, J., Zhang, C., Shokat, K.M., Stroud, R.M., and Walter, P. (2009). The unfolded protein response signals through high-order assembly of Ire1. Nature *457*, 687-693.

Koyano, Y., Kawamoto, T., Kikuchi, A., Shen, M., Kuruta, Y., Tsutsumi, S., Fujimoto, K., Noshiro, M., Fujii, K., and Kato, Y. (2001). Chondrocyte-derived ezrin-like domain containing protein (CDEP), a rho guanine nucleotide exchange factor, is inducible in chondrocytes by parathyroid hormone and cyclic AMP and has transforming activity in NIH3T3 cells. Osteoarthritis Cartilage *9 Suppl A*, S64-68.

Koyano, Y., Kawamoto, T., Shen, M., Yan, W., Noshiro, M., Fujii, K., and Kato, Y. (1997). Molecular cloning and characterization of CDEP, a novel human protein containing the ezrin-like domain of the band 4.1 superfamily and the Dbl homology domain of Rho guanine nucleotide exchange factors. Biochem Biophys Res Commun *241*, 369-375.

Kristelly, R., Gao, G., and Tesmer, J.J. (2004). Structural determinants of RhoA binding and nucleotide exchange in leukemia-associated Rho guanine-nucleotide exchange factor. J Biol Chem *279*, 47352-47362.

Kruger, R.P., Aurandt, J., and Guan, K.L. (2005). Semaphorins command cells to move. Nature reviews Molecular cell biology *6*, 789-800.

Kubo, T., Yamashita, T., Yamaguchi, A., Sumimoto, H., Hosokawa, K., and Tohyama, M. (2002). A novel FERM domain including guanine nucleotide exchange factor is involved in Rac signaling and regulates neurite remodeling. The Journal of neuroscience : the official journal of the Society for Neuroscience *22*, 8504-8513.

Kumanogoh, A., and Kikutani, H. (2013). Immunological functions of the neuropilins and plexins as receptors for semaphorins. Nat Rev Immunol *13*, 802-814.

Love, C.A., Harlos, K., Mavaddat, N., Davis, S.J., Stuart, D.I., Jones, E.Y., and Esnouf, R.M. (2003). The ligand-binding face of the semaphorins revealed by the high-resolution crystal structure of SEMA4D. Nat Struct Biol *10*, 843-848.

Luo, L. (2002). Actin cytoskeleton regulation in neuronal morphogenesis and structural plasticity. Annu Rev Cell Dev Biol *18*, 601-635.

Lutz, S., Shankaranarayanan, A., Coco, C., Ridilla, M., Nance, M.R., Vettel, C., Baltus, D., Evelyn, C.R., Neubig, R.R., Wieland, T.*, et al.* (2007). Structure of Galphaq-p63RhoGEF-RhoA complex reveals a pathway for the activation of RhoA by GPCRs. Science *318*, 1923-1927.

McCoy, A.J., Grosse-Kunstleve, R.W., Adams, P.D., Winn, M.D., Storoni, L.C., and Read, R.J. (2007). Phaser crystallographic software. J Appl Crystallogr *40*, 658-674.

Miki, H., and Takenawa, T. (2003). Regulation of actin dynamics by WASP family proteins. J Biochem *134*, 309-313.

Millard, T.H., Sharp, S.J., and Machesky, L.M. (2004). Signalling to actin assembly via the WASP (Wiskott-Aldrich syndrome protein)-family proteins and the Arp2/3 complex. Biochem J *380*, 1-17.

Mitin, N., Betts, L., Yohe, M.E., Der, C.J., Sondek, J., and Rossman, K.L. (2007). Release of autoinhibition of ASEF by APC leads to CDC42 activation and tumor suppression. Nat Struct Mol Biol *14*, 814-823.

Miyamoto, Y., Yamauchi, J., and Itoh, H. (2003). Src kinase regulates the activation of a novel FGD-1-related Cdc42 guanine nucleotide exchange factor in the signaling pathway from the endothelin A receptor to JNK. J Biol Chem *278*, 29890-29900.

Murata, T., Ohnishi, H., Okazawa, H., Murata, Y., Kusakari, S., Hayashi, Y., Miyashita, M., Itoh, H., Oldenborg, P.A., Furuya, N.*, et al.* (2006). CD47 promotes neuronal development through Src- and FRG/Vav2-mediated activation of Rac and Cdc42. The Journal of neuroscience : the official journal of the Society for Neuroscience *26*, 12397-12407.

Murayama, K., Shirouzu, M., Kawasaki, Y., Kato-Murayama, M., Hanawa-Suetsugu, K., Sakamoto, A., Katsura, Y., Suenaga, A., Toyama, M., Terada, T.*, et al.* (2007). Crystal structure of the rac activator, Asef, reveals its autoinhibitory mechanism. J Biol Chem *282*, 4238-4242.

Neufeld, G., Sabag, A.D., Rabinovicz, N., and Kessler, O. (2012). Semaphorins in angiogenesis and tumor progression. Cold Spring Harb Perspect Med *2*, a006718.

Oinuma, I., Katoh, H., Harada, A., and Negishi, M. (2003). Direct interaction of Rnd1 with Plexin-B1 regulates PDZ-RhoGEF-mediated Rho activation by Plexin-B1 and induces cell contraction in COS-7 cells. J Biol Chem *278*, 25671-25677.

Ortiz, M.L., Calero, M., Fernandez Patron, C., Patron, C.F., Castellanos, L., and Mendez, E. (1992). Imidazole-SDS-Zn reverse staining of proteins in gels containing or not SDS and microsequence of individual unmodified electroblotted proteins. FEBS Lett *296*, 300-304.

Pascoe, H.G., Wang, Y., and Zhang, X. (2015). Structural mechanisms of plexin signaling. Prog Biophys Mol Biol *118*, 161-168.

Pasterkamp, R.J. (2012). Getting neural circuits into shape with semaphorins. Nat Rev Neurosci *13*, 605-618.

Pasterkamp, R.J., and Kolodkin, A.L. (2003). Semaphorin junction: making tracks toward neural connectivity. Curr Opin Neurobiol *13*, 79-89.

Pellegrin, S., and Mellor, H. (2005). The Rho family GTPase Rif induces filopodia through mDia2. Curr Biol *15*, 129-133.

Rapley, J., Tybulewicz, V.L., and Rittinger, K. (2008). Crucial structural role for the PH and C1 domains of the Vav1 exchange factor. EMBO Rep *9*, 655-661.

Ridley, A.J. (2011). Life at the leading edge. Cell *145*, 1012-1022.

Riento, K., and Ridley, A.J. (2003). Rocks: multifunctional kinases in cell behaviour. Nature reviews Molecular cell biology *4*, 446-456.

Rohm, B., Rahim, B., Kleiber, B., Hovatta, I., and Puschel, A.W. (2000). The semaphorin 3A receptor may directly regulate the activity of small GTPases. FEBS Lett *486*, 68-72.

Rossman, K.L., Cheng, L., Mahon, G.M., Rojas, R.J., Snyder, J.T., Whitehead, I.P., and Sondek, J. (2003). Multifunctional roles for the PH domain of Dbs in regulating Rho GTPase activation. J Biol Chem *278*, 18393-18400.

Rossman, K.L., Der, C.J., and Sondek, J. (2005). GEF means go: turning on RHO GTPases with guanine nucleotide-exchange factors. Nature reviews Molecular cell biology *6*, 167-180.

Rossman, K.L., Worthylake, D.K., Snyder, J.T., Siderovski, D.P., Campbell, S.L., and Sondek, J. (2002). A crystallographic view of interactions between Dbs and

Cdc42: PH domain-assisted guanine nucleotide exchange. EMBO J *21*, 1315-1326.

Rujescu, D., Meisenzahl, E.M., Krejcova, S., Giegling, I., Zetzsche, T., Reiser, M., Born, C.M., Moller, H.J., Veske, A., Gal, A.*, et al.* (2007). Plexin B3 is genetically associated with verbal performance and white matter volume in human brain. Mol Psychiatry *12*, 190-194, 115.

Scheuermann, T.H., Padrick, S.B., Gardner, K.H., and Brautigam, C.A. (2016). On the acquisition and analysis of microscale thermophoresis data. Anal Biochem *496*, 79-93.

Schneider, C.A., Rasband, W.S., and Eliceiri, K.W. (2012). NIH Image to ImageJ: 25 years of image analysis. Nat Methods *9*, 671-675.

Shang, G., Brautigam, C.A., Chen, R., Lu, D., Torres-Vazquez, J., and Zhang, X. (2017). Structure analyses reveal a regulated oligomerization mechanism of the PlexinD1/GIPC/myosin VI complex. eLife *6*.

Solski, P.A., Wilder, R.S., Rossman, K.L., Sondek, J., Cox, A.D., Campbell, S.L., and Der, C.J. (2004). Requirement for C-terminal sequences in regulation of Ect2 guanine nucleotide exchange specificity and transformation. J Biol Chem *279*, 25226-25233.

Takegahara, N., Kang, S., Nojima, S., Takamatsu, H., Okuno, T., Kikutani, H., Toyofuku, T., and Kumanogoh, A. (2010). Integral roles of a guanine nucleotide exchange factor, FARP2, in osteoclast podosome rearrangements. FASEB J *24*, 4782-4792.

Tong, Y., and Buck, M. (2005). 1H, 15N and 13C Resonance assignments and secondary structure determination reveal that the minimal Rac1 GTPase binding domain of plexin-B1 has a ubiquitin fold. J Biomol NMR *31*, 369-370.

Tong, Y., Chugha, P., Hota, P.K., Alviani, R.S., Li, M., Tempel, W., Shen, L., Park, H.W., and Buck, M. (2007). Binding of Rac1, Rnd1, and RhoD to a novel Rho GTPase interaction motif destabilizes dimerization of the plexin-B1 effector domain. J Biol Chem *282*, 37215-37224.

Toyofuku, T., Yoshida, J., Sugimoto, T., Zhang, H., Kumanogoh, A., Hori, M., and Kikutani, H. (2005). FARP2 triggers signals for Sema3A-mediated axonal repulsion. Nat Neurosci *8*, 1712-1719.

Tran, T.S., Kolodkin, A.L., and Bharadwaj, R. (2007). Semaphorin regulation of cellular morphology. Annu Rev Cell Dev Biol *23*, 263-292.

Turner, L.J., Nicholls, S., and Hall, A. (2004). The activity of the plexin-A1 receptor is regulated by Rac. J Biol Chem *279*, 33199-33205.

Van Aelst, L., and D'Souza-Schorey, C. (1997). Rho GTPases and signaling networks. Genes Dev *11*, 2295-2322.

Vega, F.M., and Ridley, A.J. (2008). Rho GTPases in cancer cell biology. FEBS Lett *582*, 2093-2101.

Vetter, I.R., and Wittinghofer, A. (2001). The guanine nucleotide-binding switch in three dimensions. Science *294*, 1299-1304.

Vikis, H.G., Li, W., and Guan, K.L. (2002). The plexin-B1/Rac interaction inhibits PAK activation and enhances Sema4D ligand binding. Genes Dev *16*, 836-845.

Vikis, H.G., Li, W., He, Z., and Guan, K.L. (2000). The semaphorin receptor plexin-B1 specifically interacts with active Rac in a ligand-dependent manner. Proc Natl Acad Sci U S A *97*, 12457-12462.

Wang, H., Hota, P.K., Tong, Y., Li, B., Shen, L., Nedyalkova, L., Borthakur, S., Kim, S., Tempel, W., Buck, M*., et al.* (2011). Structural basis of Rnd1 binding to plexin Rho GTPase binding domains (RBDs). J Biol Chem *286*, 26093-26106.

Wang, Y., He, H., Srivastava, N., Vikarunnessa, S., Chen, Y.B., Jiang, J., Cowan, C.W., and Zhang, X. (2012). Plexins are GTPase-activating proteins for Rap and are activated by induced dimerization. Science signaling *5*, ra6.

Wang, Y., Pascoe, H.G., Brautigam, C.A., He, H., and Zhang, X. (2013). Structural basis for activation and non-canonical catalysis of the Rap GTPase activating protein domain of plexin. eLife *2*, e01279.

Wennerberg, K., Forget, M.A., Ellerbroek, S.M., Arthur, W.T., Burridge, K., Settleman, J., Der, C.J., and Hansen, S.H. (2003). Rnd proteins function as RhoA antagonists by activating p190 RhoGAP. Curr Biol *13*, 1106-1115.

Wienken, C.J., Baaske, P., Rothbauer, U., Braun, D., and Duhr, S. (2010). Protein-binding assays in biological liquids using microscale thermophoresis. Nat Commun *1*, 100.

Worzfeld, T., and Offermanns, S. (2014). Semaphorins and plexins as therapeutic targets. Nat Rev Drug Discov *13*, 603-621.

Yohe, M.E., Rossman, K., and Sondek, J. (2008). Role of the C-terminal SH3 domain and N-terminal tyrosine phosphorylation in regulation of Tim and related Dbl-family proteins. Biochemistry *47*, 6827-6839.

Yohe, M.E., Rossman, K.L., Gardner, O.S., Karnoub, A.E., Snyder, J.T., Gershburg, S., Graves, L.M., Der, C.J., and Sondek, J. (2007). Auto-inhibition of the Dbl family protein Tim by an N-terminal helical motif. J Biol Chem *282*, 13813-13823.

Yu, B., Martins, I.R., Li, P., Amarasinghe, G.K., Umetani, J., Fernandez-Zapico, M.E., Billadeau, D.D., Machius, M., Tomchick, D.R., and Rosen, M.K. (2010). Structural and energetic mechanisms of cooperative autoinhibition and activation of Vav1. Cell *140*, 246-256.

Zanata, S.M., Hovatta, I., Rohm, B., and Puschel, A.W. (2002). Antagonistic effects of Rnd1 and RhoD GTPases regulate receptor activity in Semaphorin 3A-induced cytoskeletal collapse. The Journal of neuroscience : the official journal of the Society for Neuroscience *22*, 471-477.

Zhang, X., Gureasko, J., Shen, K., Cole, P.A., and Kuriyan, J. (2006). An allosteric mechanism for activation of the kinase domain of epidermal growth factor receptor. Cell *125*, 1137-1149.

Zheng, M., Cierpicki, T., Momotani, K., Artamonov, M.V., Derewenda, U., Bushweller, J.H., Somlyo, A.V., and Derewenda, Z.S. (2009). On the mechanism of autoinhibition of the RhoA-specific nucleotide exchange factor PDZRhoGEF. BMC Struct Biol *9*, 36.

Zhuang, B., Su, Y.S., and Sockanathan, S. (2009). FARP1 promotes the dendritic growth of spinal motor neuron subtypes through transmembrane Semaphorin6A and PlexinA4 signaling. Neuron *61*, 359-372.